PHYSICS REPORTS (Review Section of Physics Letters) 237, No. 5 (1994) 249–324.
North-Holland

PHYSICS REPORTS

Melting, freezing and colloidal suspensions

Hartmut Löwen

Sektion Physik der Universität München, Theresienstr. 37, D-80333 München, Germany

Received September 1993; editor: M.L. Klein

Contents:

Abstract:

Melting and freezing are very common phenomena in everyday life. This review focusses on the statistical mechanics of these ubiquitous phase transitions and highlights recent work on the bulk and surface melting of solids, crystal growth from the melt, and the kinetic glass transition of supercooled liquids. Both phenomenological and microscopic density functional approaches are discussed. Particular emphasis is placed on colloidal suspensions, which are realizations of simple liquids on a mesoscopic length scale that also exhibit melting and freezing phenomena.

SSDI 0370-1573(93)E0043-N

MELTING, FREEZING AND COLLOIDAL SUSPENSIONS

Hartmut LÖWEN

Sektion Physik der Universität München, Theresienstr. 37, D-80333 München, Germany

NORTH-HOLLAND

Introduction

One of the best known phase transformations is the melting of a solid or freezing of a liquid into a crystal or a glass. This important phase transition occurs in quite different situations ranging from ice formation in clouds and the preparation of rapidly quenched metallic alloys to the production of window glass. During the last centuries a lot of technical experience in quite different areas has accumulated where freezing and melting phenomena are exploited in order to facilitate everyday life. Despite of this rapidly increasing empirical and phenomenological knowledge it is only since the last decades that *molecular* aspects were addressed aiming to a *microscopic* understanding of the solid–liquid phase transformation. Important recent progress was made using three different methods:

(i) well-aimed *experimental* studies, in particular scattering experiments with a resolution on a microscopic length and time scale,

(ii) *computer simulation* starting from relatively simple models for the inter-particle interaction,

(iii) microscopic and semi-phenomenological *theories* capturing the essential physical mechanisms relevant for the thermodynamics and dynamics of melting and freezing.

It is enormously difficult to construct a general comprehensive picture of three-dimensional melting and freezing phenomena. There are at least two reasons for that. Firstly, the melting transition is first order, accompagnied by a density jump, which means that it is highly *non-universal,* i.e. the detailed scenario depends on the kind of material considered. Secondly, the solid–liquid transition typically occurs in concentrated, strongly interacting systems. This implies that it is a collective phenomenon of a *many-particle* system.

As regards experiments, bulk phase diagrams of monatomic materials are well-studied and precisely known. The bulk melting temperature of lead under atmospheric pressure, for instance, is known with a relative uncertaincy of less than 10^{-5}! What is less clear are effects at the surface between a coexisting liquid and solid, and also dynamical (time-dependent) processes which happen on a small and intermediate time scale. Among these questions are crystal growth from the melt, dynamics of glass formation in the supercooled liquid, surface melting of solids etc.

Computer simulations are designed for a relatively small system size with $N = 100$–$100\,000$ particles in a box with periodic boundary conditions. They are very helpful and a necessary tool in order to get "exact" results for a well-defined model in the framework of statistical mechanics. Usually the interactions between particles are specified as an input. By computer simulation bulk phase diagrams, structural and dynamical quantities and also interfacial problems could be addressed. The main caveats are limitations due to finite system size and statistical errors.

Microscopic theories for freezing and melting based on statistical mechanics are still very rudimentary. Strictly speaking, there is to date no general theory of melting and freezing. Even a simple exactly soluble statistical mechanics model with nontrivial interactions is missing where one could study the melting process as a paradigm. Also there are no rigorous results from mathematical physics even for relatively simple (e.g. Lennard-Jones) systems. There is no rigorous proof for the existence of a liquid and solid phase in three spatial dimensions. However, in developing a general theory, an important step was recently done in viewing freezing as a condensation of liquid density modes within the framework of classical density functional theory. This theory is quite general but still a bit ad hoc. Nevertheless it makes some reasonable predictions for certain model systems.

This review focusses on recent molecular aspects of melting and freezing including experiments, computer simulations and theory. A particular emphasis is put on the structure and dynamics of solid–fluid interfaces and the diffusion of the latent heat in solidification examined on the basis of classical statistical mechanics. In parallel, special attention is paid to colloidal suspensions which are simple liquids on a mesoscopic length scale. Colloids also exhibit all kinds of melting and freezing phenomena and represent excellent experimental systems for simple models of classical statistical mechanics such that sometimes even a quantitative comparison between experiment and theory is possible.

The article is organized as follows. In chapter 1, we review some of the basic of classical statistical mechanics and discuss some intrinsic properties of atomic and colloidal systems. In chapters 2 and 3, both phenomenological and microscopic density functional theories of bulk melting are described. In chapter 4 the melting of a solid from its surface close to the triple point is studied. In contrast to bulk melting, surface melting can occur at temperatures where the bulk liquid phase is still metastable. The dynamics and kinetics of interfaces are discussed in chapter 5, with emphasis on the dynamics of surface melting and a dynamical mechanism for the creation of metastable phases. Recent results on crystal growth, hindered by thermal diffusion of the latent heat, are then described within a phenomenological phase-field model in chapter 6. Finally we consider the kinetic glass transition in supercooled atomic and colloidal liquids and conclude with a summary and an outlook.

1. Classical statistical mechanics

For conceptual and notational clarity let us consider only simple systems interacting via a *pair* potential. Realizations of such systems in nature are found both on an atomic and mesoscopic level. They include rare gases and ions for which a Lennard-Jones respectively a Coulomb pair potential is an adequate description, and colloidal suspensions. For the latter one has to distinguish between sterically stabilized colloids with a hard core interaction, and charge-stabilized suspensions, whose interaction may be described by an effective Yukawa potential. Interesting fundamental questions which form an area of intense recent research concern the bulk phase diagram, and the structure and dynamics of a given bulk phase and of interfaces between two bulk phases. A particularly rich behaviour is expected near the coexistence of three phases.

1.1. Basics and definitions

A *classical many-body system* consists of N particles, confined to a volume V, and is also characterized by a temperature T. The number N is much larger than 1 and typically of the order of 10^{23} for an atomic system. A simple criterion, to decide whether an atomic system can be considered as *classical*, is the ratio of the thermal de Broglie wavelength Λ and a typical nearest neighbour separation $a = \rho^{-1/3}$ where $\rho = N/V$ is the particle number density. The de Broglie length Λ is defined as

$$\Lambda = \sqrt{h^2/2\pi m k_B T} \tag{1}$$

where m is the particle mass, h is Planck's constant and k_B Boltzmann's constant. It turns out that all of the heavier atoms (except H_2, He of course) have a ratio $\Lambda/a \ll 1$ at "moderate" conditions, which means that quantum corrections are negligible.

In the following, only *simple* systems are considered, i.e. *one-component* systems with particles interacting via *pairwise* forces derivable from a *spherical symmetric* potential $V(r)$, r denoting the mutual particle distance. The classical Hamiltonian H_N therefore reads

$$H_N = H_{\text{kin}} + H_{\text{ext}} + U \tag{2}$$

where

$$H_{\text{kin}} = \sum_{i=1}^{N} \boldsymbol{p}_i^2/2m, \tag{3}$$

$$H_{\text{ext}} = \sum_{i=1}^{N} V_{\text{ext}}(\boldsymbol{r}_i), \tag{4}$$

$$U = \frac{1}{2} \sum_{i,j=1;i\neq j}^{N} V(|\boldsymbol{r}_i - \boldsymbol{r}_j|). \tag{5}$$

Here, $\boldsymbol{p}_i$, $\boldsymbol{r}_i$ are the momenta and positions of particle i and $V_{\text{ext}}(\boldsymbol{r})$ denotes an external potential e.g. gravity or external walls confining the system.

The central quantity in classical statistical mechanics is the equilibrium canonical probability density $w_N(\{\boldsymbol{p}_i\}, \{\boldsymbol{r}_i\}; i = 1, \ldots, N)$ for N particles at temperature T which is defined as

$$w_N(\{\boldsymbol{p}_i\}, \{\boldsymbol{r}_i\}) = Z^{-1} \exp(-H_N/k_B T) \tag{6}$$

where the normalization factor Z is the canonical partition function

$$Z = \text{Tr}_N \exp(-H_N/k_B T). \tag{7}$$

Here, Tr_N denotes a classical trace

$$\text{Tr}_N(\cdots) = \frac{1}{h^{3N} N!} \int \mathrm{d}^3 r_1 \cdots \int \mathrm{d}^3 r_N \int \mathrm{d}^3 p_1 \cdots \int \mathrm{d}^3 p_N \, (\cdots). \tag{8}$$

Z is related to the canonical free energy F by

$$F = -k_B T \ln Z. \tag{9}$$

It is clear that F depends on the three external quantities T, V, N. In the *thermodynamic limit* $N, V \to \infty$, $N/V = \rho = \text{const.}$, F is an extensive quantity for $V_{\text{ext}}(\boldsymbol{r}) \equiv 0$, i.e. the canonical free energy density $f = F/V$ only depends on T and ρ. For further purposes it is useful to introduce a short notation for the statistical configuration average. We write

$$\langle A(\{\boldsymbol{p}_i\}, \{\boldsymbol{r}_i\}) \rangle = \text{Tr}_N [w_N(\{\boldsymbol{p}_i\}, \{\boldsymbol{r}_i\}) A(\{\boldsymbol{p}_i\}, \{\boldsymbol{r}_i\})]. \tag{10}$$

An important and fundamental quantity is the equilibrium density $\rho_0(\boldsymbol{r})$ which is the statistical average of the particle positions

$$\rho_0(\boldsymbol{r}) = \left\langle \sum_{i=1}^{N} \delta(\boldsymbol{r} - \boldsymbol{r}_i) \right\rangle. \tag{11}$$

One can often distinguish different thermodynamic phases by qualitatively different equilibrium densities, then $\rho_0(\boldsymbol{r})$ plays the role of an *order parameter.*

For theoretical and practical reasons it is often more convenient to move from the canonical to the *grand canonical* ensemble by a Legendre transform with respect to N. One arrives at a grand canonical partition function Ξ depending now on T, V and the chemical potential μ which can formally be interpreted as the Lagrange multiplier for the constraint of fixed averaged particle number. Ξ is defined as

$$\Xi = \sum_{N=1}^{\infty} \mathrm{Tr}_N \exp(-H_N - \mu N/k_B T) \tag{12}$$

and the corresponding grand canonical free energy Ω reads

$$\Omega = -k_B T \ln \Xi. \tag{13}$$

Its density $\omega = \Omega/V$ only depends on T and μ in the thermodynamic limit. This ensemble can be shown to be "equivalent" to the canonical description in the thermodynamic limit. The physical significance of the grand canonical free energy Ω is that it represents the key quantity for a calculation of a phase diagram. It also obeys an important variational principle that we shall discuss in section 2.1. The definition of $\langle \cdots \rangle$ for a statistical average, see eq. (10), can be easily generalized to the grandcanonical case, now with a trace

$$\mathrm{Tr}(\cdots) = \sum_{N=1}^{\infty} \mathrm{Tr}_N(\cdots) \tag{14}$$

and with an added term $-\mu N$ in the Hamiltonian. In the thermodynamic limit, the results do not depend on the kind of ensemble one choses for the average. The definition of $\rho_0(\boldsymbol{r})$ for instance, see (11), can therefore also be read as in the grandcanonical ensemble including now an additional sum over N.

Apart from trivial noninteracting cases ($V(r) \equiv 0$), the trace operation in (8) and (12) cannot be done explicitly in three spatial dimensions. Analytical results are sparse in classical statistical mechanics, even for very simple models.

1.2. Realizations of classical statistical mechanics systems

In this section, we discuss systems in nature that are described by a pairwise radial symmetric potential $V(r)$. There are both realizations on a microscopic and on a mesoscopic length scale, namely atomic and colloidal systems, although there are some caveats since often the systems intrinsically contain also higher-than-two-body interactions.

1.2.1. Atomic systems

At very high temperature, atomic or molecular systems do not feel details of the interactions but only the strong Born repulsion due to overlapping electronic shells of two neighbouring particles. In such a situation, it is often sufficient to describe the interaction by a repulsive pairwise potential or – even more approximate – just by a *hard sphere* interaction

$$V_{\mathrm{HS}}(r) = \begin{cases} \infty & \text{for } r \leq \sigma. \\ 0 & \text{for } r > \sigma. \end{cases} \tag{15}$$

The experimental measured structure then can be fitted by just one parameter, the effective diameter σ of the system. The hard-sphere interaction is the simplest nontrivial interaction one can think about. Due to its scaling behaviour $\Lambda V_{\mathrm{HS}}(r) = V_{\mathrm{HS}}(r)$ for any positive Λ, it has relatively simple thermodynamic properties. However, it is clear that this potential remains a caricature for the interaction of atomic and molecular liquids. At moderate conditions and at relatively high density, the interaction is certainly more complicated than the hard-sphere model. It normally also includes more than two-body interactions, due to a mutual polarization of the electronic clouds if three or more particles are present.

Rare gases have spherical symmetric electronic shells and can, at moderate conditions, be described by the *Lennard-Jones* pair potential

$$V(r) = 4\varepsilon[(\sigma/r)^{12} - (\sigma/r)^6] \tag{16}$$

which includes the repulsive as well as the attractive van der Waals interaction. Here, σ sets the microscopic length scale and ε the energy scale of the Lennard-Jones potential. (σ should not be confused with the hard sphere diameter of the potential (15).) A more refined version of a pairwise potential for rare gases, the so-called Barker potential [1], is also available. However, at high concentration and in strongly inhomogeneous situations, triplet forces become important which are usually incorporated by the Axilrod–Teller three-body potential [2, 3].

The interaction of ions in a *homogeneous non-responding electronic background* is dominated by the Coulomb repulsion. The *one-component classical plasma* (OCP) is defined by the potential

$$V(r) = V_0\sigma/r \tag{17}$$

where σ again sets the length and V_0 the energy scale. *Molten salts* represent another simple though two-component system where the Coulomb interaction is dominating. In such a mixture of oppositely charged ions, a pair potential with a $1/r$ tail and a repulsive e.g. hard core part is an appropriate description of the interaction.

The case of monatomic *metals* is more difficult due to the extended nature of the conduction electrons. The latter clearly directly induce many-body forces between the ions at least at high densities. A similar situation occurs for *semiconductors*. What one can do here is to find an *effective pair potential* that depends on the thermodynamic parameters (e.g. temperature T and density ρ). By now there exist suitable tabulations of effective pair potentials for most of the simple monatomic materials, giving a structure which is very close to the experimental data [4]. Of course, this effective pair potential description fails in strongly inhomogeneous situations as for a liquid–gas or solid–gas interface. At this stage, it is useful to point out that there are recent ab initio theories combining quantum mechanical density functional theory for the electrons and molecular dynamics for the ions, by which one can simulate the structure and dynamics of crystalline and disordered metals and semiconductors. This very attractive and widely applied scheme includes systematically many-body forces and compares favorably well with the experimental data. It was invented by Car and Parrinello in 1985 [5].

1.2.2. Colloidal systems

A *colloidal suspension* consists of *mesoscopic* particles, with a diameter σ typically varying between 10^{-8} and 10^{-4} m, which are dispersed in a suspending microscopic fluid. There are lots of examples for such dispersions including gelatin sol, solutions of proteins, soap and microemulsions. Well-characterized experimental model systems are aqueous suspensions of polystyrene spheres and polymethylmethacrylate (PMMA) macromolecules. Such a suspension of "macroparticles"

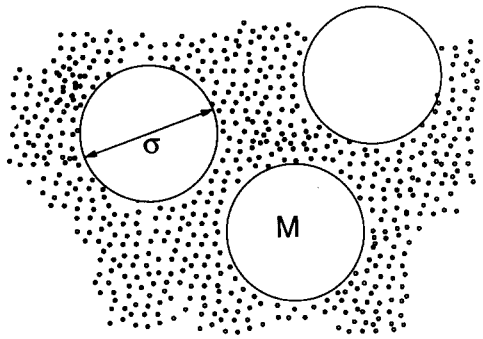

Fig. 1.1. Colloidal particles (big spheres) characterized by a mesoscopic diameter σ and a mass M, which are dispersed in a suspending atomic liquid (small spheres).

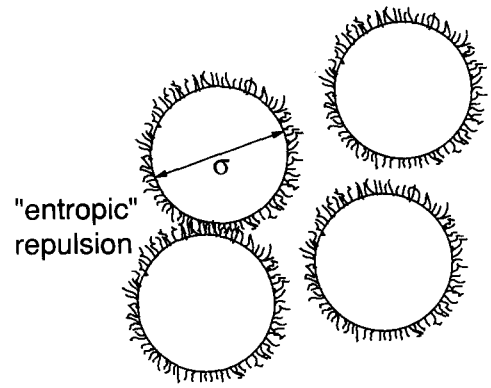

Fig. 1.2. Sterically stabilized colloidal particles with a diameter σ which are coated by polymer brushes. Typically the length of the polymeric chains is much smaller than the colloidal diameter. If two colloidal particles come very close to eachother, the polymer brushes overlap and a repulsion of entropic origin prevents the particles from sticking together.

embedded in an atomic liquid is sketched in fig. 1.1. Since the mass M of the colloidal particles is much bigger than the atomic mass of the solvent, there is a complete separation of time scales of colloidal and solvent motion. The latter is of the order of 0.1 ps whereas the motion of the big particles happens on a time scale of about 1–10 000 ns. Furthermore, it becomes clear that a typical trajectory of a particle is Brownian on a time scale relevant for macroion motion, due to random kicks with the solvent. This is very different to the atomic case where a particle trajectory is smooth and obeys Newtonian or molecular dynamics. This difference has important implications on time dependent quantities in atomic and colloidal systems.

Let us now focus on the forces between the colloidal particles. The first contribution naturally stems from the van der Waals dipole–induced-dipole attraction. This attraction *diverges* at particle contact and vanishes as r^{-6} for intermediate and as r^{-7} for very large interparticle distances r. Would this be the only interparticle interaction, a coagulation instability would result where the particles stick together and form a large cluster. Only the strong Born repulsion of the contacting big particles would prevent a complete collapse of the system. Therefore, to ensure the stability of a colloidal suspension with respect to irreversible flocculation, an additional stabilizing force is needed. There are two different stabilization mechanisms for colloidal systems: (a) steric stabilization and (b) charge stabilization.

As regards *steric stabilization*, the colloidal particles are coated with polymer brushes which leads to an "entropic" repulsion if polymer brushes of two neighbouring particles do overlap. This is visualized in fig. 1.2. Since the length of a polymer chain typically is much smaller than the colloidal diameter σ, one can describe this repulsive force simply by the pairwise *hard sphere potential* (15). The PMMA particles represent a paradigm of sterically stabilized colloidal particles. By "index-matching" of the colloidal particles and the solvent, one can practically suppress the van der Waals interaction such that the simple hard-sphere interaction dominates the interparticle forces. Careful experiments on the structure and the phase diagram reveal that the interaction of PMMA particles is really very well described by excluded volume effects only. Thus they represent an excellent experimental system for the hard sphere model which existed until recently only in the brains of the theoreticians! The characteristic parameter determining the bulk phase diagram and

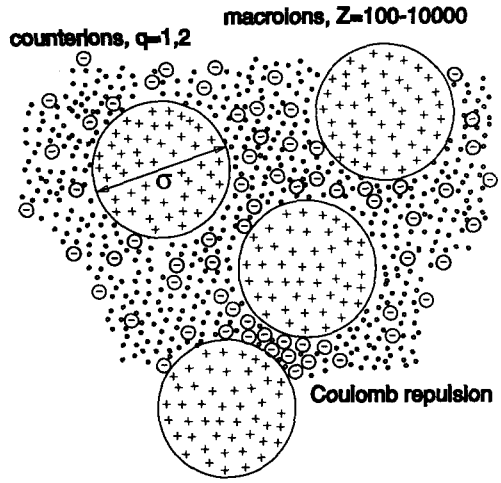

Fig. 1.3. A charge-stabilized colloidal suspension consists of macroions with a mesoscopic diameter σ and a charge Z of 100–10000 elementary charges, microscopic counterions with a charge of $q = 1, 2$ and the microscopic polar solvent shown as small dots. Here, the macroions have a negative and the counterions a positive charge; this can of course also be reversed. Two macroions repel themselves due to the Coulomb repulsion of an overlapping electric double layer.

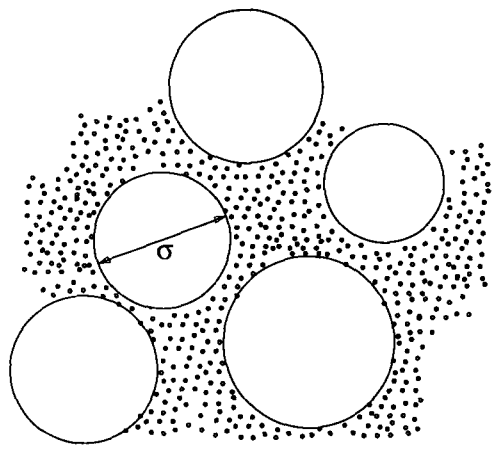

Fig. 1.4. Size-polydisperse colloidal suspension. The diameters of each big particle are not equal but distributed around a mean value with a second moment that defines the relative polydispersity.

the structure is the number density $\rho = N/V$ of the big particles or the packing fraction

$$\eta = \pi\rho\sigma^3/6. \tag{18}$$

Due to the scaling property of the hard sphere potential, the temperature T only enters in the time scale of dynamical processes. Interestingly enough, η can be varied experimentally from few percent to 0.74, the limiting value for a densed packed fcc or hcp crystal structure. So one can scan the whole relevant parameter space experimentally.

On the other hand, a *charge-stabilized* colloidal suspension results when big particles with surface radicals are put into a polar solvent like water. Most of the these charged surface groups dissociate into the solvent and form *counterions* carrying one or two elementary charges. Consequently, the colloidal particles become highly charged and may be called *macroions*; they carry typically $Z = 100$–$10\,000$ elementary charges. Essentially, the counterions are located around the charged colloidal surfaces forming a diffuse electric double layer. Since the counterion distribution is diffuse due to their finite temperature, screening of the macroions is imperfect and a screened Coulomb repulsion between the macroions results. In fig. 1.3, such a charge-stabilized colloidal suspension is shown as a three-component system consisting of macroions, counterions and the solvent. A typical experimental system which forms a charge-stabilized colloidal suspensions is an aqueous solution of polystyrene spheres. One fundamental problem in characterizing such a suspension experimentally concerns the direct determination of the macroion charge Z. One can only get upper bounds on Z by conductometric titration. If one compares experimental data with theories, one is therefore forced to treat Z as a fit parameter. Typically, a charge-stabilized suspension is rather dilute, i.e. the macroion packing fraction η is small (0.001–0.4). Nevertheless due to the high macroion

charge, the interaction is very strong resulting in a marked structure. Such a very dilute system can even exhibit crystallization. For packing fractions of about $\eta \simeq 0.3$ the suspension represents a *concentrated* strongly interacting system whose theoretical description is of course much more complex than in the dilute case.

The question after the interaction between macroions has a long history. An explicit expression for a pairwise potential incorporating corrections due to a finite macroion diameter σ was given by Derjaguin, Landau, Verwey and Overbeek (DLVO) [6]. This DLVO potential was derived by linear Debye–Hückel screening theory and consists of an electrostatic and the van der Waals part. The electrostatic part has the *Yukawa* or screened Coulomb form:

$$V(r) = Z^{*2}e^2 \exp(-\kappa r)/\varepsilon r \tag{19}$$

where ε is the dielectric constant of the solvent and

$$\kappa = \sqrt{4\pi\rho_c(qe)^2/\varepsilon k_B T} \tag{20}$$

is the inverse Debye–Hückel screening length, ρ_c denoting the mean counterion number density and qe their charge. Furthermore the renormalized charge Z^* is related to the bare charge Z via

$$Z^* = Z\frac{\exp(\kappa\sigma/2)}{1+\kappa\sigma/2}. \tag{21}$$

If $\rho \equiv N/V$ is the number density of macroions, global charge neutrality requires

$$Z\rho = -q\rho_c. \tag{22}$$

The celebrated DLVO potential is an *effective* pair potential between the macroions. The complex *three-component* system has been reduced to *a one-component* system. The discrete nature of the solvent has been neglected completely. It only enters via its dielectric constant ε in the effective potential. The counterionic degrees of freedom have also been integrated out approximately. They determine the screening parameter κ. In addition, the DLVO potential depends on the thermodynamic parameters like the temperature T and, via (22), the macroion density ρ.

Although the description via the effective DLVO-pair potential is expected to work for very dilute suspensions, the assumption of linear screening must break down for concentrated suspensions. In particular, one would expect that effective many-body forces on the macroions, induced by the counterions, become relevant [7].

In order to reduce the screened Coulomb repulsion between the macroions in a charge-stabilized colloidal suspensions, one usually adds salt to the solution. If the ions of the salt have the same charge q as the counterions, the colloidal suspension consists of *four* components: macroions, counterions, coions and the solvent. Within DLVO-theory, one can again find an effective pair potential between the macroions. In the high dilution limit, the effective interaction remains Yukawa-like, see (19), but the inverse Debye screening length κ is enhanced to

$$\kappa = \sqrt{[4\pi(qe)^2/\varepsilon k_B T](\rho_c q^2 e^2 + \rho_{co} q^2 e^2)} \tag{23}$$

where $\rho_{co} = N_{co}/V$ is the coion concentration.

1.3. Polydispersity in colloidal suspensions

In a real colloidal suspension, the particles are not identical but differ in size and charge. This property is called *polydispersity*. Polydispersity makes a direct comparison of experimental data

with that of simple liquid models difficult. Therefore one has to introduce more complex models. Polydisperse fluids can also be viewed as infinite-component mixtures.

1.3.1. Polydispersity in size

For sterically stabilized colloidal suspensions, polydispersity in size is conveniently described by the hard sphere potential between two particles i and j

$$V_{ij}(r) = \begin{cases} \infty & \text{for } r \leq \frac{1}{2}(\sigma_i + \sigma_j), \\ 0 & \text{else} \end{cases} \tag{24}$$

where the particle diameters $\{\sigma_i\}$ are now continuously distributed according to a distribution function $P(\sigma)$ with a *mean diameter*

$$\overline{\sigma} = \int_0^\infty d\sigma \, P(\sigma)\sigma \tag{25}$$

and a *relative polydispersity* p_σ as the second moment of the distribution

$$p_\sigma = \left(\frac{1}{\overline{\sigma}^2} \int_0^\infty d\sigma \, (\sigma - \overline{\sigma})^2 P(\sigma) \right)^{1/2}. \tag{26}$$

Such a size-polydisperse suspension is sketched in fig. 1.4.

1.3.2. Polydispersity in charge

In a charge-stabilized colloidal suspension, there occurs both, polydispersity in size *and* charge. Such a polydisperse suspension is shown in fig. 1.5.

Assuming the DLVO potential (19) for the interaction between macroions, it is the *effective charge* which is continuously distributed. Note that within linear screening theory, the Debye screening parameter κ (20) remains unaffected by polydispersity. Hence the corresponding potential is

$$V_{ij}(r) = Z_i Z_j U_0 \exp(-\kappa r)/r =: Z_i Z_j U(r) \tag{27}$$

where now the effective charges are distributed according to a function $P(Z)$ and one can again define a mean value $\overline{Z}$ and a relative charge polydispersity p_Z as the first and second moment of the distribution $P(Z)$.

1.4. Atomic versus colloidal systems: analogies and differences

The main analogy between atomic and colloidal systems is that they both represent classical statistical mechanics systems whose interactions can be described in terms of a *pair potential.* Consequently, theories known from statistical mechanics can be applied to both kind of systems. The first important difference is that the parameters of the pair potential can be *tuned* in the colloidal case, e.g. by adding salt or by sample preparation, whereas they are *fixed* for atomic systems. This permits an flexible exploration of the relevant parameter space.

As already emphasized earlier, the inherent *length scale* (called σ in the previous section) is different: it is microscopic (1–10 Å) for atomic and mesoscopic (100–10^6 Å) for colloidal systems. Thus, the structure and the phase diagram is expected to be similar in the two cases, but it occurs

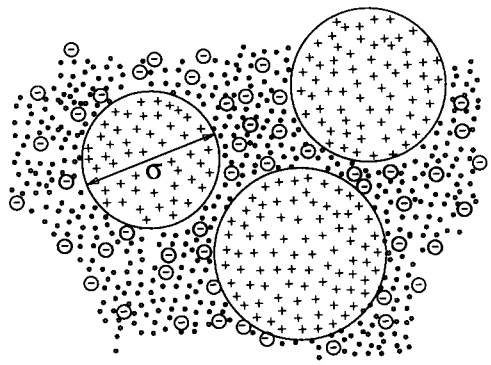

Fig. 1.5. Charge-stabilized colloidal suspension which is polydisperse in size and charge. This leads to a polydispersity in the effective charge within the DLVO-picture where the interaction between the macroions is described by a Yukawa potential.

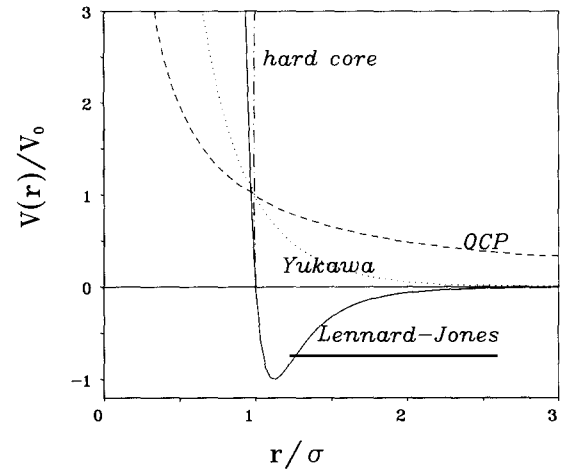

Fig. 1.6. Shape of the different pair potentials used to model various simple systems of classical statistical mechanics: hard-sphere potential (dot-dashed line), Lennard-Jones potential $V(r) = 4V_0[(\sigma/r)^{12} - (\sigma/r)^6]$ (solid line), OCP potential $V(r) = V_0\sigma/r$ (dashed line), and Yukawa potential $V(r) = V_0(\sigma/r)\exp(-\kappa(r-\sigma)/\sigma)$ with $\kappa = 2$. Here, σ denotes a length scale and V_0 an energy scale.

on a different length scale. Experimentally, the mesoscopic length scale implies that diffraction experiments of visible light rather than X-rays are necessary in order to explore the structure. There are also real space techniques like direct image processing which are only possible in the colloidal case.

The *time scale* relevant for dynamical processes of the atomic or colloidal particles is different, too. For an atomic system, one typically has a relaxation time of 0.1 ps whereas this time is shifted to 1–10000 ns for a colloidal suspension. This implies that dynamical phenomena like crystal growth etc. may occur on a time scale more convenient for experimental resolution, which constitutes another advantage of colloidal suspensions. The *dynamics* themselves, however, are different: they are Newtonian (Molecular Dynamics (MD)) for atomic systems and Brownian (BD) for colloidal suspensions. This has an important influence on time-dependent processes and will be extensively discussed in section 1.5.3. For a concentrated colloidal suspension, the solvent mediates *hydrodynamic interactions*, such that the actual dynamics of a colloidal system are much more complicated than for atomic systems. Only in the dilute limit, the dynamics are simple Brownian without any hydrodynamic forces. These hydrodynamic effects, however, fortunately do not affect static structural quantities.

One disadvantage of colloidal suspensions is their intrinsic *polydispersity* in size and charge. By a careful sample preparation, the polydispersity can be kept small, but cannot be always completely neglected. In this case the much more complicated models discussed in section 1.3 have to be used.

Summarizing, we have discussed different realizations for classical statistical mechanical systems in atomic and colloidal context. We found that the possible pair potentials are of hard-sphere, Coulomb, Lennard-Jones and Yukawa form. The shape of these different potentials is plotted in fig. 1.6 which clearly shows that they are qualitatively different. The phase diagrams and the static and dynamical behaviour depends crucially on the detailed form of the interaction.

1.5. Questions of classical statistical mechanics

1.5.1. Bulk phase diagrams

The first fundamental question concerns the nature of the different thermodynamic phases. Henceforth let us set $V_{\text{ext}}(\boldsymbol{r}) \equiv 0$; then the question is: How many and what kind of phases do occur for a given interaction potential $V(r)$ as a function of the thermodynamical parameters temperature T and density ρ (or chemical potential μ)?

For a classical many body system, this is a nontrivial difficult question, in general. During the last decade progress was made using the following methods:

(1) *Computer simulation* methods, mainly Monte Carlo and Molecular Dynamics codes.

(2) *Experiments* on well-characterized model systems (e.g. sterically stabilized colloidal suspensions).

(3) *Ab initio* theories starting from first principles, i.e. with the pair potential $V(r)$ as the only input. Up to now, there is no such generally applicable theory but there is some remarkable progress during the last decade with so-called *density functional theory* that starts from the phase with homogeneous density and then predicts a freezing transition into a solid.

The liquid to solid phase transition takes place along a coexistence line in the (T,μ)-plane and is first order, in general. It is also called *melting* or *freezing* transition depending on whether one goes from the solid to the liquid state or vice versa.

As for example for the freezing transition, let us first consider purely repulsive potentials $V(r)$ that are governed by one length scale σ. Typical examples are inverse power potentials

$$V(r) = V_0(\sigma/r)^\nu, \quad \nu > 0. \tag{28}$$

In this case, there are two phases: a crystal for low temperatures and a liquid for high temperatures. For a liquid, the equilibrium density is a constant, $\rho_0(\boldsymbol{r}) \equiv \rho$ whereas in the solid the density exhibits peaks on a regular lattice. The structure of the lattice at freezing depends on the "softness" of the repulsion: it is face centered cubic (fcc) for hard repulsions, i.e. for $\nu \gtrsim 6$, and body centered cubic (bcc) for soft cores ($\nu \lesssim 6$). Thus a *hard sphere* system, formally obtained from (28) by setting $\nu = \infty$, freezes into an fcc solid. The transition is strongly first order with $\eta_f = 0.49$ and $\eta_s = 0.54$ for the packing fractions of the coexisting fluid and solid phases [8]. On the other hand, a *one-component plasma* ($\nu = 1$) freezes isochorically into a bcc crystal if the dimensionless coupling parameter $\Gamma \equiv (4\pi\rho/3)^{1/3}\sigma V_0/k_B T$ equals 180 [9]. The lattice spacing and the width of the solid density peaks clearly depend on T and μ.

The softness of the *Yukawa potential* $\sim \exp(-\kappa(r-\sigma))/r$ depends on the screening parameter κ. For $\kappa = 0$, one recovers the OCP case whereas for large κ the repulsion becomes harder. Correspondingly, as a function of κ, the bulk phase diagram of the Yukawa system shows liquid, bcc and fcc solid phases. This result was confirmed by extensive computer simulations [10, 11].

The *Lennard-Jones* potential (16) has also an attractive tail. In this case, there are three phases, two of them with homogeneous density, namely the solid, liquid and gas phase. Most conveniently, the phase diagram is shown in the (P, T)-plane, where P denotes the pressure. There are three coexistence lines which meet at a *triple point*. Furthermore the liquid–gas coexistence line terminates at the *critical point*. This is schematically illustrated in fig. 1.7.

1.5.2. The structure of a given phase

The second question addresses the detailed structural properties of a given thermodynamic bulk phase. A basic static quantity is the *two particle probability density* $\rho^{(2)}(\boldsymbol{r},\boldsymbol{r}')$ that gives the joint

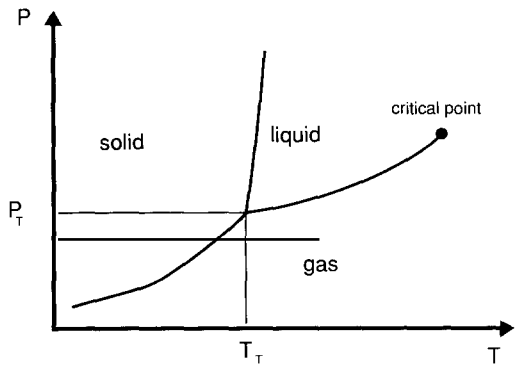

Fig. 1.7. Schematic phase diagram of a Lennard-Jones potential in the $P - T$ plane. There are three phases solid, liquid, gas meeting at the triple point (P_T, T_T). The gas–liquid coexistence line ends at the critical point.

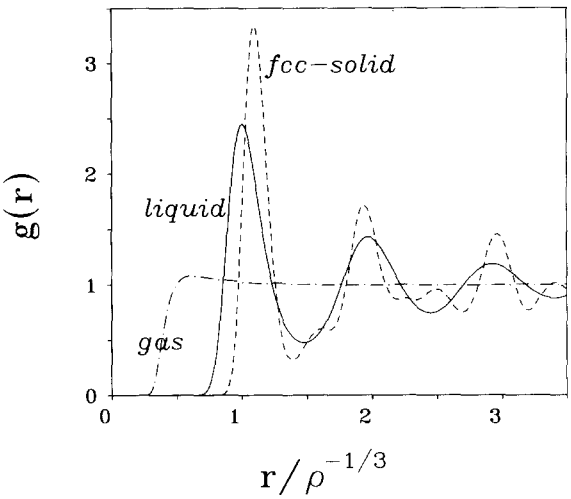

Fig. 1.8. Qualitative shape of the pair distribution function $g(r)$ for a dense liquid (solid line), a gas (dot-dashed line) and an fcc solid (dashed line). In the latter case, the spherical averaged pair distribution function is plotted. The peaks correspond to next and further nearest neighbour shells in the solid.

probability density to find a particle at position $\boldsymbol{r}$ and another particle at position $\boldsymbol{r}'$. It is naturally defined in the canonical ensemble as

$$\rho^{(2)}(\boldsymbol{r},\boldsymbol{r}') = \left\langle \sum_{i,j=1;i\neq j}^{N} \delta(\boldsymbol{r}-\boldsymbol{r}_i)\delta(\boldsymbol{r}'-\boldsymbol{r}_j) \right\rangle . \tag{29}$$

By normalization, the *pair distribution function* $g(\boldsymbol{r},\boldsymbol{r}')$ is defined as

$$g(\boldsymbol{r},\boldsymbol{r}') = \rho^{(2)}(\boldsymbol{r},\boldsymbol{r}')/\rho_0(\boldsymbol{r})\rho_0(\boldsymbol{r}'). \tag{30}$$

For a homogeneous phase with density $\rho_0(\boldsymbol{r}) = \rho$, $g(\boldsymbol{r},\boldsymbol{r}')$ is a function only of the separation $|\boldsymbol{r}-\boldsymbol{r}'|$ and (30) can be rewritten as

$$g(r) = \frac{1}{\rho}\left\langle \frac{1}{N} \sum_{i,j=1,i\neq j}^{N} \delta(\boldsymbol{r}-(\boldsymbol{r}_i-\boldsymbol{r}_j)) \right\rangle . \tag{31}$$

The pair distribution function plays a central role in the physics of liquids and solids. There are two main reasons for that. Firstly, the Fourier transform of the pair distribution function is measurable by scattering experiments. Secondly, for a homogeneous phase, thermodynamic properties of a fluid can be written as integrals over $g(r)$; so one can recover the free energies that determine the bulk phase diagram. A famous example is the virial expression for the pressure P

$$P = k_B T\rho\left(1 - \frac{2}{3}\frac{\pi\rho}{k_B T}\int_0^\infty \mathrm{d}r\, r^3 \frac{\mathrm{d}V}{\mathrm{d}r} g(r)\right). \tag{32}$$

Whereas $g(\boldsymbol{r},\boldsymbol{r}')$ shows long-ranged positional order in the solid phase, $g(r)$ decays to 1 for large r in a homogeneous phase. In a gas, $g(r) \approx exp(-V(r)/(k_BT))$ does not exhibit marked oscillations, but in a dense liquid it is strongly peaked around $r \approx \rho^{-1/3}$. There are also less pronounced second and higher order peaks at higher r which correspond to next and further nearest neighbour ordering in the liquid. In fig. 1.8, the qualitative different shape of $g(r)$ is shown for the gas, liquid and solid phase.

Another important quantity is the *direct correlation function* $c^{(2)}(\boldsymbol{r},\boldsymbol{r}')$ that is implicitly defined by the *Ornstein–Zernike* equation

$$h(\boldsymbol{r},\boldsymbol{r}') = c^{(2)}(\boldsymbol{r},\boldsymbol{r}') + \int \mathrm{d}^3 r''\, \rho_0(\boldsymbol{r}'')h(\boldsymbol{r},\boldsymbol{r}'')c^{(2)}(\boldsymbol{r}'',\boldsymbol{r}') \tag{33}$$

with

$$h(\boldsymbol{r},\boldsymbol{r}') = g(\boldsymbol{r},\boldsymbol{r}') - 1. \tag{34}$$

For a homogeneous system $c^{(2)}(\boldsymbol{r},\boldsymbol{r}')$ and $h(\boldsymbol{r},\boldsymbol{r}')$ only depend on $|\boldsymbol{r}-\boldsymbol{r}'|$ and the Ornstein–Zernike relation reduces to

$$h(r) = c^{(2)}(r) + \rho \int \mathrm{d}^3 r'\, h(r')c^{(2)}(|\boldsymbol{r}-\boldsymbol{r}'|). \tag{35}$$

This can be solved by Fourier transformation

$$\tilde{c}^{(2)}(k) = \int \mathrm{d}^3 r \exp(-\mathrm{i}\boldsymbol{k}\cdot\boldsymbol{r})c^{(2)}(r) \tag{36}$$

to express $\tilde{c}^{(2)}(k)$ by $\tilde{h}(k)$:

$$\tilde{c}^{(2)}(k) = \tilde{h}(k)/(1 + \rho\tilde{h}(k)) \tag{37}$$

$c^{(2)}(r)$ is typically negative for small r and approaches $-V(r)/k_BT$ for large r.

Finally, one can also define the static *structure factor* $S(k)$ by

$$S(k) = 1 + \rho\tilde{h}(k) \tag{38}$$

that is directly measured in scattering experiments. In a dense liquid, $S(k)$ has its main peak at $k \approx 2\pi\rho^{1/3}$ and is then oscillating and approaches 1 as $k \to \infty$. An example of $S(k)$ is shown in fig. 1.9.

So our second question is: How can one obtain structural properties embodied in the functions $g(r)$, $c^{(2)}(r)$, $S(k)$? Firstly, of course, there are experimental scattering techniques. Another possibility is provided by computer simulation. Thirdly, there are now well-established theories (mainly integral equations in the liquid state) to calculate $S(k)$ (or equivalently $c^{(2)}(r)$, $g(r)$) for a given pair potential $V(r)$. As an example, a very successfull theory for the structure of the hard sphere system is the *Percus–Yevick* closure [12, 13]. Combining the exact relation $g(r) = 0$ for $r < \sigma$ and the approximation $c^{(2)}(r) = 0$ for $r > \sigma$, one gets an explicit expression for the direct correlation function

$$c^{(2)}_{\mathrm{PY}}(r) = \begin{cases} 0 & \text{for } r \geq \sigma, \\ -\Lambda_1 + 6\eta\Lambda_2 r/\sigma - \frac{1}{2}\eta\Lambda_1(r/\sigma)^3 & \text{else} \end{cases} \tag{39}$$

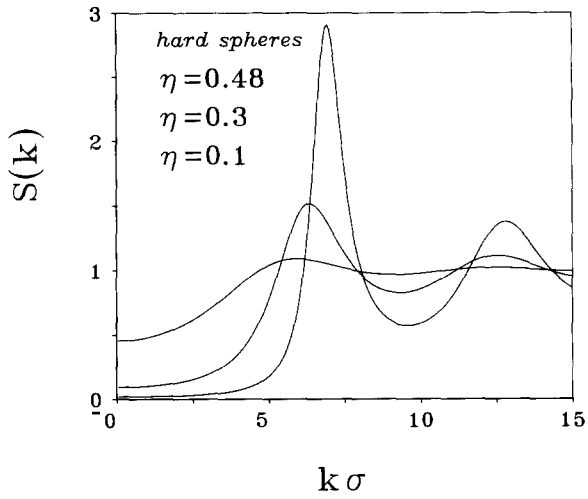

Fig. 1.9. Structure factor $S(k)$ versus $k\sigma$ within the Percus–Yevick approximation for a hard-sphere system. The results for three different packing fractions $\eta = 0.1$, 0.3,0.48 are given. The main peak increases for increasing packing fraction.

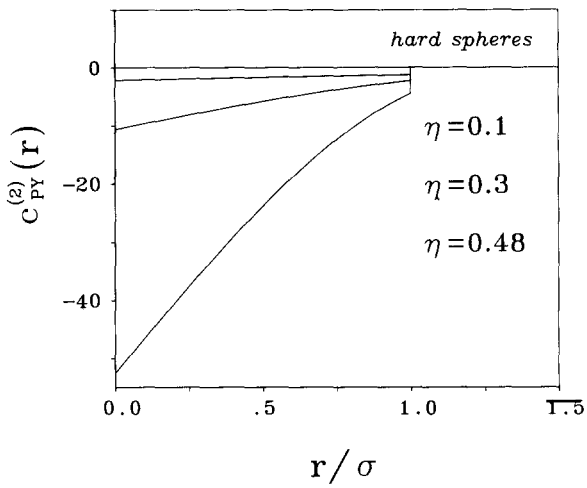

Fig. 1.10. Direct correlation function $c^{(2)}_{PY}(r)$ versus r/σ within the Percus–Yevick approximation for a hard-sphere system. The results for three different packing fractions $\eta = 0.1$, (upper curve) 0.3, and 0.48 (lowest curve) are given.

with $\Lambda_1 = (1 + 2\eta)^2/(1-\eta)^4$ and $\Lambda_2 = (1 + \frac{1}{2}\eta)^2/(1-\eta)^4$. Here, η is the packing fraction of the hard spheres, see (18), and σ is the hard-sphere diameter. This expression compares fairly well with computer simulations up to packing fractions $\eta \lesssim 0.3$. It is displayed in fig. 1.10 for three different packing fractions. An improved version for $c^{(2)}(r)$ was given in refs. [14, 15]. Also, the structure factor $S(k)$ of a hard sphere system was plotted within the Percus–Yevick approximation for three different packing fractions in fig. 1.9. One advantage of the Percus–Yevick approximation is that it can be solved also for a polydisperse hard-sphere fluid (24) [16, 17]). As expected, it turns out that the structure is smoothened out by polydispersity. This means, for instance, that the height of the main peak of the liquid structure factor decreases for increasing relative polydispersity. On the other hand, for a charge-polydisperse liquid, described by the Yukawa potential (27), much less is known compared to the size-polydisperse case. The so-called mean-sperical approximation can be handled analytically [18]. Recent attempts have focused on the applicability of more sophisticated liquid integral equations [19, 20] and on a mapping to a size-polydisperse reference system [21].

1.5.3. Dynamics; time-dependent correlation functions

Until now we have only considered static quantities, i.e. time-independent correlations. Obviously, one can also correlate quantities at different times provided the dynamics of the system are specified. In a classical *atomic* system the dynamics are just simply Newtonian and are called *Molecular Dynamics* (MD) which means that the particle trajectories in phase space obey Newton's coupled differential equations

$$\mathrm{d}\boldsymbol{r}_i/\mathrm{d}t = m^{-1}\boldsymbol{p}_i, \tag{40}$$

$$\mathrm{d}\boldsymbol{p}_i/\mathrm{d}t = \boldsymbol{F}_i, \tag{41}$$

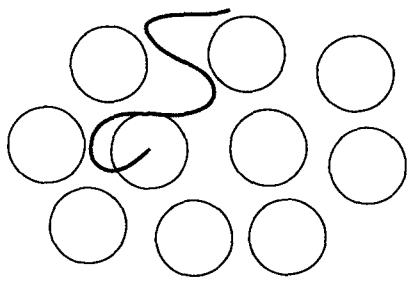

Fig. 1.11. Typical trajectory of a particle in a dense liquid for Molecular Dynamics. For a smooth pair potential, the trajectory is smooth and an analytical function of the time t.

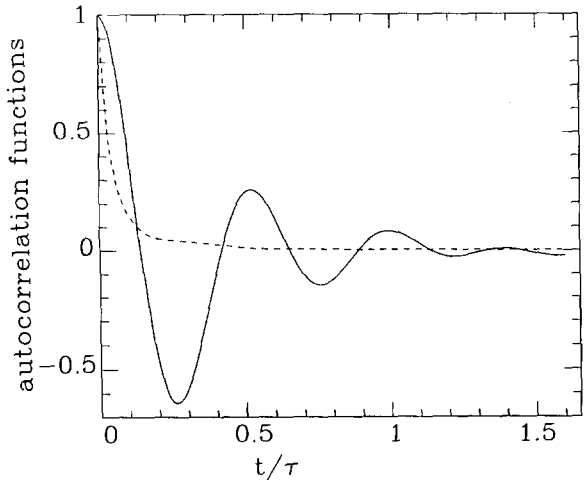

Fig. 1.12. Force autocorrelation function versus reduced time t/τ where τ is a characteristic relaxation time, for a Yukawa system. The solid curve is for Newtonian Dynamics and the dashed curve for Brownian Dynamics. Note that the shapes are completely different, although the same thermodynamic parameters and the same potential was used for both curves.

with the force

$$\boldsymbol{F}_i = -\frac{\partial}{\partial \boldsymbol{r}_i} V_{\text{tot}} = -\frac{\partial}{\partial \boldsymbol{r}_i}\left(\sum_{i \neq j} V(|\boldsymbol{r}_i - \boldsymbol{r}_j|) + V_{\text{ext}}(\boldsymbol{r}_i)\right). \tag{42}$$

A finite difference version of Newton's equations for the particle displacement is

$$\boldsymbol{r}_i(t + \Delta t) = \boldsymbol{r}_i(t) + \frac{1}{m}\boldsymbol{p}_i(t)\Delta t + \frac{\boldsymbol{F}_i(t)}{2m}\Delta t^2 + \mathrm{O}(\Delta t^3). \tag{43}$$

A typical particle trajectory in a dense liquid is sketched in fig. 1.11. In particular, it is a smooth, analytical function of time t if the interparticle potential and the external potential are smooth. The time-development of a general dynamical variable $A(t)$ depending on positions and momenta

$$A(t) = A(\{\boldsymbol{r}_i(t)\}, \{\boldsymbol{p}_i(t)\}) \tag{44}$$

is governed by the Liouville operator

$$\mathcal{L} = \sum_{j=1}^{N}\left(\frac{\mathrm{d}\boldsymbol{r}_j}{\mathrm{d}t} \cdot \frac{\partial}{\partial \boldsymbol{r}_j} + \frac{\mathrm{d}\boldsymbol{p}_j}{\mathrm{d}t} \cdot \frac{\partial}{\partial \boldsymbol{p}_j}\right) \tag{45}$$

and explicitly given by

$$A(t) = \exp(\mathcal{L}t)A(0). \tag{46}$$

We can construct an autocorrelation function associated to the dynamical variable A that correlates $A(t)$ with $A(0)$ by

$$C_A(t) \equiv \langle A(0)A(t)\rangle = \langle A(0)\exp(\mathcal{L}t)A(0)\rangle \tag{47}$$

where the average is now over the initial conditions $\{\boldsymbol{r}_i(0)\},\{\boldsymbol{p}_i(0)\}$. Due to the time inversion symmetry of Newton's equations, we get the short time expansion

$$C_A(t) = C_A(0) + \mathrm{O}(t^2). \tag{48}$$

Among physical interesting examples is the velocity autocorrelation function

$$Z(t) = \frac{1}{3k_\mathrm{B}Tm}\left\langle \frac{1}{N}\sum_{j=1}^{N}\boldsymbol{p}_j(0)\cdot\boldsymbol{p}_j(t)\right\rangle. \tag{49}$$

The value of $Z(t)$ at $t = 0$ is 1 which can be derived immediately from the equipartition theorem. In a solid, $Z(t)$ has long-lived oscillations associated with phonons. In a dense liquid, on the other hand, $Z(t)$ decays to zero for large times, but has an oscillatory behaviour on a time scale $\tau = \sqrt{m\sigma^2/k_\mathrm{B}T}$, where σ is a typical microscopic length scale. A second example is the force autocorrelation function that is just the second time derivative of $Z(t)$:

$$C_F(t) = \left\langle \frac{1}{N}\sum_{j=1}^{N}\boldsymbol{F}_j(0)\cdot\boldsymbol{F}_j(t)\right\rangle = -3k_\mathrm{B}Tm\frac{\mathrm{d}^2}{\mathrm{d}t^2}Z(t). \tag{50}$$

An example of the force autocorrelation in a dense liquid is plotted in fig. 1.12 (solid line). According to (50), it exhibits oscillations on the same time scale as the velocity autocorrelation function does.

Another important representative is the density autocorrelation in real space as well as in Fourier space. If we take $A(t)$ to be the density operator

$$A(t) = \sum_{j=1}^{N}\delta(\boldsymbol{r}-\boldsymbol{r}_j(t)) \tag{51}$$

we can define the general density autocorrelation function

$$C_\rho(t) \equiv C_\rho(\boldsymbol{r},\boldsymbol{r}',t) = \left\langle \sum_{i,j=1}^{N}\delta(\boldsymbol{r}-\boldsymbol{r}_j(0))\delta(\boldsymbol{r}'-\boldsymbol{r}_i(t))\right\rangle. \tag{52}$$

This can be splitted into a self (s) and distinct (d) part

$$C_\rho(\boldsymbol{r},\boldsymbol{r}',t) = C_\rho^{(\mathrm{s})}(\boldsymbol{r},\boldsymbol{r}',t) + C_\rho^{(\mathrm{d})}(\boldsymbol{r},\boldsymbol{r}',t), \tag{53}$$

$$C_\rho^{(\mathrm{s})}(\boldsymbol{r},\boldsymbol{r}',t) = \left\langle \sum_{j=1}^{N}\delta(\boldsymbol{r}-\boldsymbol{r}_j(0))\delta(\boldsymbol{r}'-\boldsymbol{r}_j(t))\right\rangle, \tag{54}$$

$$C_\rho^{(\mathrm{d})}(\boldsymbol{r},\boldsymbol{r}',t) = \left\langle \sum_{i,j=1;i\neq j}^{N}\delta(\boldsymbol{r}-\boldsymbol{r}_j(0))\delta(\boldsymbol{r}'-\boldsymbol{r}_i(t))\right\rangle. \tag{55}$$

$C_\rho^{(s)}(\boldsymbol{r},\boldsymbol{r}',t)$ (respectively $C_\rho^{(d)}(\boldsymbol{r},\boldsymbol{r}',t)$) give the joint probability density to find a particle at position $\boldsymbol{r}'$ after a time t and the same (respectively another) particle at position $\boldsymbol{r}$ for zero time. Obviously, for $t = 0$, the distinct part reduces to the static two particle distribution function $\rho^{(2)}(\boldsymbol{r},\boldsymbol{r}')$ as defined in the previous section.

By normalization, we obtain the *van Hove correlation function*

$$G(\boldsymbol{r},\boldsymbol{r}',t) = C_\rho(\boldsymbol{r},\boldsymbol{r}',t)/\rho_0(\boldsymbol{r})\rho_0(\boldsymbol{r}') \tag{56}$$

which also naturally splits into a self and distinct part

$$G(\boldsymbol{r},\boldsymbol{r}',t) = G_s(\boldsymbol{r},\boldsymbol{r}',t) + G_d(\boldsymbol{r},\boldsymbol{r}',t). \tag{57}$$

For a homogeneous phase, the distinct part of the van Hove correlation function is the time-dependent generalization of the pair distribution function $g(r)$

$$G_d(r,t) = \frac{1}{\rho N}\left\langle \sum_{i,j=1;i\neq j}^{N} \delta(\boldsymbol{r} - \boldsymbol{r}_i(0) + \boldsymbol{r}_j(t))\right\rangle. \tag{58}$$

Of course, $G_d(r,0) = g(r)$ and $\lim_{t\to\infty} G_d(r,t) = 1$ in a liquid, whereas the van Hove function has frozen-in components for large times in a solid. The self part simplifies for a homogeneous system correspondingly:

$$G_s(r,t) = \frac{1}{\rho N}\left\langle \sum_{j=1}^{N} \delta(\boldsymbol{r} - \boldsymbol{r}_j(0) + \boldsymbol{r}_j(t))\right\rangle. \tag{59}$$

For $t = 0$, we get $G_s(r,0) = \delta(\boldsymbol{r})/\rho$ and the long time limit is given by the hydrodynamic behaviour

$$G_s(r,t) \cong \rho^{-1}(4\pi D_L t)^{3/2}\exp(-r^2/4D_L t) \tag{60}$$

where

$$D_L = \lim_{t\to\infty}\left(\frac{1}{6t}\left\langle \sum_{j=1}^{N}\frac{1}{N}(\boldsymbol{r}_i(t) - \boldsymbol{r}_i(0))^2\right\rangle\right) \tag{61}$$

is the long time diffusion coefficient. Again, for a solid, D_L is extremely small, and there is a frozen structure for large times. The van Hove functions $G_s(r,t)$ and $G_d(r,t)$ play an important role as dynamical diagnostics of the kinetic glass transition in supercooled liquids.

Furthermore, one can take the Fourier transforms of $G_s(r,t)$ and $G_d(r,t)$ with respect to r to obtain the corresponding k-dependent structure factors $F_s(k,t)$, $F_d(k,t)$ which are defined as

$$F_s(k,t) = \frac{1}{\rho N}\sum_{j=1}^{N}\langle\exp[i\boldsymbol{k}\cdot(\boldsymbol{r}_j(t) - \boldsymbol{r}_j(0))]\rangle, \tag{62}$$

$$F_d(k,t) = \frac{1}{\rho N}\sum_{l,j=1;l\neq j}^{N}\langle\exp[i\boldsymbol{k}\cdot(\boldsymbol{r}_j(t) - \boldsymbol{r}_l(0))]\rangle. \tag{63}$$

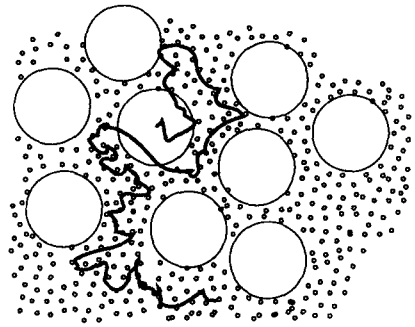

Fig. 1.13. Typical particle trajectory in a dense colloidal liquid with Brownian Dynamics. The solvent kicks the colloidal particle randomly on a time scale relevant for the big particles. Consequently, the trajectory is not smooth; there are no particle velocities. This is completely different to the Molecular Dynamics case (fig. 1.11).

It is clear that $F_d(k,0) = S(k)$, i.e. $F_d(k,t)$ equals the static structure factor for $t = 0$. Further Fourier transformation with respect to time t then leads to the dynamical structure factors $S_s(k,\omega)$, $S_d(k,\omega)$. The latter quantity is directly accessible in dynamical scattering experiments.

Mesoscopic *colloidal* systems, on the other hand, are embedded in a microscopic solvent and obey irreversible *Brownian Dynamics* (BD) on a time scale relevant for the mesoscopic particles, due to solvent friction. Consequently the velocities are not defined and do not occur as independent statistical variables; just the positions occur in the partition function integral. For given interparticle forces, the static properties are exactly the same for BD and MD, but the time dependence of the correlation functions is different.

The irreversible coupled equations of motion read

$$\xi \frac{d\boldsymbol{r}_i}{dt}(t) = \boldsymbol{F}_i(t) + \boldsymbol{R}(t) \tag{64}$$

where $\boldsymbol{R}$ denotes a Langevin random force and ξ the solvent friction coefficient.

In concentrated colloidal systems, *hydrodynamic forces* induced by the solvent are relevant. In principle, they could be approximately included by replacing ξ by a $3N \times 3N$ matrix depending parametrically on the positions $\{\boldsymbol{r}_i\}$ although the explicit form of this matrix is not known exactly. Hence, also for simplicity, we shall take ξ to be diagonal and constant in the following, which is a reasonable assumption for dilute suspensions.

Finite difference integration of equations (64) leads to the BD algorithm [22, 23]:

$$\boldsymbol{r}_i(t + \Delta t) = \boldsymbol{r}_i(t) + \xi^{-1}\boldsymbol{F}_i(t)\Delta t + (\Delta \boldsymbol{r})_R + O(\Delta t^2) \tag{65}$$

where the random displacement $(\Delta \boldsymbol{r})_R$ is sampled from a Gaussian distribution of zero mean, $\overline{(\Delta \boldsymbol{r})_R} = 0$, and variance $\overline{(\Delta \boldsymbol{r})_R^2} = 6k_B T \Delta t/\xi$. This should be contrasted with (43). A typical trajectory of a colloidal particle is visualized in fig. 1.13. Hence, also on a short time scale ("short" with respect to a typical time for the movement of the big colloidal particles) the motion is diffusive with the short-time diffusion constant:

$$D_0 = k_B T/\xi. \tag{66}$$

D_0 provides a natural scale to measure the long-time diffusion coefficient D_L defined by (61).

The time development of any dynamical variable

$$A(t) = A(\{\mathbf{r}_i(t)\}) \tag{67}$$

is now governed by the adjoint Smoluchowski operator

$$\tilde{O} = \sum_{j=1}^{N} \xi^{-1}[-\partial(H_{\text{ext}} + U)/\partial \mathbf{r}_j + k_B T \partial/\partial \mathbf{r}_j] \cdot \partial/\partial \mathbf{r}_j \tag{68}$$

and given by

$$A(t) = \exp(\tilde{O}t)A(0). \tag{69}$$

The short time expansion of an autocorrelation function

$$C_A(t) = \langle A(0)A(t)\rangle = \langle A(0)\exp(\tilde{O}t)A(0)\rangle \tag{70}$$

has now a linear term due to the irreversibility of solvent friction:

$$C_A(t) = C_A(0) + O(t) \tag{71}$$

which should be contrasted to the MD expansion (48). In fig. 1.12 the force auro-correlation function is shown for Newtonian and Brownian dynamics. Clearly their shape is completely different although the thermodynamic parameters are the same.

So our third question concerns the time dependence of correlation functions in a given bulk phase. This is of course more difficult than the corresponding question for the static structure since the dynamical quantities depend more sensitive on the microscopic interaction potential $V(r)$ and since the dynamics itself also depend on the physical nature of the system (atomic or colloidal).

Again information on the dynamics can be gained by three different methods: computer simulations with molecular dynamics or Brownian dynamics codes, dynamical scattering experiments, and theories. In theoretical approaches, one often starts from the Mori–Zwanzig projector formalism and constructs so-called mode coupling theories by which one arrives at a closed set of equations for the correlation functions. Here the static quantities serve as an input.

1.5.4. Interfaces between two coexisting bulk phases

Our fourth class of questions concerns interfacial problems. If the thermodynamic variables (e.g. temperature T and chemical potential μ) are such that two phases coexist, an equilibrium situation with an interface between these two phases is conceivable. The surface tension, the density profile, the structure and the role of fluctuations at such interfaces are the key quantities that are of interest here. The simplest example is the liquid–gas interface that was studied already in the last century by van der Waals [24], see ref. [25] for an extensive review. Solid–liquid or solid–gas interfaces are more complicated since their structure depends on the orientation of the solid phase.

Another interesting question concerns interfaces near the triple point where *three* phases (solid, liquid, gas, for a simple material) are in coexistence. If two phases A and B coexist and one moves along their coexistence line towards the triple point where the phase C also becomes thermodynamically stable as a bulk phase, one may think about *wetting*: the third phase may intervene between phases A and B, even when the triple point is not yet reached. The thickness l of the layer with phase C will be finite, depending on the distance to the triple point. *Complete wetting* is defined by a divergence of l as one moves to the triple point. For an extensive review of

wetting phenomena, see ref. [26]. An important example that will be pursued further in chapter 3 is *surface melting* where one moves on the sublimation line towards the triple point. The question here is whether there is a quasiliquid layer formation at the solid–gas interface.

A very much related situation is a phase in contact with an external wall, where one may examine interfacial phenomena at the wall like wetting, drying or wall-induced melting transitions.

Fluctuations are important in particular near the *critical point*; they also drive roughening transitions of interfaces. Here we shall consider exclusively first order phase transitions where fluctuations may be neglected. For a review on the role of interfacial fluctuations, we refer e.g. to ref. [27].

Again, computer simulations have given much insight into interfacial problems, but also powerful experimental techniques like X-ray and ion scattering, low energy electron diffraction (LEED) and other methods have been successfully applied to study interfaces, see ref. [28] for a recent review. Last but not least microscopic theories, mainly density functional theories, can be used to calculate the interfacial structure. An example will be given in the context of surface melting in chapter 4. One can also reduce these microscopic theories to a Ginzburg–Landau description that can then be considered as a phenomenological approach with few parameters that are determined microscopically. These simple square-gradient models have frequently been used to study qualitative features of interfaces with and without fluctuations. We shall give an example in chapter 4. A great advantage is that the qualitative features should be universal and therefore also be applicable to more complex systems. In the simplest setting, one considers a functional for the surface tension $\Sigma[m]$ of a dimensionless order parameter field $m(z)$, only depending on a surface normal coordinate z, where $m \equiv 0$ in the A and $m \equiv 1$ in the B phase:

$$\Sigma[m] = \int_{-\infty}^{\infty} \mathrm{d}z \, [\tfrac{1}{2} f_0 \zeta_m^2 \partial^2 m(z)/\partial z^2 + f(m(z))]. \tag{72}$$

Here ζ_m is a microscopic bulk correlation length, f_0 an energy density scale, and $f(m)$ denotes the bulk free energy density for a spatially constant order parameter. At AB coexistence, $f(m)$ has two minima at $m = 0, 1$ of equal depth. The mean field solution of a planar interfacial profile in z direction, is then obtained by the minimization

$$\delta\Sigma/\delta m = 0 \tag{73}$$

with the boundary conditions

$$\lim_{z\to\infty} m(z) = 0, \quad \lim_{z\to-\infty} m(z) = 1. \tag{74}$$

1.5.5. Dynamics of interfaces

Suppose that a phase A is present and the thermodynamic parameters are changed (e.g. by cooling) so that phase B is now thermodynamically stable as a bulk phase. A description of the temporal evolution of the conversion from phase A into phase B represents a formidable challenge to theory and experiments. Of course, this situation is at least one order of magnitude more complicated than the equilibrium case of the last section, since we are dealing now with a *nonequilibrium situation*. Normally one can distinguish between two stages: *nucleation* of phase B, taking place at inhomogeneities and forming small germs of phase B, and the subsequent *growth* of phase B. For long times, one frequently arrives at a *steady state* situation, i.e. the interface grows with a constant velocity v. Evidently the description of a steady state situation is easier than the nucleation process.

It is important whether the phases themselves are described by a conserved or non-conserved order parameter. Their dynamics clearly are different: a conserved order parameter has to obey a generalized continuity equation whereas a nonconserved order parameter can be created and annihilated arbitrarily. Consequently, growth is slower if a conserved order parameter is involved.

Physically important examples are crystal growth from the undercooled liquid, dynamics of wetting transitions and a dynamical creation of metastable phases. A full microscopic theory for all such phenomena is still missing, although there are some first attempts in dynamical extensions of density functional theories. One therefore restricts oneself to phenomenological Ginzburg–Landau models and studies simple model dynamics for conserved and nonconserved order parameters (Cahn–Hilliard respectively Ginzburg–Landau dynamics), see ref. [29] for a review. Explicitly, with the notation of the previous section, the dynamical evolution of a nonconserved order parameter profile $m(z,t)$ is governed by the equation

$$\partial m/\partial t = -\Gamma_n \delta\Sigma/\delta m \tag{75}$$

whereas the Cahn–Hilliard picture of a conserved order parameter is

$$\partial m/\partial t = \Gamma_c (\partial^2/\partial z^2)\delta\Sigma/\delta m. \tag{76}$$

Here, Γ_n and Γ_c are phenomenological kinetic coefficients that set the microscopic time scale and the functional Σ is taken from (72).

The growing and kinetics of an A–B interface provided phase B has been nucleated may be more complicated and non-steady-state if latent heat is produced as A is converted into B. This heat also has to diffuse away and can hinder the growth of the B phase. This is examined in more detail in chapter 6.

There are also lots of growth experiments in different setups and for different physical systems. Recently also detailed investigations of crystal growth in *colloidal suspensions* were performed, see e.g. refs. [30, 31]. Since here also powerful direct image technique are applicable, one can be optimistic that much more details of growth effects are experimentally accessible in near future. Computer simulations for nonequilibrium situations are much harder than equilibrium simulations but, in the last decade, interesting results on nucleation and growth have been obtained.

2. Criteria and theories for freezing and melting

2.1. Phenomenological criteria for freezing and melting

Although in general the melting and freezing transition is non-universal, there are some useful phenomenological criteria which are usually based on the properties of only one of the two coexisting phases. The advantages of these empirical rules is that they permit an estimation of the solid–liquid coexistence line avoiding any free energy calculation. Typically they predict quasi-universal values of certain static or dynamical quantities. By quasi-universal we mean that a quantity is not exactly constant but is close to a fixed number within $\approx 10\%$.

One has to distiguish between two kinds of universalities. First, one can vary the temperature for a given system with a fixed pair potential and study properties along the melting line of this material. By scaling properties of inverse power potentials, for instance, it becomes immediately clear that any dimensionless suitable scaled quantity is universal along the melting and freezing line. This first universality is thus trivial for inverse power potentials but less trivial for more complicated

(e.g. Lennard-Jones) potentials. The second more general universality holds if a property has the same value for freezing/melting even for different systems (with different pair potentials).

2.1.1. The Lindemann criterion of melting

A first phenomenological melting rule was put forward as early as 1910 by Lindemann [32, 33]. It states that the ratio L of the root-mean-square displacement and the average interparticle distance at the melting line of the solid has a universal value in the sense of the first weaker universality. More interesting is the question whether L is quasi-universal with respect to different potentials. This was a question of intense research during the last decade. In fact, by computer simulation, it turned out that the actual value of L depends a bit on the detailed form of the microscopic interaction. However, it always has the same order of magnitude of ≈ 0.15. For the extremely soft interaction of the classical OCP one gets $L = 0.185$ [34] at melting of the OCP bcc crystal. For a Yukawa potential, L was calculated by Meijer and Frenkel [11] and subsequently by Stephens and Robbins [35]. As a result, L is also close to 0.17. On the other hand, for the hard sphere fcc solid, L equals 0.129 at melting [36, 37]. Intuitively one can understand the Lindemann criterion as a breakdown of the ordered cage formed by neighbouring solid particles if the particle displacement exceeds a critical value which is one order of magnitude smaller than the mean distance to the neighbours. A generalization of the Lindemann rule was discussed by Ross [38].

2.1.2. The Hansen–Verlet freezing rule

A second criterion was formulated by Hansen and Verlet in 1969 [39]. For a Lennard-Jones liquid they found by computer simulation that the first maximum of the liquid structure factor $S(k)$ has a constant amplitude of ≈ 2.85 along the freezing line. It is thus universal with respect to the first kind of universality. Indeed it was confirmed by scattering experiments and by computer simulation of other than Lennard-Jones systems that the maximum of $S(k)$ is always close to 3 at freezing and that thus the Hansen–Verlet criterion is also universal in the more general sense. It shows that freezing sets in if the order in the liquid system, measured by the first maximum of $S(k)$, exceeds a certain quasi-universal value. Another criterion, working with the bridge function, was discussed by Rosenfeld [40].

2.1.3. Dynamical criterion for freezing in colloidal suspensions

It is tempting to look for quasi-universal *dynamical* quantities at the freezing and melting line. Since dynamical quantities depend much more sensitive on details of the microscopic interaction, it is clear that such quantities are much harder to obtain. Recently, a dynamical criterion was found by Löwen, Palberg and Simon [41] for Brownian dynamics: the ratio of the long-time self-diffusion coefficient, D_L, and the short-time self-diffusion constant, D_0, is very close to 0.1 along the freezing line of a colloidal liquid. This was confirmed both by Brownian dynamics computer simulations along the freezing line of a Yukawa liquid (including the OCP and the hard sphere case) and also by forced Rayleigh scattering experiments on charge-stabilized colloidal suspensions. The criterion is thus universal in the more general sense since it is valid for different pair potentials. It should be emphasized that this criterion is only valid for Brownian dynamics. In contrast, for Newtonian dynamics, a simple scale for the long-time self-diffusion is missing and consequently a dynamical criterion is only valid in the weak universality sense.

A theoretical justification of the dynamical freezing criterion is still missing and its relation to the static Hansen–Verlet criterion is not yet fully understood. Some simple theories for D_L/D_0 only involve k-integrals over a function of $S(k)$ [42–44]. Due to the universality of $S(k)$ at freezing [45]

the results for D_L/D_0 are practical the same for soft and hard spheres. Thus universality of D_L/D_0 at freezing follows in such theories but they typically strongly overestimate D_L/D_0. Another theoretical approach to D_L/D_0 is an Enskog theory which was discussed by Leegwater and Szamel [46]. This theory is superior to the simple ones from a theoretical point of view, since it incorporates the two-particle dynamics *exactly* and weightes the solution with the pair correlation function $g(r)$. The theories discussed before only sum up a part of the complete two-particle dynamics corresponding to two particles going apart and coming back only once. The Enskog theory gets reasonable values for D_L/D_0 for hard spheres, but underestimates D_L/D_0 strongly for soft repulsive potentials. This was shown recently in the context of Yukawa potentials by Löwen and Szamel [47]. Finally a modified Enskog approach, originally introduced by Cichocki [48], was investigated [47]. It yields good results for soft spheres but overestimates D_L/D_0 for hard spheres. Since the expressions for D_L/D_0 of both Enskog theories also involve the potential itself, they fail in predicting universality of D_L/D_0. Nonetheless their absolute results are closer to the results of computer simulation than that of the simple approaches.

At present the approximations involved in the dynamical theories remain somewhat uncontrolled for long times and have to be checked carefully by simulations. In conclusion, a theory which predicts a value of D_L/D_0 close to 0.1 at freezing *and* universality is still missing.

2.2. *Theories for freezing and melting*

There are two different theoretical approaches to bulk melting and freezing. The first starts from the liquid phase and the second from the solid phase. Still there are some difficulties in constructing a more general theory which includes properties from both, liquid and solid, phases although quite recently some first steps were made in this direction, see e.g. refs. [49, 50].

2.2.1. *Liquid-based theory*

In this kind of approach one uses the density functional formulation of classical statistical mechanics which is discussed in detail in the following chapter. Basically one uses properties of the uniform liquid phase, as the equation of state, static pair and triplet correlations, at any uniform density. With these inputs, one then constructs an approximate free energy density functional. The physically realized density minimizes the functional. Here the solid is parameterized by a periodic density ansatz on a regular lattice. Hence the long-ranged positional order of the solid is assumed and not an output of the theory. The key point is that the short range order in the solid is not very much different than that in the liquid at a suitable density. Consequently *freezing is viewed as a condensation of liquid density modes.* The first important output of the theory is the bulk phase diagram. For hard sphere and Lennard-Jones potentials the resulting phase diagrams are in good agreement with the simulational data. For soft potentials there are at the moment still some difficulties with the density functional approach. Also the structure of the solid, like its density distribution or its pair correlations are a further nontrivial output. Details of these properties, however, are not reproduced exactly [37].

Although the denisty functional approach has shed much more light on the microscopic points of the freezing process, the disadvantage of the approach is that the construction of the approximative functional is ad hoc and only the results justify the approximation. There is no unique recipe to construct a functional and thus the construction is arbitrary. Despite this criticism, the density functional approach is the best theory of freezing to date.

2.2.2. Crystal-based theory

The second approach is a crystal based theory where one starts from a crystal with defects. *Melting is viewed as an accumulation and unbinding of defects.* The melting point is identified with the situation where the free energy of dislocations cores assumes negative values. When this happens, dislocation cores are spontaneously created to fill the crystal to capacity, the crystal absorbs latent heat and loses its resistance against shear forces.

In two spatial dimensions, this concept was used by Kosterlitz and Thouless in 1973 [51] and further developed by Nelson and Halperin in 1980 (see e.g. ref. [52]). Thermally excited dislocation dipoles do indeed drive a phase transition from a dilute gas of dipole pairs to a plasma of unbound dislocations in which translational order is lost. This two-dimensional melting transition is continuous and predicts the existence of an intermediate hexatic phase with long-ranged orientational order, between the solid and liquid. In the absence of firm experimental evidence of this phase, however, there appears to be an unsolved issue with computer simulations that favor a first order transition, see ref. [53] for a review. Strictly speaking there is no solid phase with a long-ranged positional order in two dimensions, see the proof of Fröhlich and Pfister [54], which applies to any relevant pair potential except for hard-discs.

In three dimensions, there are some attempts to construct a dislocation theory of melting, see refs. [55, 56] and the textbook of Kleinert [57]. The topology of defects is more complicated in 3D than in 2D [58], and thus the theory is more difficult in 3D. Also computer simulations of defect generation in superheated solids were performed to support the picture of dislocation generation [59]. Recently, Lund [60] re-examined the instability driven by dislocation loops in three dimensions and found that the solid shear modulus vanishes as a power law of the temperature distance to the instability with exponent ≈ 0.5. In his analysis, the 3D dislocation-mediated melting is achieved without a sudden proliferation of unbound dislocation loops in contrast to the simpler earlier calculations.

The main critique for these kind of approach is that the melting transition in three dimensions is first order. At the melting point, the shear modulus is finite and the defect concentration small. It becomes thus clear that the defect generation cannot be the physical mechanism for bulk melting. In contrast, experimental observations as well as theoretical studies show that melting is not initiated by dislocations but by the crystalline *surface.* It is via the surface which is a natural defect in the solid order that disorder sets in. This important mechanism which is extensively discussed in chapter 4 already shows up well below the bulk melting temperature. Despite this fact a solid can, under suitable conditions e.g. by coating it with another material, be overheated and finally loses its stability due to spontaneous defect generation. All theories based on dislocation generation thus do not decribe the bulk melting transition but may be applicable to an superheated crystal.

3. Density functional theory

The fundamental microscopic tool for calculating melting and freezing is the classical density functional theory. We discuss concrete approximations of the functional and explain how phase diagrams are obtained for hard spheres and other given pair potentials. We also mention applications of density functional theory to interfaces and related topics.

3.1. Fundamental aspects

Adopting the notation of section 1.1, we consider a grandcanonical free energy functional $\overline{\Omega}(T, \mu, [w])$ of distribution functions w depending on the number N of particles and on the positions and momenta of those particles:

$$\overline{\Omega}(T, \mu, [w]) = \mathrm{Tr}\{w(H_N - \mu N + k_B T \ln w)\}. \tag{77}$$

$\overline{\Omega}(T, \mu, [w])$ also depends parametrically on the grandcanonical thermodynamic parameters, temperature T and chemical potential μ. All distribution functions are subject to the normalization constraint

$$\mathrm{Tr}\{w\} = 1. \tag{78}$$

The equilibrium distribution function w_0 of the grandcanonical ensemble is given by

$$w_0 = \Xi^{-1} \exp(-(H_N - \mu N)/k_B T) \tag{79}$$

which is the grandcanonical extension of w_N, see eq. (6). If one evaluates the functional $\overline{\Omega}$ at w_0, one finds that it equals the real equilibrium grandcanonical free energy

$$\overline{\Omega}(T, \mu, [w_0]) = \Omega(T, \mu). \tag{80}$$

If it is evaluated at some other distribution function $w \neq w_0$, one gets via the Gibbs-inequality [61] (or the *convexity* of the logarithmic function)

$$\overline{\Omega}(T, \mu, [w]) - \overline{\Omega}(T, \mu, [w_0]) = k_B T\{\mathrm{Tr}(w \ln w) - \mathrm{Tr}(w \ln w_0)\} > 0. \tag{81}$$

For a fixed interaction potential $V(r)$, the distribution function w_0 is determined entirely by the external potential $V_{\mathrm{ext}}(\boldsymbol{r})$. One can show [62] that $V_{\mathrm{ext}}(\boldsymbol{r})$ is uniquely determined by the equilibrium density $\rho_0(\boldsymbol{r})$. This then implies the important result that w_0 is a functional of $\rho_0(\boldsymbol{r})$ which we call $w_0[\rho_0]$. Chayes and Chayes [63] have proved that *any* positive density $\rho(\boldsymbol{r})$ can be viewed as an equilibrium density for a system in a suitable external potential $V_{\mathrm{ext}}(\boldsymbol{r})$. Consequently,

$$\mathcal{F}(T, [\rho]) = \mathrm{Tr}\{w_0[\rho](H_{\mathrm{kin}} + U + k_B T \ln w_0[\rho])\} \tag{82}$$

is a well-defined functional of $\rho(\boldsymbol{r})$. We can construct one further functional by the extension

$$\Omega(T, \mu, [\rho]) = \mathcal{F}(T, [\rho]) + \int \mathrm{d}^3 r\, \rho(\boldsymbol{r}) V_{\mathrm{ext}}(\boldsymbol{r}) - \mu \int \mathrm{d}^3 r\, \rho(\boldsymbol{r}). \tag{83}$$

If one takes this functional at the equilibrium density, one gets the equilibrium grandcanonical free energy

$$\Omega(T, \mu, [\rho_0(\boldsymbol{r})]) = \Omega(T, \mu). \tag{84}$$

Next, one can show that Ω is minimized at $\rho(\boldsymbol{r}) = \rho_0(\boldsymbol{r})$, which follows directly from the fact that $\overline{\Omega}$ is minimal at $w = w_0$. Thus the equilibrium density minimizes the functional $\Omega(T, \mu, [\rho])$ and it follows

$$\delta\Omega(T, \mu, [\rho])/\delta\rho|_{\rho=\rho_0(\boldsymbol{r})} = 0. \tag{85}$$

Equations (84) and (85) constitute the basic *variational principle*: there exists a unique functional $\Omega(T, \mu, [\rho])$ which becomes minimal for the equilibrium density $\rho_0(\boldsymbol{r})$ and then equals the real grandcanonical free energy.

Let us now discuss the implications of this variational principle: first, consider an external potential $V_{\text{ext}}(\boldsymbol{r})$ which breaks any symmetry and is strong enough to avoid any two phase region. In this case, there is a unique minimum of the functional which corresponds to the one-particle density realized experimentally. In particular, all fluctuations from the thermodynamic average are taken into account *exactly* provided one knows the exact functional.

If the external potential is zero, the minimizing equilibrium density defined via (11) is homogeneous but it is not necessarily a "laboratory" density since it can be an average over a set of possible densities which are experimentally realizable. To see this, consider a point in the phase diagram where the solid is stable. Then the equilibrium density $\rho_0(\boldsymbol{r})$, as defined in (11), is homogeneous. It can be thought of as a superposition of solid density realizations with peaks on a periodic crystal lattice. Different realizations just differ by a translation in real space. A fundamental problem is how to decompose the homogeneous equilibrium density uniquely into experimentally realized densities and how to do a reduced thermodynamical average around a "laboratory" density. Closely connected to this problem is the proper incorporation of all experimentally realized fluctuations. One possible strategy to get a "laboratory" density for $V_{\text{ext}}(\boldsymbol{r}) = 0$ is to switch on a small symmetry breaking potential $V_{\text{ext}}(\boldsymbol{r})$, calculate the equilibrium density and then take the limit $V_{\text{ext}}(\boldsymbol{r}) \to 0$. But even here, it remains obscure which fluctuations are properly accounted for. For example, one can get a realization of a *solid* density by this procedure, but one does not know whether all fluctuations in the solid state like defects, dislocations etc. are incorporated properly into the density.

For a *practical* calculation, the usual procedure is as follows: first, the functional is not known exactly, so one is forced to make an *approximation* for the functional. Next, one makes a density ansatz which corresponds to an experimentally realizable density (for example: peaks on a fixed crystalline lattice to characterize the solid). Third, one normally does *not* perform a calculation explicitly with a symmetry-breaking external potential. If, for a given T and μ, there are two solutions with equal grand canonical free energy, one interprets this as the coexistence of the two realizable densities. Using this strategy, it is unclear which fluctuations are accounted for; one ends up with a picture which is a *mean-field*-like description of a statistical mechanics system. Nevertheless, on this mean-field level, density functional theory remains a useful tool to study phase transitions, in particular the freezing transition: One gets an approximation of the free energy for the solid and the liquid which can be used to calculate the bulk phase diagram.

Before we describe concrete approximation schemes for the functional in the next section, let us introduce some further useful relations.

(a) For the noninteracting case (the ideal gas), $V(r) = 0$ and one knows $\mathcal{F}(T, [\rho])$ exactly

$$\mathcal{F}(T, [\rho]) \equiv \mathcal{F}_{\text{id}}(T, [\rho]) = k_{\text{B}}T \int \mathrm{d}^3 r\, \rho(\boldsymbol{r}) [\ln(\Lambda^3 \rho(\boldsymbol{r})) - 1] \tag{86}$$

where Λ is the thermal wavelength, see (1). Minimization of $\Omega(T, \mu, [\rho])$ then immediately leads to the generalized barometric expression for the equilibrium density of an ideal gas in an external potential:

$$\rho_0(\boldsymbol{r}) = \Lambda^{-3} \exp[-(V_{\text{ext}}(\boldsymbol{r}) - \mu)/k_{\text{B}}T]. \tag{87}$$

(b) For the general interacting case, it is convenient to introduce the separation

$$\mathcal{F}(T, [\rho]) = \mathcal{F}_{\text{id}}(T, [\rho]) + \mathcal{F}_{\text{excess}}(T, [\rho]) \tag{88}$$

which is just a definition of $\mathcal{F}_{\text{excess}}(T,[\rho])$. In general, $\mathcal{F}_{\text{excess}}(T,[\rho])$ is not known. One can, however, prove that the direct correlation function, introduced in section 1.3.2, can be obtained from $\mathcal{F}_{\text{excess}}(T,[\rho])$ by

$$c^{(2)}(\boldsymbol{r},\boldsymbol{r}') \equiv c^{(2)}(\boldsymbol{r},\boldsymbol{r}',[\rho_0(\boldsymbol{r})]) = -\frac{1}{k_B T}\frac{\delta^2 \mathcal{F}_{\text{excess}}}{\delta\rho(\boldsymbol{r})\delta\rho(\boldsymbol{r}')}\bigg|_{\rho=\rho_0(\boldsymbol{r})}. \tag{89}$$

For an arbitrary density, this relation can directly be generalized by taking the derivative at this arbitrary density to define a functional $c^{(2)}(\boldsymbol{r},\boldsymbol{r}',[\rho])$. Integrating this twice in density space leads to the exact relation [25]

$$\mathcal{F}_{\text{excess}}(T,[\rho]) = k_B T \int_0^1 \mathrm{d}\alpha\ (\alpha-1)\int \mathrm{d}^3 r \int \mathrm{d}^3 r'\ c^{(2)}(\boldsymbol{r},\boldsymbol{r}',[\alpha\rho])\rho(\boldsymbol{r})\rho(\boldsymbol{r}') \tag{90}$$

which forms the basis for different approximations.

3.2. *Approximations for the density functional*

The simplest approximation is the *local density approximation* (LDA)

$$\mathcal{F}_{\text{excess}}(T,[\rho]) = \int \mathrm{d}^3 r\, f_{\text{excess}}(T,\rho(\boldsymbol{r})) \tag{91}$$

where $f_{\text{excess}}(T,\rho)$ is the excess free energy density of a homogeneous system with density ρ at temperature T. Henceforth we assume that this homogeneous state exists and is thermodynamically stable. In the LDA, the direct correlation function is just approximated (see (89)) by a δ-peak

$$c^{(2)}(\boldsymbol{r},\boldsymbol{r}'[\rho]) = -\frac{1}{k_B T}\frac{\partial^2 f_{\text{excess}}(T,\rho(\boldsymbol{r}))}{\partial\rho^2}\delta(\boldsymbol{r}-\boldsymbol{r}'). \tag{92}$$

So, LDA can only be used for weak inhomogeneities.

The local density approximation can be improved by adding a nonlocal mean-field energy, quadratic in the density, as follows:

$$\mathcal{F}_{\text{excess}}(T,[\rho]) = \int \mathrm{d}^3 r\,[f_{\text{excess}}(T,\rho(\boldsymbol{r})) - \tfrac{1}{2}V_0\rho^2(\boldsymbol{r})] + \frac{1}{2}\int \mathrm{d}^3 r \int \mathrm{d}^3 r'\ V(|\boldsymbol{r}-\boldsymbol{r}'|)\rho(\boldsymbol{r})\rho(\boldsymbol{r}') \tag{93}$$

with V_0 being the zeroth moment of the interparticle potential $V(r)$

$$V_0 = \int \mathrm{d}^3 r\, V(r) \tag{94}$$

which we have assumed to exist. The approximation (93) can be called *LDA plus mean-field approximation.* In this approach, the corresponding direct correlation function is approximated by

$$c^{(2)}(\boldsymbol{r},\boldsymbol{r}'[\rho]) = -\frac{1}{k_B T}\left[\left(\frac{\partial^2 f_{\text{excess}}(T,\rho(\boldsymbol{r}))}{\partial\rho^2} - \frac{V_0}{2}\right)\delta(\boldsymbol{r}-\boldsymbol{r}') + V(|\boldsymbol{r}-\boldsymbol{r}'|)\right]. \tag{95}$$

The LDA plus mean-field approximation is generally applicable to inhomogeneous liquids, but not to very inhomogeneous situations like packing effects in a dense liquid at an external wall or freezing.

In 1979, Ramakrishnan and Yussouff [64] proposed the first functional that describes freezing. This was also reformulated in familiar density functional language in 1981 by Haymet and Oxtoby [65]. It consists of a Taylor expansion up to second order around a homogeneous system with a *fixed* liquid reference density $\rho(\boldsymbol{r}) \equiv \overline{\rho}$:

$$\mathcal{F}_{\text{excess}}(T,[\rho]) = F_0 + \int \mathrm{d}^3 r \left.\frac{\delta \mathcal{F}_{\text{excess}}(T,[\rho])}{\delta \rho(\boldsymbol{r})}\right|_{\rho(\boldsymbol{r})\equiv\overline{\rho}} [\rho(\boldsymbol{r}) - \overline{\rho}]$$

$$+ \frac{1}{2}\int \mathrm{d}^3 r \int \mathrm{d}^3 r' \left.\frac{\delta^2 \mathcal{F}_{\text{excess}}(T,[\rho])}{\delta\rho(\boldsymbol{r})\delta\rho(\boldsymbol{r}')}\right|_{\rho(\boldsymbol{r})\equiv\overline{\rho}} [\rho(\boldsymbol{r}) - \overline{\rho}][\rho(\boldsymbol{r}') - \overline{\rho}]. \tag{96}$$

Constants like F_0 are irrelevant for the minimizing density and the term linear in $\rho(\boldsymbol{r})$ only renormalizes the chemical potential μ. So the relevant term is the quadratic one whose kernel is essentially the direct correlation function $c^{(2)}(|\boldsymbol{r}-\boldsymbol{r}'|,\rho)$ for a homogeneous system, see eq. (89). Thus the corresponding direct correlation function is incorporated *exactly*, but only for one single liquid reference state, and higher-than-second-order direct correlations do vanish in this approach. The Ramakrishnan–Yussouff functional can be systematically improved by extending the expansion in (96) to the third term and using liquid state theory [66] for the triplet direct correlation function, see e.g. ref. [67].

A better but more complicated functional is constructed in such a way that it reproduces the direct correlation function for *any* density in the homogeneous limit. In particular, a so-called *weighted density approximation* (WDA) has been proposed by Tarazona [68] and Curtin and Ashcroft [69]. Here one chooses

$$\mathcal{F}_{\text{excess}}(T,[\rho]) = \int \mathrm{d}^3 r\, \rho(\boldsymbol{r}) \Psi(T, \bar{\rho}(\boldsymbol{r})) \tag{97}$$

where $\Psi(T,\rho)$ is the excess free energy per particle in the homogeneous case (used as an input), and the weighted density is given implicitly by

$$\bar{\rho}(\boldsymbol{r}) = \int \mathrm{d}^3 r\, \bar{w}(|\boldsymbol{r}-\boldsymbol{r}'|, \bar{\rho}(\boldsymbol{r}))\rho(\boldsymbol{r}'). \tag{98}$$

The weight function $\bar{w}(r,\rho)$ is normalized and chosen in such a way that the second functional derivative equals the direct correlation function for any homogeneous density. In this approach, one systematically includes all informations from the liquid state, i.e. $f_{\text{excess}}(T,\rho) \equiv \rho\Psi(T,\rho)$ and $c^{(2)}(|\boldsymbol{r}-\boldsymbol{r}'|,\rho)$. Also this density functional yields freezing, so we have developed a theory of freezing based on the liquid state. The higher-than-second-order direct correlations are non-zero in general and, for certain geometries, agree in principle with computer simulation data [66, 70–73]. Although it has several inconsistencies and shortcomings, the WDA functional seems to be the best generally applicable functional that is known so far, at least for hard sphere systems.

Another functional, called *modified weighted density approximation* (MWDA) was introduced by Denton and Ashcroft [74]. It is computationally much simpler than the original WDA but has the same underlying philosophy. However, it is not written in a local form and therefore not directly applicable to interfacial situations. Here, one approximates

$$\mathcal{F}_{\text{excess}}(T,[\rho]) = N\Psi(T,\hat{\rho}) \tag{99}$$

with a *scalar* density $\hat{\rho}$ given by the implicit relation

$$\hat{\rho} = \frac{1}{N} \int d^3r \int d^3r' \, \rho(\boldsymbol{r}) \rho(\boldsymbol{r}') \hat{w}(|\boldsymbol{r} - \boldsymbol{r}'|, \hat{\rho}). \tag{100}$$

The weight function $\hat{w}(r, \rho)$ is normalized and $c^{(2)}(r, \rho)$ is reproduced for any homogeneous density. There is also an attempt to combine both approaches, MWDA and WDA, and construct a hybrid weighted density approximation (HWDA) by Leidl and Wagner [75]. In the context of hard-sphere systems, the MWDA and WDA are inconsistent since they admit densities with overlapping hard spheres [76, 77]. A modification of the MWDA that produces a consistent functional was proposed by Ohnesorge et al. [78].

There have been many other approximations discussed in the literature, often constructed for special applications and special systems (like hard spheres or OCP-freezing), for a review see refs. [79, 80]. Simpler variants of the WDA with an explicit form for the weight function were examined by Tarazona [81]. We also mention different kinds of effective liquid approximations by Baus and coworkers [82–85] and Lutsko [86], the variants of Meister and Kroll [87], Igloi and Hafner [88], Groot and van der Eerden [89], and other related forms [90–99].

There are also some fundamentally different approaches using only thermodynamic properties of the *solid* as an input for the functional [49, 50]. Then the liquid structure is predicted from the solid side, i.e. one has a solid-based theory of melting.

3.3. Calculation of bulk phase diagrams

If the concrete form of the functional $\Omega(T, \mu, [\rho])$ has been chosen the next step is to find a suitable parameterization for the density $\rho(\boldsymbol{r})$ with some variational parameters. The energy of the homogeneous phase is easily obtained by plugging a constant $\rho(\boldsymbol{r}) \equiv \rho$ into the functional $\Omega(T, \mu, [\rho])$ and minimize with respect to ρ. For a solid, the parameterization most frequently employed are Gaussian peaks with a variable width α on a fixed solid lattice. The solid lattice is described by the lattice vectors $\{\boldsymbol{R}_n\}$, with one particle per lattice site:

$$\rho(\boldsymbol{r}) = \left(\frac{\alpha}{\pi}\right)^{3/2} \sum_{\boldsymbol{R}_n} \exp[-\alpha(\boldsymbol{r} - \boldsymbol{R}_n)^2]. \tag{101}$$

The lattice structure is an input (normally the lattice constant is varied, too), but in principle one can try with different lattice types and take that with the lowest free energy; also one can vary with respect to the form of the [100]. Parameterizations going beyond the Gaussian parameterization (101) [101, 76, 102, 37] indeed reveal that the corrections are very small. The parameter α plays the role of an *crystalline order parameter*. It is zero in the liquid phase and nonzero in the solid phase indicating long-range crystalline order.

In order to get the bulk phase, one looks at which T and μ the functional $\Omega(T, \mu, [\rho])$ has two equal minima. This means that two phases with same temperature T, chemical potential μ and pressure $P = -\Omega/V$ do coexist.

In the following, we shall discuss the success of density functional theory in describing freezing for different potentials, namely for hard and soft spheres, Yukawa and Lennard-Jones interactions.

3.3.1. Hard spheres

The hard-sphere system represents the simplest nontrivial liquid with a freezing transition, and is thus the prototyp of a model where theories and simulations of freezing can directly be compared. In

fact, it is for this system that density functional theory has had its most notable success. The liquid correlations, used as an input for density functional theory, are well known, see e.g. the Percus–Yevick expression (39). The Ramakrishnan–Yussouff as well as WDA, MWDA-type functionals all yield a freezing transition with coexisting densities that are in pretty good agreement with the simulation data, for a review see refs. [103, 79]. This success motivates a hard-sphere perturbation theory for other potentials. However, details of the solid phase deviate from simulational data; for example the Lindemann-parameter of the solid at coexistence turns out to be too small, and the direct correlation function in the solid is inconsistent within the MWDA [78].

3.3.2. *Soft cores*

Much effort was put into the challenge to find a functional that describes freezing of the OCP into a bcc crystal [104–106, 67, 107–109]. An MWDA-type approximation was proposed recently by Likos et al, 1992 [110]. It turns out that higher-than-second-order direct correlations, at least liquid triplet correlations, should be incorporated into the functional. Furthermore, the free energy difference between a bcc lattice and a fcc or hcp lattice is tiny; so this difference will sensitively depend on details of the approximations used.

Freezing of soft cores, described by a general inverse power law in r, see (28), was examined by Barrat and coworkers [111, 112], see also refs. [113, 114]. The usual schemes (like the WDA or the MWDA) do fail for soft cores. A hard sphere perturbation theory, performed by Lutsko and Baus [115], on the other hand, gives good results compared to the simulation data.

3.3.3. *Yukawa systems*

Kesavamoorthy et al. [116] applied the Ramakrishnan–Yussouff theory of freezing to Yukawa systems, described by the potential (19). Also, the MWDA was applied to Yukawa systems by Laird and Kroll [114]. For high screening, i.e. large κ, the potential is pretty hard and good agreement of the density functional and simulational data was obtained. For small κ, of course, one gets the same failure as for soft core potentials, discussed in the previous paragraph. The bcc–fcc coexistence was studied with the Ramakrishnan–Yussouff density functional by Sengupta and Sood [117]. There was also a study for a Yukawa plus hard core potential by Kloczkowski and Samborski [118].

3.3.4. *Lennard-Jones potentials*

The Lennard-Jones potential (16) exhibits three different phases and density functional theory has been successfully applied using both Ramakrishnan–Yussouff [120, 102] and other schemes [112]. A quantitative agreement with the simulational phase diagram was also obtained by using a hard sphere reference system and hard sphere perturbation theory. This was both performed for the WDA by Curtin and Ashcroft, 1986 [121], and for the MWDA with its consistent formulation by Ohnesorge et al [78]. The latter result is shown as a T–ρ diagram in fig. 3.1. In fact, in this figure, a short-ranged fit for the Lennard-Jones potential is used and compared with the simulation data of a short ranged cutoff Lennard-Jones potential. The quantitative agreement of the microscopic density functional theory is really convincing. Thus this theory can be used as a starting point for an interfacial study near the triple point.

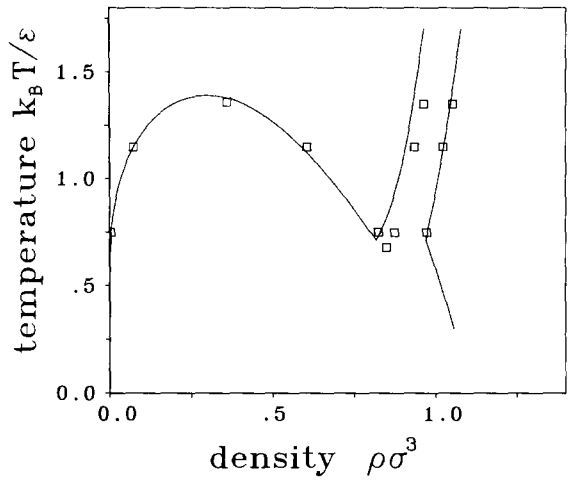

Fig. 3.1. Bulk phase diagram for a Lennard Jones system without long ranged potential tail. Squares denote simulation data from refs. [119, 39], for a truncated Lennard-Jones potential. From ref. [78].

3.4. *Density functional theory of interfaces*

3.4.1. *Direct minimization*

The ideal procedure for a calculation of a density profile and the surface tension for a planar interface would be a free minimization of the density functional $\Omega(T, \mu, [\rho])$ where one of the coexisting phase (A) is on the left and the other (B) is on the right side. Of course for complicated e.g. WDA-type functionals this is a very hard numerical problem. The first promising attempts of a free minimization were made using the simulated annealing method in order to find the minimum in a very high-dimensional (of the order one million) parameter space by Ohnesorge et al. [37]. A concrete calculation for the solid–liquid interface was done by Curtin within the original WDA both for hard sphere systems [122], and a Lennard-Jones potential [123]. But here only two variational parameters were taken to determine the interfacial profile. Another successful calculation of the hard-sphere and Lennard-Jones solid–liquid interface was recently performed by Marr and Gast [124]. They used a laterally averaged density and a planar weigthed density approximation for the density functional.

We add a final remark concerning interfacial fluctuations. As we discussed in section 3.1, it is not clear how they are contained in the density functional solution. In this aspect, density functional theory remains a "mean-field-type" description.

3.4.2. *Gradient expansion, Landau and van der Waals theories*

Let us consider a multicomponent order parameter $\boldsymbol{m} = (m_1, m_2, \ldots, m_N)$ parameterizing the density

$$\rho(\boldsymbol{r}) = \rho(\boldsymbol{m}, \boldsymbol{r}). \tag{102}$$

A concrete choice is the mean density for m_1 and for m_i, $i > 1$, the Fourier coefficients of the density on a fixed solid lattice. Then one can define a bulk grandcanonical free energy density $f(\boldsymbol{m})$ by

$$f(\boldsymbol{m}) \equiv \Omega(T, \mu, [\rho(\boldsymbol{m}, \boldsymbol{r})])/V. \tag{103}$$

At coexistence of two phases A and B, $f(\boldsymbol{m})$ has two equal minima at $\boldsymbol{m}_A$ and $\boldsymbol{m}_B$, the order parameters describing the two bulk phases. If the perpendicular coordinate of a planar interface between A and B is denoted by z, we can parameterize the density by a z-dependent set of order parameters $\rho(\boldsymbol{r}) = \rho(\boldsymbol{m}(z), \boldsymbol{r})$. As long as the order parameters vary slowly with respect to a microscopic length scale, a gradient expansion up to second order in the order parameters is justified. This approximation has frequently been employed in the literature for various applications, see e.g. refs. [65, 125–128]. The most general and systematic derivation was given by Löwen et al. [129, 130]. The final result for the interfacial grandcanonical free energy per area A, alias the surface tension $\Sigma = \Omega/A$, is

$$\Sigma[\boldsymbol{m}] = \int_{-\infty}^{\infty} \mathrm{d}z \left(\frac{1}{2} \sum_{i,j=1}^{N} g_{ij}(\boldsymbol{m}(z)) \frac{\partial m_i}{\partial z} \frac{\partial m_j}{\partial z} + f(\boldsymbol{m}(z)) \right) \tag{104}$$

with the matrix

$$g_{ij}(\boldsymbol{m}) = -\frac{1}{2V} \int \mathrm{d}^3 r \int \mathrm{d}^3 r' \, (z - z')^2 c^{(2)}(\boldsymbol{r}, \boldsymbol{r}', [\rho(\boldsymbol{m}, \boldsymbol{r})]) \frac{\partial \rho(\boldsymbol{m}, \boldsymbol{r})}{\partial m_i} \frac{\partial \rho(\boldsymbol{m}, \boldsymbol{r}')}{\partial m_j} \tag{105}$$

where $c^{(2)}(\boldsymbol{r}, \boldsymbol{r}', [\rho])$ is given by (89). This expansion is valid for short ranged interparticle potentials $V(r)$; if $V(r)$ is long ranged, $g_{ij}(\boldsymbol{m})$ does not exist since $c^{(2)}(\boldsymbol{r}, \boldsymbol{r}', [\rho]) \sim V(|\boldsymbol{r} - \boldsymbol{r}'|)$ for large $|\boldsymbol{r} - \boldsymbol{r}'|$) in the liquid phase. In this case, one separates

$$V(r) = V_s(r) + V_\ell(r) \tag{106}$$

where $V_s(r)$ is short ranged and $V_\ell(r)$ is a slowly varying long ranged tail. Then, one treats $V_\ell(r)$ in mean-field fashion and does the square gradient expansion only for the short-ranged part. One arrives at (104) where one has to add a long ranged term $\mathcal{F}_\ell$ to $\Sigma[m]$. If m_1 is the mean density and m_i for $i > 1$ are crystallinity order parameters that vanish in the liquid phase, $\mathcal{F}_\ell$ only depends on m_1

$$\mathcal{F}_\ell[m_1] = \frac{1}{4} \int_{-\infty}^{\infty} \mathrm{d}z \int_{-\infty}^{\infty} \mathrm{d}z' \, w(|z - z'|) [m_1(z) - m_1(z')]^2 \tag{107}$$

where

$$w(z) = \int \mathrm{d}^2 r'' \, V_\ell(\sqrt{r''^2 + z^2}) \tag{108}$$

is the parallel-integrated long-range tail. Furthermore, in (104), $c^{(2)}$ has to be replaced by the direct correlation function for the system described by $V_s(r)$.

If one starts from the reduced functional (104) one deals with a (generalized) *Landau theory*, whereas an added long range term leads to a *van der Waals* type *theory* (since van der Waals was the first to write down a long range expression like (107) for the liquid–gas interface [24]).

The physical realized solution is obtained by solving

$$\delta \Sigma / \delta m_i = 0 \tag{109}$$

with the boundary conditions

$$\lim_{z \to -\infty} \boldsymbol{m}(z) = \boldsymbol{m}_A, \quad \lim_{z \to \infty} \boldsymbol{m}(z) = \boldsymbol{m}_B. \tag{110}$$

If there are multiple solutions, one has to take that with minimal surface tension Σ in order to get the physical realized one.

At this stage, let us note an interesting analogy to classical mechanics. The functional (104) looks like a classical Lagrangian of a fictitious "particle" in order parameter space; z plays the role of "time"; $g_{ij}(\boldsymbol{m})$ is a position dependent anisotropic but positive definite 'mass' tensor, and $-f(\boldsymbol{m})$ defines a "potential" in which the particle moves. At coexistence, $-f(\boldsymbol{m})$ has two equal maxima ("hills"), the boundary condition (110) means that we are looking for connecting trajectories of the fictitious classical "particle" starting from "hill" A and ending at "hill" B. This classical analogy helps in understanding the qualitative behaviour of the solutions. For long range forces, however, there is also a "memory-term", associated with the kernel $w(z)$ in (107) which resembles a "polaron action" [131].

In the context of the liquid–vapour interface where the density itself is the order parameter, the corresponding square gradient expansion has a long history, see ref. [25] for a review. It was also transferred to solid–liquid interfaces but often the mass tensor is approximated by a diagonal *constant* matrix and $f(\boldsymbol{m})$ is taken to have an ad hoc form with two equal minima. Then one recovers the functional Σ discussed in the first chapter, see eqs. (72)–(74). The microscopic interactions only enter via few numbers and one can also use these kind of theories as phenomenological approaches to more complex systems. If one takes the full expressions (103), (105), on the other hand, the solution of (109) still represents a full though approximate reduced theory, since details of the interaction and the T, μ-dependence enter in a set of functions $g_{ij}(\boldsymbol{m})$ and $f(\boldsymbol{m})$. If one wants to calculate numbers, the m-dependence of g_{ij} and the full function $f(\boldsymbol{m})$, containing all informations on the bulk phase diagram, is essential. We shall examine surface melting (i.e. solid–vapour interfaces near the triple point) within this van der Waals approach in the next chapter. In addition, (104) establishes a microscopic foundation and justification of purely phenomenological Landau theories.

3.5. *Other applications of density functional theory*

Until now we have discussed the application of density functional theory to calculate bulk phase diagrams, interfacial structures and noncrystalline solids for simple systems. There is a huge variety of other related applications for simple three-dimensional liquids.

First some details of the *crystalline* phase were studied within the liquid-based density functional theory: successfull density functional studies for the elastic constants of the an fcc hard sphere crystal were done by Velasco and Tarazona [132] and Xu and Baus [133]. Also *vacancies* in the crystal [134, 135], *dislocations* [136] and non-Gaussian and *anisotropic* behaviour of the solid peak density [102, 37] were investigated. Recently, also *phonon frequencies* in the solid were studied [137, 138]). With density functional theory one can also calculate the free energy of a *metastable* phase. Such applications in the context of hard-sphere systems were done for *quasicrystals* (e.g. ref. [139]) and *glasses* [140–142].

Other situations which were attacked by density functional theory include *adsorption* at interfaces [143, 144], and the *crystallization of a liquid in an external periodic potential* [145].

Density functional theory was also applied to others than classical liquids: *liquid metals* [146] where the quantum character of the electrons is relevant, freezing of different *quantum fluids* [147–154], and such "exotic" systems like *vortex liquids* in high-T_c superconductors [155].

Finally, we mention *dynamical* (though still phenomenological) *extensions* of density functional theories [156, 157].

4. Surface melting

The decisive mechanism initiating bulk melting of a crystal is via the solid surface. We describe recent experiments, theories and simulational studies of surface melting. In addition, for complete surface melting, scaling laws for the crystallinities in the quasiliquid film are given and the influence of gravity and finite crystal size is examined.

4.1. Introductory remarks

4.1.1. What is surface melting?

In chapter 2 we discussed already that solid bulk melting is not accompagnied by a sudden proliferation of dislocations. How does melting manifest itself microscopically? One may conjecture that bulk melting may be initiated at point defects, vacancies [158, 159], grain-boundaries [160–163] or at the crystal *surface* which is a natural and omnipresent defect in the crystalline order. This is based on the common experience that liquids may easily be undercooled due to kinetic obstacles of nucleation but crystals can hardly be overheated. That the crystal surface plays a decisive role to initiate melting gains further support from the experimental observation that silver crystals (melting temperature 1234 K) coated by a thin film of gold (melting temperature 1337 K) can be substantially overheated [164]. This was also recently confirmed by a simulation of Broughton [165]. Let us first focus on an idealized *planar* and *equilibrium* situation of surface melting. A semi-infinite three-dimensional crystal being in coexistence with its gas is heated up along the sublimation line until the temperature approaches the triple point temperature T_T where the liquid phase becomes thermodynamically stable. The corresponding path in the P–T diagram is visualized in fig. 4.1.

The distance to the triple point is conveniently measured by the reduced temperature distance

$$\tau \equiv (T_T - T)/T_T > 0. \tag{111}$$

The crystal is cut along a fixed plane with an area A, the position perpendicular to this plane is z. A key quantity in characterizing the solid–gas interface is the parallel-integrated density $\bar{\rho}(z)$

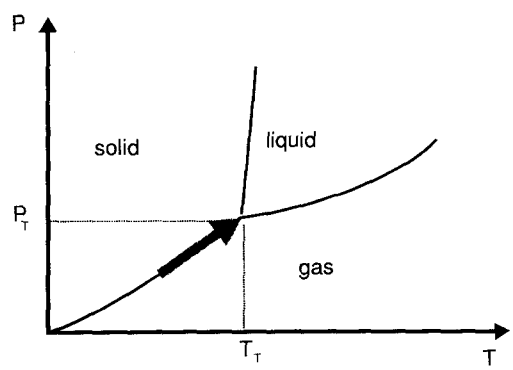

Fig. 4.1. Schematic (P, T) bulk phase diagram. T_T and P_T are the temperature and pressure at which the solid, liquid and vapour phases are at coexistence. The path along the solid–vapour coexistence curve, indicated by the arrow, corresponds to the trajectory studied in the context of surface melting.

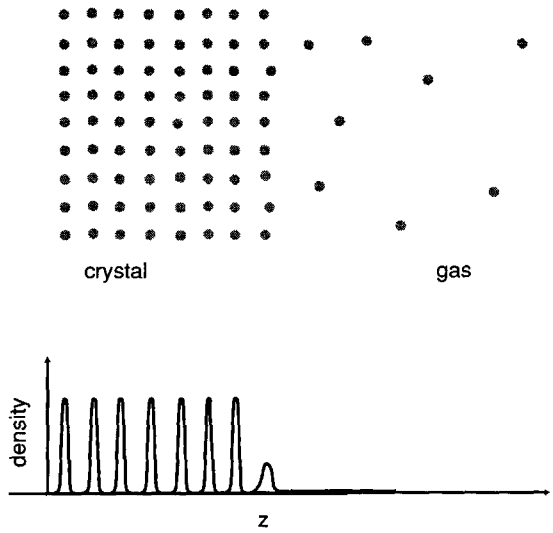

Fig. 4.2. Crystal–gas interface away from the triple point. The upper plot shows the positions of the particles for a typical configuration (schematic). The crystal on the left side has long-ranged order whereas the gas on the right has a homogeneous density. Also, the parallel-integrated density $\overline{\rho}(z)$ is shown.

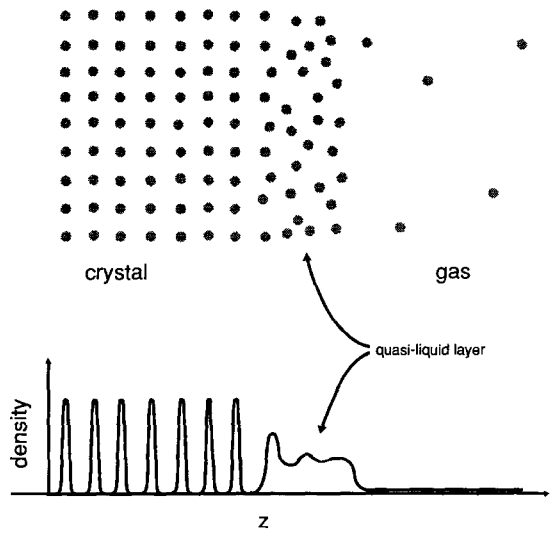

Fig. 4.3. Same as fig. 4.2 but now near the triple point. In the case of surface melting, a quasiliquid layer intervenes between the solid and the gas which is characterized by a thickness l. The upper plot shows the positions of the particles for a typical configuration, one sees that disorder sets in at the solid surface.

which is obtained from the full density $\rho(\boldsymbol{r})$ via

$$\overline{\rho}(z) = \frac{1}{A}\int_A \mathrm{d}x\,\mathrm{d}y\,\rho(\boldsymbol{r}) \tag{112}$$

The typical shape of the parallel-integrated density for a solid–gas interface far away from the triple point is shown in fig. 4.2. In the solid phase $\overline{\rho}(z)$ consists of sharp peaks reflecting the periodic crystal lattice while it equals the gas bulk density in the gas phase. Between the two phases there is a sharp interface typically involving only few crystalline layers.

As one approaches the triple point, two different situations can occur. In the first case, the *non-melting* case, there is no drastic change in the structure of the solid gas interface at $T = T_T$, i.e. the solid remains nonwet at its surface, even at T_T, and there is a sharp solid–gas interface. Apart from a broadening of the solid peaks due to the higher temperature, the parallel-integrated density across the solid–gas interface then is very similar to the one far from the triple point, see again fig. 4.2. In the second case, near T_T, a *quasiliquid layer* intervenes between the solid and the gas exhibiting a certain *width* l and a residual crystallinity at the quasiliquid–gas interface. This is visualized in fig. 4.3. One speaks about *complete surface melting*, if l diverges as $\tau \searrow 0$; correspondingly the residual crystallinity does vanish as $\tau \searrow 0$. One may express this also within the surface tensions at the triple point between solid–gas, σ_{sg}, solid–liquid, $\sigma_{s\ell}$, and liquid–gas, $\sigma_{\ell g}$: complete surface melting occurs if at $T = T_T$

$$\sigma_{sg} = \sigma_{s\ell} + \sigma_{\ell g}. \tag{113}$$

A peculiar case is *blocked surface melting*: Here, a quasiliquid layer starts to develop for $T < T_T$, grows and then stays and remains finite at T_T.

Of course, the behaviour depends on the orientation of the crystalline plane. One can surmise that melting is more likely in looser packed planes, whereas in denser packed planes the atoms are bound more tightly and disorder cannot get in easily. Generalizations to nonplanar geometries are studied in section 4.7 and surface melting away from equilibrium is considered in section 5.3.

Motivated by these considerations, the following questions are interesting: (1) Does the crystal melt from its surface or not? Equivalently: does the crystal exhibit non-melting or complete surface melting (or perhaps blocked surface melting)? (2) If there is complete melting, what is the divergence law for $l(\tau)$ and the decay law for the residual crystallinity as a function of the reduced temperature τ (as $\tau \searrow 0$)? What is the detailed structure of the solid–quasiliquid-gas interface?

4.1.2. Historical remarks

The problem of surface melting is as old as 1842 when Faraday [166, 167] started investigations on melting and freezing of pieces of ice, see ref. [168], for more details. Of course, this is not the idealized equilibrium situation, just discussed in 4.1.1, since there is a temperature gradient. In 1910, Tammann [169] pointed out that the surface has a decisive role to initiate bulk crystal melting. Later in 1942, this idea was supplied with macroscopic, qualitative considerations, including the dependence on the orientation of the solid plane by Stranski [170]. Then, in the last decade, microscopic aspects of surface melting were studied: new powerful surface-sensitive experimental methods were developed and thereby the problem of surface melting was revitalized. Theories and extensive computer simulations were then also performed. We shall review this recent work in the next three chapters.

4.2. Experiments on surface melting

Experimentally, surface melting was mainly studied for simple metals (most notably lead) and rare gases (argon and neon). In fact, *lead* represents the material for which the most detailed studies were made and is thus the "paradigm" for surface melting. Starting in 1985, van der Veen, Frenken and later Pluis and collaborators used ion scattering [171–175] and X-ray reflectivity ([176], see also refs. [177–179]) to prove that the (110)-plane does and the denser packed (111)-plane of the lead fcc-crystal does not melt. The (100)-surface was later found to show incomplete melting [180]. The onset of disorder in the first layer of the loosely packed (110)-plane is at a temperature $T \approx 450$ K whereas the triple point is about 600.7 K. The first layer is practically molten at $T \approx 580$ K which means that surface melting effects set in already well below the triple temperature. High precision data for the divergence of the width $l(\tau)$ were obtained, such that one could even exclude a discontinuous layer-by-layer surface melting process for the (110)-plane as T is raised. In particular, $l(\tau)$ was found to diverge logarithmically as $-\ln\tau$ and to cross over to a power law $\tau^{-\nu}$ with exponent $\nu = 0.315 \pm 0.015$ very near T_T. Lead was also examined by Bonzel, Breuer and coworkers [181, 182] (see also ref. [183]) using low energy electron diffraction (LEED). These observations confirm the ion scattering data and give also information on the anisotropic residual crystalline order in the quasiliquid film. Also spin-polarized LEED was applied to study surface melting of lead [184]. Note that the experiments are performed in ultrahigh vacuum, i.e. not exactly at coexistence but below the true sublimation line (see again fig. 43.1). In section 4.3, however, we shall estimate that the corrections with respect to an equilibrium situation are negligibly small.

Second, there are specific heat measurements for *argon* [185] and *neon* [186] films on graphite by Zhu and Dash and also by Brushi et al. [187]. Also a divergence law of the liquid film thickness $l(\tau) \sim -\ln\tau$ with a crossover to a $\tau^{-1/3}$ law was detected.

Let us also mention the early, pioneering optical measurements on copper and gold surfaces by Stock and Menzel [188, 189] and Stock and Grosser [190]. Likewise, experimental evidence for surface melting has been obtained for oxygen films on graphite [191, 192], methane films on MgO [193, 194], for aluminium [195–198], for the (111) surface of germanium [199], for the (001) and (111) surfaces of gold [200–202] and for the (110)-surface of nickel [203]. Also the surface melting behaviour of an *anisotropic* crystal (caprolactan) was recently studied by Chandavarkar et al. [204].

Last but not least surface melting of *ice* was controversial for a long time. Ice is probably the material where surface melting has most pronounced applications ranging from charge transfer between ice crystallites in thunderstorm clouds and frost heaves to ice-skating. Recent careful and reproducible X-ray scattering experiments by Lied et al. [205] strongly indicate that ice exhibits complete surface melting for every high-symmetry surface orientation. In addition, non-basal orientations show a temperature-dependent facetting.

Occurrence of surface melting for quite a number of different materials proves that it is, in this sense, universal, although details depend on the kind of the material.

4.3. Theoretical approaches

A necessary condition for a microscopic theory of surface melting is a good description of the bulk phase diagram of the material studied which forms the starting point of an interface calculation and defines the sublimation line and the triple point temperature T_T. It then should describe well the solid-gas interface up to T_T.

4.3.1. Phenomenological theories

A simple phenomenological theory of surface melting starts from the free energy difference between the solid–quasiliquid-gas interface and the solid bulk phase [206–208]. This difference per unit area is called *interfacial potential* $V^*(l)$. As a function of the thickness l of the quasiliquid layer, the interfacial potential reads

$$V^*(l) = \sigma_{s\ell} + \sigma_{\ell g} + L\tau l + \sigma_0 \exp(-l/a_L) + W/l^2. \tag{114}$$

The term $L\tau l$ results from the bulk free energy difference between the solid and the metastable liquid; L denotes a latent heat. The exponential term describes interfacial repulsion due to short range interparticle forces where a_L denotes a liquid correlation length while the W/l^2 term stems from the van der Waals attraction, W being the Hamaker constant.

The expression (114) for the interfacial potential can be derived either by calculating the free energy difference of a sharp-kink density profile with density functional theory [26] or by considering a Landau-model (see eq. (72)) for an order parameter $m(z)$ [209, 210, 129, 130]). In the Landau model, the bulk free energy density $f(m)$ has three minima corresponding to the gas, liquid and solid state, two of them (gas, solid) of equal depth zero. Around the liquid phase, $f(m)$ has the expansion

$$f(m) = L\tau + \tfrac{1}{2}g(m - m_L)^2/a_L^2 \tag{115}$$

where m_L is the dimensionless order parameter for the liquid phase and g is the prefactor of the square gradient term in the Landau functional (72).

All these approaches are phenomenological in the sense that one cannot decide whether there is complete surface melting or not for a given material, since the surface tensions (113) cannot

be calculated microscopically. However, one can make definitive predictions for the width of the quasi-liquid layer $l(\tau)$ provided the material exhibits surface melting. Minimization of $V^*(l)$ with respect to l immediately yields the following results: for short-ranged interparticle forces ($W = 0$), there is a logarithmic growth law for the width of the quasiliquid film $l \simeq -a_L \ln(\tau)$. With a long range van der Waals tail, $l(\tau)$ diverges algebraically as $l \simeq (2W/L\tau)^{-1/3}$. For a weak long range tail, $l(\tau)$ crosses over from logarithmic to algebraic divergence. More general, for an algebraic long range tail $\sim r^{-d}$, $d \geq 3$, in the interparticle pair potential, $l(\tau)$ diverges algebraically as $\tau^{-\nu}$ with $\nu = 1/(d-3)$. Finally, if the solid density is smaller than the liquid density at the triple point, the Hamaker constant becomes negative and there is blocked melting.

Since the interaction in rare gases is pairwise with a van der Waals tail, this explains the experimental growth law $\propto \tau^{-1/3}$ described in the previous section. For large particle separations, Van der Waals interactions are dominant for any polarizable material, also for metals like lead. For very long distances, however, the interaction becomes retarded $\sim r^{-7}$ such that the exponent ν crosses finally over to $\nu = 1/4$. For lead, this means that the observed crossover from a logarithmic to an algebraic growth law is in agreement with the theory and also the experimental value $\nu = 0.315 \pm 0.015$ consistently fits into the considerations above.

4.3.2. Density functional theories

In principle, a direct minimization of a density functional which has a good bulk phase diagram would be an ideal way to get quantitative results for the solid–gas interface for a given interaction potential (see the discussion in section 2.4.1). Attention was restricted to the Lennard-Jones system which represents a model system for rare gases. Chereponova et al. [211, 212] followed this strategy and obtained surface melting . However, they used a density functional whose phase diagram is not in good agreement with the simulations and their minimization was in a strongly restricted density space. Recently, Ohnesorge et al. [37], used the better WDA functional and performed a free minimization of the density functional. Surface melting was found to occur for the (110) and (100) directions. This calculation is very promising for further details of the solid–quasi-liquid–gas interface.

4.3.3. A density functional van der Waals approach

In this approach, the approximate but microscopically well-founded functional (104) for the surface tension is minimized. The model with *two* order parameters and neglection of long range forces yields an *odd* number of solutions [129, 130]; the one with minimal surface tension corresponds to the physically realized solution. Here the classical analogy, discussed in section 2.4, of a fictitious "particle" moving in a three-hill "potential" helps a lot to classify and understand the qualitative behaviour. Different solutions may correspond to non-melting, melting and blocked-melting situations, see fig. 4.4. If there are three solutions, the intermediate blocked-melting solution is dynamically unstable [213].

Ohnesorge et al. [78], discussed the van der Waals approach for a Lennard-Jones system and used the MWDA with the hard-sphere nonoverlapping modification to calculate the necessary microscopic input data. This was done with and without long range tail in the interparticle potential. The density was parameterized by *two* order parameters, the local mean density $m_1(z) \equiv \rho_0(z)$ and a crystallinity $m_2(z) \equiv \chi(z)$. Explicitly, one takes for the parameterization

$$\rho(\boldsymbol{m}(z), \boldsymbol{r}) = 2a_0^3 \rho_0(z) [\alpha(z)/\pi]^{3/2} \sum_{\boldsymbol{R}_n} \exp[-\alpha(z)(\boldsymbol{r} - \boldsymbol{R}_n)^2]. \tag{116}$$

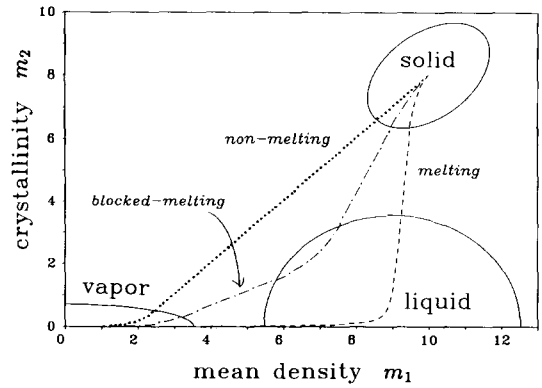

Fig. 4.4. Illustration of three types of solutions in a two-dimensional order parameter space spanned by the mean density m_1 and a crystallinity order parameter m_2: (i) melting (dashed line), (ii) blocked-melting (dot-dashed line), (iii) non-melting (dotted line). The units are arbitrary. The "potential" $-f(\boldsymbol{m})$ has a three-peak structure which is indicated by the three ellipses around the gas, liquid and solid phases.

The crystallinity $\chi(z)$ is related to $\alpha(z)$ by

$$\chi(z) = \rho_0(z)\exp[-G_1^2/4\alpha(z)]. \tag{117}$$

This density parameterization describes Gaussian peaks on a *fixed* underlying solid fcc lattice with

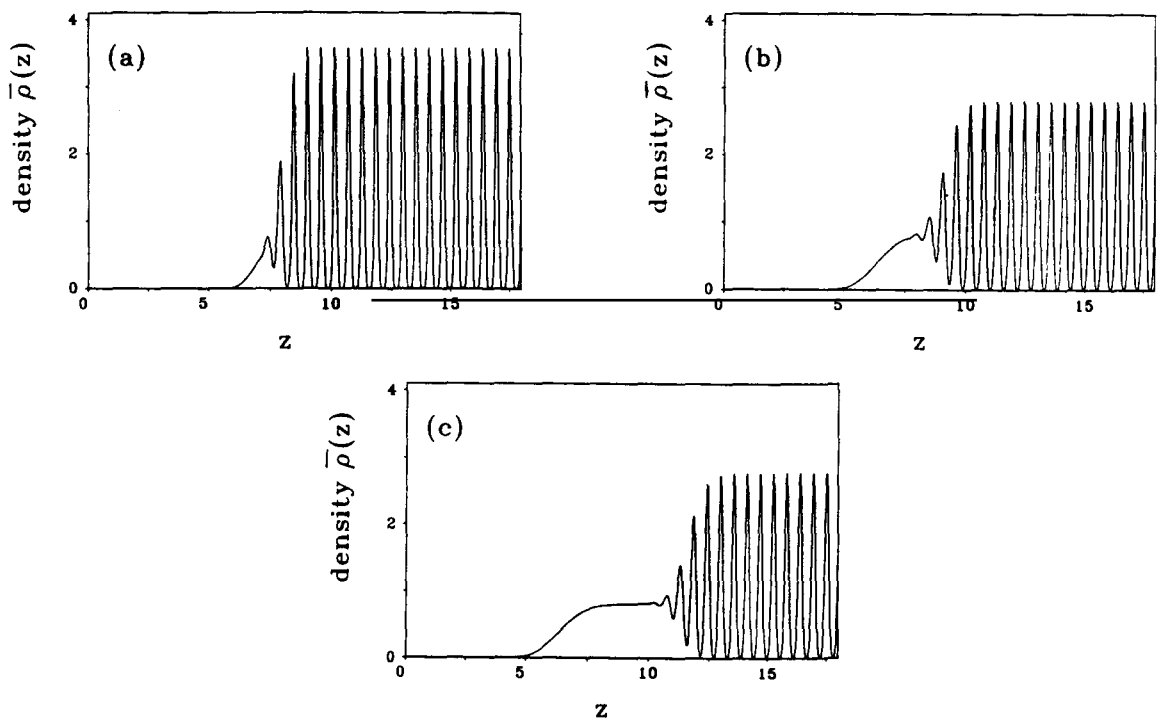

Fig. 4.5. The laterally integrated density $\bar{\rho}(z)$ in units of σ^{-3} in (110) direction at the reduced temperatures (a) $\tau = 0.343$, (b) $\tau = 0.015$, (c) $\tau = 1.2 \times 10^{-4}$, for a Lennard-Jones system. From ref. [78].

lattice constant a_0 which coincides with the lattice of the bulk solid phase. Furthermore, in eq. (117), $G_1^2 = 3\pi^2/a_0^2$ is the square of the first reciprocal lattice vector. According to eqn. (103) and (105), the basic input quantities $f(\boldsymbol{m})$ and $g_{ij}(\boldsymbol{m})$ were calculated for different temperatures along the sublimation line and the surface tension functional was minimized numerically. The corresponding parallel-integrated density $\overline{\rho}(z)$ is shown for different reduced temperatures τ in fig. 4.5 for a Lennard-Jones system without long range tail. It clearly exhibits surface melting near T_T, i.e. a quasiliquid layer emerges as $\tau \searrow 0$.

One disadvantage of the two-order-parameter parameterization is that it is not suited to describe anisotropies, i.e. the resulting surface tension is the same for any surface orientation in this approximation. For a system described by pairwise Lennard-Jones forces, this anisotropy of the surface tension is expected to be small [214].

4.3.4. *Other approaches*

Classical phonon theory was applied to surface melting [215–217]). In this approach one finds a lattice instability which starts at the surface and propagates into the bulk as the temperature is raised. Here, the description of the liquid is poor; the pressure dependence of the melting line is not in agreement with measurements [38].

Last, a *lattice theory* has been developed and successfully applied to a Lennard-Jones system by Trayanov and Tosatti [218, 219]. In this approach the Lennard-Jones system exhibits surface melting but the underlying bulk phase diagram is not in good agreement with the simulation data.

4.4. *Simulations of surface melting*

In the last ten years, the problem of surface melting was also attacked by direct numerical Molecular Dynamics simulation. Here one can in principle also gain information on the *dynamics* in the solid–quasi-liquid–gas interface. Motivated by the experiments, mainly two types of materials were studied, namely Lennard-Jones systems and metals.

Extensive simulations for the *Lennard-Jones system* were carried out by Broughton and Woodcock [220] and Broughton and Gilmer [214]. They obtain surface melting for any surface orientation and only a slight orientational dependence of the interfacial tension. On the other hand, Rosato et al. [221, 222], refuse the possibility of surface melting for the (110) plane, so the situation remains a bit inconclusive. For a critical review of the different simulations for a Lennard-Jones system, the reader is referred to Pontikis and Sindzingre [223]. In recent simulations of van der Eerden et al. [224], the (111) and (100) orientations of a Lennard-Jones crystal exhibit surface melting. The authors also propose the vanishing of the shear modulus at the solid surface as a criterion for surface melting. Schommers et al. [225, 226], used more realistic pair potentials for rare gases and included triplet forces. They obtain surface melting for the (100) orientation. Valkealahti and Nieminen [227] simulated the (111) plane of a Lennard-Jones system and get surface melting via a layer-by-layer process. Also a long-range potential tail $\sim 1/r^4$ was extensively studied in a simulation by Chen [228].

Next, simple *metals* were simulated. The basic difficulty is that many-body forces are present. Carnevalli et al. [229] have applied an empirical potential which includes many-body interactions to the melting of the (111) surface of gold. They found that there is a reconstruction of the surface; the reconstructed surface did not show surface melting. Stoltze, Nørskov and Landman [230, 231] used an ab initio effective medium interaction potential for aluminium which includes many-body aspects of the interaction but is still simple enough such that it can be employed in

simulations. They found surface melting for the (110) plane whereas the more close-packed (111) surface had a much weaker disordering. The strong orientational dependence seems thus to be due to the many-body interactions which are highly relevant in a strongly inhomogeneous situation like a solid–gas interface. This is in accordance with experiments where for lead, a metal for which many-body effects are important, different surface melting behaviour is seen for different orientations, whereas for rare gases there is no such well-pronounced dependence. Also nickel was studied around 1989 by Chen, Barnett and Landman [232, 233]. A further extensive simulation for aluminium was done in 1990 by Stoltze [234], and a direct comparison of the results of the simulation with experimental data was done by Denier van der Gon et al. [235]. The surface diffusion behaviour for the aluminium (110) surface can be explained by Molecular Dynamics simulations [236]. Recently the same effective medium theory was applied to simulate the copper (110) surface, where surface melting was found to occur too [237, 238]. Finally sulfur hexafluoride was investigated by MD simulation where also surface melting was found [239].

4.5. *Crystallinities in the quasiliquid film*

In this section we focus on scaling decay-laws for the crystallinities in the quasiliquid layer. First of all, we have to give a precise definition of what we mean with crystallinity. A concrete multicomponent order parameter parameterization of the local density for planar surface melting is

$$\rho(\boldsymbol{r}) \equiv \rho(\{m_{\boldsymbol{G}}(z)\}, \boldsymbol{r}) = \sum_{\boldsymbol{G}} m_{\boldsymbol{G}}(z) \exp(\mathrm{i}\boldsymbol{G} \cdot \boldsymbol{r}) \tag{118}$$

where $\{m_{\boldsymbol{G}}(z)\}$ is a special set of complex order parameters with $m^*_{\boldsymbol{G}}(z) = m_{-\boldsymbol{G}}(z)$, and $\boldsymbol{G} = (\boldsymbol{G}_\parallel, G_\perp) = (G_x, G_y, G_\perp)$ denotes a reciprocal lattice vector of the bulk crystal. As the sum in (118) is over all reciprocal lattice vectors, the representation (118) is very general. For $\boldsymbol{G} \equiv 0$, $m_{\boldsymbol{G}}(z)$ represents the local mean density of the system. On the other hand, for $\boldsymbol{G} \neq 0$, $m_{\boldsymbol{G}}(z)$ is called a *crystallinity* order parameter. Of course, in a homogeneous phase like a liquid or a gas, a crystallinity order parameter vanishes, whereas it is nonzero in the solid phase.

For a solid covered with a quasiliquid film, the crystallinities become smaller as one moves through the solid–quasi-liquid interface. Then just before the quasi-liquid–gas interface, there is still a nonzero crystallinity value on the quasiliquid side of this interface. This value is called *residual crystallinity* $m^R_{\boldsymbol{G}}$. Then, as one moves further through the quasi-liquid–gas interface, the crystallinities decay rapidly to zero. Of course, as the thickness of the quasimolten layer increases, the residual crystallinity decreases. The residual crystallinity is also accessible experimentally e.g. by LEED scattering techniques.

In order to construct a simple microscopic theory for the crystallinities we consider a solid–liquid interface at the triple point. Assuming that the quasi-liquid–gas interface is sharp and that it does not disturb the solid–quasi-liquid interface, the residual crystallinities on a quasi-liquid film of thickness ℓ approximately equal the crystallinities in the solid–liquid interface at a distance l from the interfacial position. One can prove that the *asymptotic* behaviour for large l (or small τ) is really the same. Of course, if only one layer is liquid like, the actual residual crystallinity may considerably deviate from this asymptotic expression since it may be strongly influenced by the solid and gas phases.

Mikheev et al. [240] as well as Löwen et al. [241, 242] have performed an asymptotic analysis around the liquid bulk phase in order to calculate the behaviour of the crystallinities very deep in the liquid phase. The analysis involves all terms bilinear in the order parameters and is thus more

general than the square gradient expansion used in section 4.3. If the liquid phase is approached as $z \to \infty$, one finds that asymptotically

$$m_{\boldsymbol{G}}(z) \sim \exp(ik_{\boldsymbol{G}} z) \exp(-z/a_{\boldsymbol{G}}). \tag{119}$$

($\boldsymbol{G} \neq 0$) with an oscillation mismatch $k_{\boldsymbol{G}}$ and a decay length $a_{\boldsymbol{G}}$ both for short range and for long range interactions. A microscopic expression for $k_{\boldsymbol{G}}$ and $a_{\boldsymbol{G}}$ can be obtained by considering the poles of the liquid structure factor $S_{\mathrm{T}}(k)$ at the triple point in the *complex* k-plane. For a given $\boldsymbol{G} = (\boldsymbol{G}_{\parallel}, G_{\perp})$ consider the complex solutions $\{q_i\}$ of the equation

$$1/S_{\mathrm{T}}(\sqrt{G_{\parallel}^2 + (G_{\perp} - q_i)^2}) = 0. \tag{120}$$

Then, the decay lengths are given by

$$a_{\boldsymbol{G}}^{-1} = \min_{q_i}[\{\mathrm{Im}(q_i)\}] \tag{121}$$

where the minimum extends over any complex solution q_i whose real part lies in the projection of the first Brillouin zone of the lattice onto the z-axis. Let q_0 be the solution with minimal imaginary part. Then, the oscillation mismatch is given by $k_{\boldsymbol{G}} = \mathrm{Re}(q_0)$.

If one has obtained the set of $a_{\boldsymbol{G}}$'s by this procedure, one can predict scaling decay laws for the residual crystallinities $m_{\boldsymbol{G}}^{R}(\tau)$ as a function of reduced temperature as $\tau \searrow 0$. For short range potentials the result is a power law

$$m_{\boldsymbol{G}}^{R}(\tau) \sim \tau^{\nu_{\boldsymbol{G}}} \tag{122}$$

with a nonuniversal and $\boldsymbol{G}$-dependent exponent $\nu_{\boldsymbol{G}}$ given by

$$\nu_{\boldsymbol{G}} = \max[2a_0, \{a_{\boldsymbol{G}}\}]/2a_{\boldsymbol{G}}. \tag{123}$$

For long-range potentials (e.g. with a van der Waals tail $\sim r^{-6}$), one gets a stretched-exponential behaviour

$$m_{\boldsymbol{G}}^{R}(\tau) \sim \exp[-(2W)^{1/3}\tau^{-1/3}/a_{\boldsymbol{G}}]. \tag{124}$$

This result is obtained by plugging the algebraic divergence law into the exponential decay (119) (see also ref. [243]). W is the Hamaker constant. The stretched exponential form was also obtained numerically by Trayanov and Tosatti [219].

For surface scattering experiments only the $\boldsymbol{G}_{\parallel}$ dependence is relevant and one can define a decay length of the lateral crystallinity as

$$a(\boldsymbol{G}_{\parallel}) := \max_{G_{\perp}}[a_{(\boldsymbol{G}_{\parallel}, G_{\perp})}]. \tag{125}$$

Using experimental data for the structure factor $S_{\mathrm{T}}(k)$ and continuating it into the complex plane, the results of the present theory are shown in fig. 4.6 for the lead (110) surface. They are compared with the experimental data and with a simple algebraic expression derived by Lipowsky et al. [208] within a phenomenologocal ansatz. The results from the microscopic theory described above and the experimental data are in reasonable agreement. However, there is a caveat since the LEED experiments have not yet reached the true asymptotic regime and there is also some curve fitting involved in extracting a decay length from the experimental output.

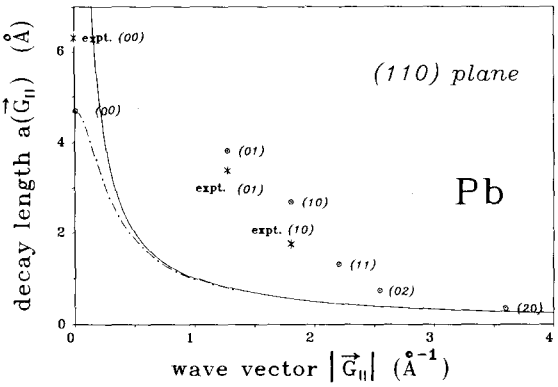

Fig. 4.6. Decay lengths $a(\boldsymbol{G}_{\parallel})$ plotted versus $|\boldsymbol{G}_{\parallel}|$ ($\odot$) for a lead (110)-plane at the triple point (T = 600.7 K). Units are in Å^{-1} and Å. Each point is labelled by the pair of integers (nm) resulting from the decomposition $\boldsymbol{G}_{\parallel} = n\boldsymbol{G}_{\parallel 1} + m\boldsymbol{G}_{\parallel 2}$ with $\boldsymbol{G}_{\parallel 1} \sim (1,-1,0)$ and $\boldsymbol{G}_{\parallel 2} \sim (0,0,1)$. The stars ($*$) denote experimental values. For the (00) beam, they are from ref. [174], for the (01) and (10) beam results are taken from LEED data from ref. [178]. The dotted-dashed line is the phenomenological expression from ref. [208] $a(G_{\parallel}) = a(0)/\sqrt{1 + (G_{\parallel}a(0))^2}$, where $a(0)$ is a fit parameter. For any choice of $a(0)$ this expression is bounded by $1/G_{\parallel}$ (solid line) and underestimates the decay lengths. From ref. [241].

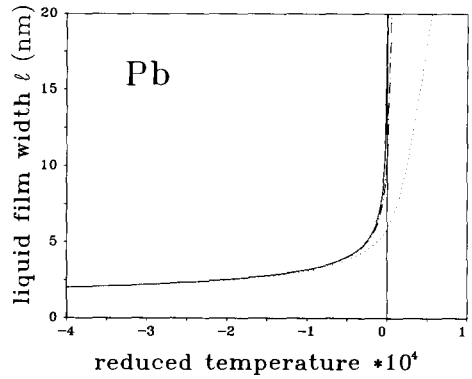

Fig. 4.7. Width of the liquid film versus reduced temperature for lead. The solid line corresponds to $g = 0$ and is the usual $\tau^{-1/3}$ divergence law for complete surface melting. The dot-dashed and dotted line are for $g = 10^8 m/s^2$, $10^9 m/s^2$ respectively. For $T = T_T$, ℓ is finite and the crystal is overheatable. From ref. [244].

4.6. *Influence of gravity on surface melting*

In the case of complete planar surface melting, the width of the quasi-liquid layer in principle diverges as the triple point is approached. Of course there are a couple of different mechanisms that finally limit the growing liquid layer such that its width remains finite at the triple point. Some of these mechanisms are external fields and walls as well as the finite size of the crystallites. We shall consider a gravitational field in this section and finite size effects in the next one. Consider planar surface melting where the normal of the solid surface has the same direction as a constant gravitational acceleration g. The corresponding interfacial potential was studied by Löwen and Beier in 1990 [244]. The main result was that gravity induces a *finite* width l^* of the liquid layer at the triple point and the solid can be overheated. l^* is given by

$$l^* = \sqrt[4]{2W\rho_S/mg\rho_L(\rho_S - \rho_L)}. \tag{126}$$

Here, m denotes the mass of a particle and W is the Hamaker constant of the material (we have assumed a long-range van der Waals attractive tail in the interparticle interaction). Furthermore, ρ_S and ρ_L ($\rho_S > \rho_L$) are the bulk solid and liquid densities at the triple point. The triple gas density is assumed to be small. For lead, the width of the liquid film is plotted versus reduced temperature τ for different gravitational accelerations in fig. 4.7. Notable deviations from the usual complete melting law do occur only for very high accelerations. It was argued in ref. [244] that in a centrifuge with very high centripetal acceleration the effect is in principle visible.

Another quite interesting realization to detect gravitational corrections to complete surface melting would be a *colloidal suspension.* Victor and Hansen [245] have shown that there is also a triple

point for a charged colloidal system characterized by a repulsive electrostatic and an attractive van der Waals potential. For colloidal particles, retardation effects which lead to an attraction $\sim r^{-7}$ are relevant. This would reduce the value of l^*. An estimation shows that, for normal gravity, l^* is of order of few interparticle spacings. Another very attractive possibility is a colloid–polymer mixtures where excluded volume effects may lead to an effective attraction between colloidal particles. The resulting phase diagram has a triple point and a critical point [246] but interfacial features have not yet been examined in detail. Also for such a system, surface melting is expected and effects of a gravitational field should be much pronounced. Therefore, whereas effects of gravity are normally negligible for atomic systems, they may be well observable for mesoscopic colloidal suspensions.

4.7. Equilibrium shapes of crystals near the triple point

Far away from the triple point, it is the orientational dependence of the solid–gas surface tension, $\sigma_{sg}(\hat{n})$, that determines the equilibrium shape of a crystal. Here, $\hat{n}$ denotes the surface normal. Within Wulff's construction [247] one can find the crystal shape for a given $\sigma_{sg}(\hat{n})$ geometrically by a Legendre transformation of $\sigma_{sg}(\hat{n})$. Very near the triple point where the liquid becomes also stable as a bulk phase, the situation is more complicated since for some orientations the solid may cover itself with a liquid film in order to reduce the free energy. This is in particular expected if a solid exhibits planar surface melting for these orientations. Such interesting phenomena were investigated experimentally, theoretically and recently also by computer simulation.

As regards *experiments*, extensive equilibrium shape measurements of lead crystallites were performed by Métois and coworkers [248–250] and by Pavlovska et al. [251]. A technical problem is that one is not always sure to be at equilibrium since the equilibration time is pretty large. As a result, the equilibrium shape of lead crystallites consists of facets and rounded parts. The (111) facet length increases with increasing temperature. The matching between the facet and the rounded part becomes angular about 20 K below the triple temperature; the discontinuity in orientation between these two parts also increases with temperature. Lead is insofar interesting as some orientations (like (111)) do and others (like (110)) do not melt, which results in a competition between nonmolten facets and molten rounded parts.

Recently, also first *simulations* were started by Stoltze [252]. The simulated system is pretty large (compared to usual bulk simulations) although the resulting crystallite is still small compared to experimental sizes. One can hope that, for a realistic interparticle interaction including many-body forces, the orientational dependence of surface melting and the corresponding change in the shape of the crystallite can be seen directly. Another recent related study was done for orientations near the nonmelting (111) surface of a lead crystal by Bilalbegovic et al. [253]. An orientational phase separation was then obtained that should be universal for vicinals of nonmelting crystal surfaces. Such surface-melting induced faceting was also confirmed experimentally by van Pinxteren and Frenkel [254].

Also phenomenological *theories* were proposed by Nozières [255] and Löwen [256]. In these references, the generalization of Wulff's construction with three temperature-dependent surface tensions, solid–gas $\sigma_{sg}(\hat{n}, T)$, solid–liquid $\sigma_{s\ell}(\hat{n}, T)$ and liquid–gas $\sigma_{\ell g}(T)$ is discussed. Strictly speaking, these three surface tensions are not always well-defined for all orientations, but one can extrapolate the orientational as well as the temperature dependence. Near the triple point, the equilibrium crystal shape then minimizes the total surface tension under the constraint of fixed mass $\rho_S V_S$ of the crystallite, V_S being the volume of the crystallite. In general, one has to consider simple solid–gas configurations as well as more complex configurations including e.g. a solid covered with liquid lenses of different density ρ_l. In this situation, one has to add also a free energy term

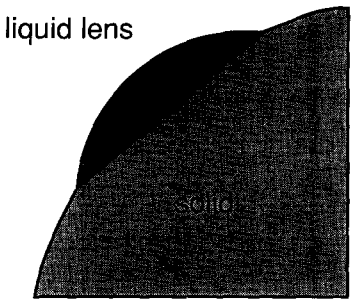

Fig. 4.8. Crystalline surface near the triple point (schematic). At certain orientations a liquid lens may occur. This implies in a drastical change of the equilibrium shape near the triple point due to surface melting.

$L\tau V_\ell$ where L is a latent heat and V_ℓ is the liquid volume. The main result of the phenomenological theories is that the crystalline surface exhibits liquid lenses roughly at those orientations where planar surface melting does occur. This is visualized in fig. 4.8. The crystal is then overheatable, since it shows a first-order transition to a liquid drop. In ref. [256], also the three-dimensional case for lead was discussed using experimental data for the temperature-dependent surface tensions as an input. In the resulting crystal shape, the (111)-facet length *increases* with temperature; there are liquid lenses with an orientation jump whose magnitude also increases with temperature. This is consistent with experimental facts. Stewart [257] explains the increasing facet length by vacancy melting in the (111) facet. In his approach, he also needs the three surface tensions $\sigma_{sg}(\hat{n}, T)$, $\sigma_{s\ell}(\hat{n}, T)$ and $\sigma_{\ell g}(T)$ as input. Since they have relative large experimental uncertainties, all such phenomenological approaches should still be considered as preliminary.

5. Dynamics of interfaces

In this chapter some basic models for interfacial dynamics away from critical points are discussed including exactly soluble cases. Also interfacial dynamics near the coexistence of three (stable or metastable) phases is considered, particularly dynamics of surface melting and the dynamical creation of metastable phases. The dynamics of the models employed is phenomenological and not ab initio in the sense of microscopic classical statistical mechanics. Therefore the universal qualitative features should be applicable to a large number of concrete systems.

5.1. Ginzburg–Landau-type models for interfacial dynamics

An interfacial profile is described by a space and time dependent scalar order parameter $m(z,t)$, z being the coordinate perpendicular to the surface plane. The order parameter is taken to be dimensionsless and normalized so that it is zero in the first (A) and 1 in the second (B) phase. We consider Ginzburg–Landau-type grandcanonical surface free energy functionals of $m(z,t)$, as discussed in section 3.4.2:

$$\Sigma[m] = \int_{-\infty}^{\infty} \mathrm{d}z \, \{\tfrac{1}{2} g(m(z,t))[\partial m(z,t)/\partial z]^2 + f(m(z,t))\}. \tag{127}$$

At coexistence of A and B, $f(m)$ has two equal minima at $m = 0, 1$. If one phase (A) grows at the expense of the other (B) , we have

$$f(1) - f(0) \equiv \varepsilon > 0 \tag{128}$$

Long ranged interactions of $m(z,t)$ can be incorporated by adding

$$\mathcal{F}_\ell[m] = \frac{1}{4} \int_{-\infty}^{\infty} \mathrm{d}z \int_{-\infty}^{\infty} \mathrm{d}z'\, w(|z - z'|)[m(z,t) - m(z',t)]^2 \tag{129}$$

to the original functional Σ (compare with (107)).

We define *relaxational dynamics* or dynamics for a *nonconserved* order parameter as follows [258]:

$$\partial m/\partial t = -\Gamma_{\mathrm{n}}(m)\, \delta\Sigma[m]/\delta m. \tag{130}$$

Here, the free energy gradient is just the driving force for the order parameter, Γ_n is a kinetic coefficient which sets the microscopic time scale and generally depends on the order parameter m, i.e. it is different in the different thermodynamic phases described by m. On the other hand, the dynamics for a *locally conserved* order parameter follows from a generalized continuity equation [258] and is given by

$$\partial m/\partial t = \Gamma_{\mathrm{c}}(m)(\partial^2/\partial z^2)\delta\Sigma[m]/\delta m \tag{131}$$

where again Γ_{c} is a generalized diffusion coefficient (with another dimension than Γ_{n}). The boundary conditions for $m(z,t)$ are

$$\lim_{z\to-\infty} m(z,t) = m_{\mathrm{A}} = 0, \quad \lim_{z\to\infty} m(z,t) = m_{\mathrm{B}} = 1. \tag{132}$$

Furthermore, in (130) and (131), we have neglected random forces; they serve only to describe thermodynamic fluctuations and are important for phenomena near critical points, but not for phases separated by first order phase transitions.

Often one looks for *steady state* solutions

$$m(z,t) = m(z - vt) \equiv m(x) \tag{133}$$

with a velocity v which is then specified as a function of the free energy difference ε. Such a solution obviously exists only for non-conserved order parameter dynamics. If one substitutes in (130) $\partial/\partial t$ by $-v\partial/\partial z$ and neglects $\mathcal{F}_\ell$ one arrives at an ordinary differential equation. As discussed in section 3.4 in the context of the equilibrium situation ($v = \varepsilon = 0$), the problem is equivalent to the classical dynamics of a fictitious "particle" in order parameter space, where z plays the role of "time". This "particle" has a "mass" g and moves in a classic potential $-f(m)$ from the "hill" of phase A to the other "hill" of phase B which is lower than the first "hill" (for $\varepsilon > 0$). In contrast to the equilibrium case, however, the particle suffers also linear "friction" with a friction constant $v\Gamma_n^{-1}$. For a given ε, the friction must be chosen such that the particle stops exactly at hill B. This requirement then yields the desired relation $v(\varepsilon)$.

5.2. Exactly soluble models

Let us first restrict attention to a single order parameter. We further assume that g and Γ_c, Γ_n do not depend on m. A simple exactly soluble model, well-known from its static kink-solution, is the *Ginzburg–Landau* model defined by a quartic free energy function $f(m)$

$$df(m)/dm = Am(m - m_0)(m - 1) \tag{134}$$

where m_0 is an additional parameter governing the free energy difference $\varepsilon = A(\frac{1}{2} - m_0)/6$. The steady state solution can be expressed as [259, 260]

$$m(x) = \frac{1}{1 + \exp(\sqrt{A/2g}\,x)} \tag{135}$$

where $x \equiv z - vt$ if the relation

$$v = 6\Gamma_n\sqrt{g/A}\,\varepsilon \tag{136}$$

is satisfied.

Another exactly soluble model that has been widely used and applied is the *parabolic* model

$$f(m) = \min[\tfrac{1}{2}Am^2, \tfrac{1}{2}A(m-1)^2 + \varepsilon] \tag{137}$$

If one neglects $\mathcal{F}_\ell$, the steady state equation of motion is piecewise linear leading to exponential solutions which can be matched to give $m(x)$ and the desired relation $v(\varepsilon)$. Although the quartic potential (134) is undoubtedly smoother and therefore more realistic than the intersecting parabola model, both are evidently ad hoc. Qualitative features should be the same in both models. The smooth Ginzburg–Landau model is more attractive for direct numerical simulation whereas the parabolic model is more appropriate to derive analytical results.

The analytical treatment within the parabolic model can also be done, when $w(z)$, the long ranged interaction kernel, is not ignored. As realized by Löwen and Oxtoby [261], the steady state solution can be found for *arbitrary* kernels $w(z)$. Long-ranged interaction kernels were studied previously, but analytical results were mainly limited to the Sullivan model in equilibrium situations [262–264] where a special Yukawa type of interaction kernel is required. In the parabolic model, the steady state solution is explicitly given by

$$m(x) = \frac{A}{2\pi}\int_{-\infty}^{x} dy \int_{-\infty}^{\infty} dk\, \frac{\exp(-iky)}{gk^2 - ikv/\Gamma_n + A + W(k)} \tag{138}$$

with

$$W(k) = \sqrt{2\pi}[\tilde{w}(k) - \tilde{w}(0)] \tag{139}$$

where $\tilde{w}$ denotes the Fourier transform. The relation between v and ε is governed by the expansion

$$\varepsilon = A_1 v + A_3 v^3 + O(v^5) \tag{140}$$

with

$$A_1 = A^2 I_0/2\pi\Gamma_n, \quad A_3 = A_1 I_2/I_0\Gamma_n^2, \tag{141}$$

$$I_m = \int_{-\infty}^{\infty} dk\, \frac{k^m}{[gk^2 + A + W(k)]^{m+2}}. \tag{142}$$

Finally, the full time-dependent analytical solutions were found for the equilibrium case $\varepsilon = 0$ in ref. [261].

5.3. Dynamics of surface melting

In this section and the following one, we study the interfacial dynamics, particularly the steady state solutions, for a situation where *three* phases are (meta)stable. Then, $f(m)$ has three local minima and the existence of a steady state solution depends sensitively on the depth of these three minima. We shall illustrate the physical effects that may occur using two different applications: surface melting away from equilibrium and, second, a dynamical mechanism for the creation of a metastable phase.

In chapter 4, *equilibrium* aspects of surface melting were discussed. However, scattering experiments on surface melting are typically performed in ultrahigh vacuum, i.e., at large undersaturation, in order to reduce the scattering from the vapor phase. In these experiments, the crystal slowly evaporates. Therefore, the crystal studied is no longer in chemical equilibrium with the vapor. The two situations of surface melting with and without chemical equilibrium can be visualized as different paths in a P–T diagram. Whereas in equilibrium one moves exactly on the sublimation line towards the triple point, in the nonequilibrium case the path is shifted by a pressure difference ΔP from the sublimation line, see fig. 5.1.

Löwen and Lipowsky [265] proposed a simple Landau model in which the crystal–vapor interface moves at constant velocity v towards the bulk of the crystal. Following their ideas, we consider a single order parameter m like the particle mean density (eventually combined with a crystallinity order parameter).

We use the familiar Ginzburg–Landau functional (127) where $f(m)$ now has three minima at $m_V < m_L < m_S$ corresponding to the vapor, liquid and solid phase. The gas phase is globally stable, the solid respectively liquid grandcanonical free energy density is about $\Delta P > 0$ respectively $\Delta P_L > 0$ higher. As in (115), one can define a liquid correlation length a_L by the curvature around the liquid peak where $f(m)$ has the expansion

$$f(m) \cong \Delta P_L + \tfrac{1}{2} g(m_L)(m - m_L)^2 / a_L^2. \tag{143}$$

For a situation away from the sublimation line, we are interested in a system in which one has a

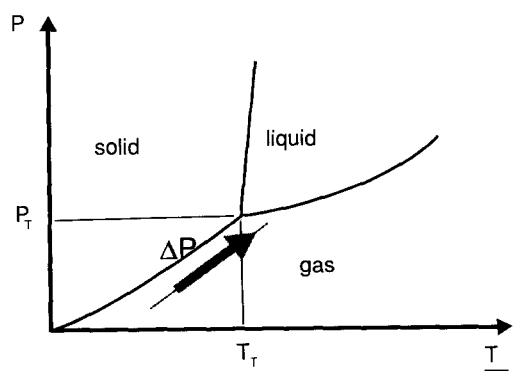

Fig. 5.1. P–T diagram and possible paths of surface melting. In the idealized equilibrium case, the path is identical with the sublimation line (solid curve). In the experimental situation without chemical equilibrium, the path (dashed line along the arrow) is shifted by a pressure difference ΔP from the sublimation line.

flux of particles away from the solid–vapor interface. This corresponds to the experimental situation where the evaporated particles are pumped away in order to sustain ultrahigh vacuum conditions. The corresponding undersaturation is governed by pressure which is a "fast" propagating mode: on the timescales relevant for the interfacial motion, the pressure within the vapour phase can be taken to be constant. In such a situation, the deposition rate of particles from the vapour phase should be proportional to this pressure while the evaporation rate should be determined by the binding energies of the molecules within the liquid vapour interface [266]. In any case, mass transport through the interface will not be limited by diffusion. In terms of the particle density, one may then study the *relaxational dynamics*, defined by (130). A steady state analysis for the profile $m(x)$ with the boundary conditions $\lim_{x\to-\infty} m(x) = m_V$ and $\lim_{x\to\infty} m(x) = m_S$ then leads to the following predictions [265]:

In the dynamical situation with $\Delta P \neq 0$ there is a characteristic temperature T_* which, in general, is different from the triple point temperature T_T. If complete surface melting occurs for the equilibrium case $\Delta P = 0$ at $T = T_T$ with a logarithmic growth law for the *width of the quasi-liquid film*, l, there is also a logarithmic growth law at $T = T_*$ for $\Delta P > 0$. In particular

$$l = l_0(v)|\ln[(T_* - T)/T_*]| \tag{144}$$

for $T \nearrow T_*$ where the prefactor depends on the steady state velocity v

$$l_0(v) = a_L[1 + va_L/2g(m_L)\Gamma_n(m_L) + O(v^2)]. \tag{145}$$

This means that the nonequilibrium condition enhances the thickness of a wetting layer.

Another interesting quantity is the *residual crystallinity* m_j^R of the order parameter m_j at the quasi-liquid–vapour interface. For the equilibrium situation, it is well-known from section 4.5 that m_j^R vanishes as a power law in $T_T - T$ with nonuniversal exponents β_j. In the generalization to the nonequilibrium situation, the exponents turn out to become v-dependent.

Finally, let us consider a long ranged algebraic tail $V_\ell(r) \sim r^{-6}$ in the interparticle potential $V(r)$. As in the case of short range forces, surface melting occurs at a characteristic temperature T_*, which differs in general from the triple point temperature T_T. The Hamaker constant W, on the other hand, is not renormalized by the dynamics, i.e. it does *not* depend on the interface velocity v [265]. The thickness l of the disordered layer diverges as $l \approx [2W/A(T_* - T)]^{1/3}$ for small $T_* - T$ where A is a latent heat. The residual crystallinity vanishes as a stretched exponential law in $T_* - T$.

Estimating typical velocity corrections, one finds that they are very small in general such that the interfacial structure observed in scattering experiments resembles very much the structure in full chemical equilibrium.

5.4. *Dynamical mechanism for the formation of a metastable phase*

One can also study three-phase Ginzburg-Landau models where one of the phases is a *metastable* phase. Although such a metastable phase cannot be thermodynamically stable as a bulk phase, one can create it dynamically. Bechhoefer et al. [267] have shown that fronts separating the stable high- and low-temperature phases can split apart into two independently moving fronts. The first front separates the phase that is stable at high temperatures (phase 0) from the metastable phase (phase 1). The second separates the metastable phase from the stable one at low temperatures (phase 2). Because the 01 front moves faster than the 12 front, a *macroscopically* large region of the metastable phase 1 is created. The mechanism explains how metastable phases may grow at the interface given that the stable phase has already been nucleated.

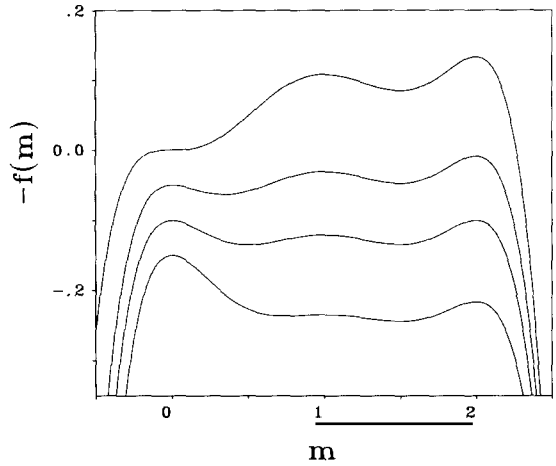

Fig. 5.2. Free energy density $-f(m)$ as a function of the order parameter m for different control parameters $b \propto (T_{02} - T)$. The curves are shifted by an arbitrary constant. From top to bottom the values of b are as follows: (a) $b = 0.5$, liquid spinodal line, (b) $b = b_c = 0.15419$, critical value for interface splitting, (c) $b = 0$, coexistence between phase 0 and 2, (d) $b = -0.25$, region where phase 0 is stable.

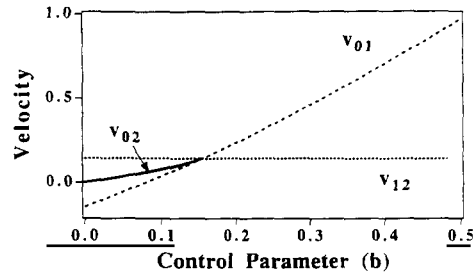

Fig. 5.3. Calculated velocities of the 01, 12, and 02 fronts as a function of b. From ref. [267].

In ref. [267], a polynomial of sixth order was chosen for the bulk free energy density $f(m)$,

$$df/dm = Am[m - (0.5 - b)](m - 1)(m - 1.5)(m - 2). \tag{146}$$

$f(m)$ is sketched in fig. 5.2 for different b exhibiting three local minima at $m = 0$, 1, and 2. The minimum at $m = 0$ represents a disordered phase (e.g. a liquid), that at $m = 2$ a stable phase (e.g. the equilibrium low-temperature solid phase), and that at $m = 1$ a metastable phase 1 (e.g. a solid phase with a different crystal structure, a martensite [268], or a quasicrystal [269]). The control parameter is $b \propto (T_{02} - T)$, where T_{02} is the coexistence temperature between phases 0 and 2. Thus, $b = 0$ corresponds to the usual melting temperature. When $0 < b < 0.5$, the stable solid phase ($m = 2$) has a lower free energy than phase 0 and 1.

In fig. 5.3 also the three front velocities are plotted versus the control parameter b. v_{01} means the velocity of the steady state interfacial profile between phase 0 and 1, to which the phase 2 is irrelevant. Accordingly, v_{12} is the velocity of the steady state profile between the phases 1 and 2 and v_{02} means the velocity of the complete profile. The most striking feature is the intersection of $v_{01}(b)$, $v_{12}(b)$, and $v_{02}(b)$ all at the same value of a *critical* control parameter $b = b_c \approx 0.154$. Although steady-state 01 and 12 fronts exist for all values of b, the steady-state 02 front ceases to exist when $b > b_c$.

For $b > b_c$, solutions connecting phases 0 and 2 are time dependent in all uniformly translating reference frames. When $b < b_c$, the width $w_{02}(t)$ converges to a constant as $t \to \infty$. When $b > b_c$, it diverges linearly for large times. The asymptotic rate of divergence satisfies

$$dw_{02}/dt = v_{01}(b) - v_{12}(b). \tag{147}$$

This, then, is the mechanism for the formation of metastable states: in the presence of the metastable phase, the 02 front can be thought of as a combined 01 and 12 front. As long as the rear part (12)

moves faster than the leading part (01), the 02 front moves with a velocity intermediate between v_{01} and v_{12}. When the rear is unable to keep up with the leading edge, the 02 state splits into two quasi-independent 01 and 12 fronts: a *macroscopic* quantity of phase 1 is created.

The splitting instability is possible even when there are multiple order parameters. This was discussed in detail by Tuckerman and Bechhoefer [213]. Finally the presence of an external field blocks metastable phase formation which was discussed by Bocquet and Löwen [270]. In this case the width of the metastable phase layer first grows to mesoscopic values and then shrinks back again to microscopic values.

6. Heat diffusion limited crystal growth

In order to describe crystal growth where the production and subsequent release of latent heat is explicitly taken into account, a simple model that couples a non-conserved order parameter to the temperature field is studied. After giving the basic equations for this "phase-field model", recent results are reviewed including two qualitative different (diffusion-limited and kinetics-limited) regimes of crystal growth and critical behaviour at the boundary between these two regimes.

6.1. Phase field model: introduction

In the simple *order-parameter model* of chapter 5, the temperature field is assumed to be uniform and constant, meaning that temperature variations due to the release of latent heat produced by freezing are ignored. Models with a non-conserved order-parameter account for various microscopic properties of the solidification process, such as the finite width of the solid–liquid interface and the deviations from thermodynamic equilibrium that drive the interface forward. They typically predict that planar fronts will propagate at a constant velocity v that is proportional to the undercooling.

By contrast, in *diffusion models*, the basic variable is the temperature field [271,272]. Although the release and subsequent diffusion of latent heat are both properly accounted for, the various microscopic features of the order-parameter models are ignored: the interface is assumed to be sharp and in local equilibrium. In contrast with the first kind of model, steady-state motion is in general impossible, but the typical asymptotic state has a front velocity decaying with time t as $t^{-1/2}$.

The ingredients of these two models can be combined by coupling an order parameter to the temperature field. This *phase-field model* was studied in the context of crystal growth by Collins et al. [273,274] and [275], and later also by Umantsev and Roitburd [276,277], Schofield and Oxtoby [278], as well as Löwen et al. [279–281], Kupfermann et al. [282], and Charach and Zaltzman [283]. The interest in this more detailed model is that it describes both diffusion- and kinetics-limited front motion in a single set of coupled equations. In addition, there are also new effects, not predicted by either of the simpler models.

6.2. The phase-field model: basic equations

Adopting the same notation as in the previous chapter, the order-parameter field, $m(z,t)$, is zero in the liquid and one in the solid at the solid–liquid coexistence temperature T_0. The temperature field $T(z,t)$ can also be scaled to be dimensionless by L/c_p, where L is the latent heat of fusion per mole and c_p is the specific heat for constant pressure at coexistence which for simplicity is

assumed to be equal in the two phases. The dimensionless-undercooling field, then, is

$$u(z,t) = c_p(T(z,t) - T_0)/L. \tag{148}$$

If one considers a solid front advancing into a liquid held at a temperature $u = -\Delta$, the latent heat released is just enough to transform the undercooled liquid into solid at the coexistence temperature when $\Delta = 1$. If $\Delta < 1$, then excess heat must be transported away from the interface. If $\Delta > 1$, the growing solid will be cooler than it would be at coexistence with the liquid.

In the phase-field model, the equation of motion for the dimensionless temperature field $u(z,t)$ is

$$\partial u/\partial t = D_T \partial^2 u/\partial z^2 + \partial m/\partial t. \tag{149}$$

Here, D_T is the thermal diffusivity, assumed to be identical in both phases and independent of temperature. Equation (149) describes the diffusion of heat, with the $\partial m/\partial t$ term acting as a source for the heat field due to the latent heat of crystallization.

On the other hand, the equation of motion for the non-conserved order-parameter field $m(z,t)$ is

$$\partial m/\partial t = -\Gamma_n \delta \Sigma[m,u]/\delta m. \tag{150}$$

The surface tension functional $\Sigma[m,u]$ is scaled by $\Delta k_B T_0/A$, where A is the cross-sectional area of the interface, and Δ is an energy (in units of $k_B T_0$) and is thus given by

$$\Sigma[m,u] = \int_{-\infty}^{\infty} \mathrm{d}z \, \{\tfrac{1}{2}\xi_m^2[\partial m(z,t)/\partial z]^2 + f[m(z,t),u(z,t)]\} \tag{151}$$

where ξ_m is a microscopic bulk correlation length. The local free-energy density $f(m,u)$ is

$$f(m,u) = f_0(m) + \tfrac{1}{2}\delta u m \tag{152}$$

where $f_0(m)$ is the local free energy density at coexistence and $\frac{1}{2}\delta u m$ is the first term in a temperature expansion around $T = T_0$. The coefficient δ can be shown to be related to the latent heat L as

$$\delta = (2/\lambda)(L/k_B T_0)(L/c_p T_0). \tag{153}$$

The local free energy density $f_0(m)$ must have equal quadratic minima at $m = 0$ and $m = 1$. As in section 5.2, one may consider two different forms for $f_0(m)$ which have this property, the *Ginzburg–Landau* model, $f_0(m) = m^2(m-1)^2$, and the *parabolic* model, $f_0(m) = \frac{1}{2}\min[m^2, (m-1)^2]$.

Defining the length scale is $z_m \equiv \sqrt{2}\xi_m$. and the time scale $\tau_m \equiv 1/\Gamma_n$, which leads to a velocity scale, $v_m = z_m/\tau_m$, the rescaled equations (149) and (150) read

$$u_t = (1/2p)u_{zz} + m_t, \tag{154}$$

$$m_t = \tfrac{1}{2}m_{zz} - \mathrm{d}f_0/\mathrm{d}m - \tfrac{1}{2}\delta u. \tag{155}$$

Material properties are now described solely by two dimensionless parameters, δ and p, where

$$p \equiv \frac{\xi_m^2/\tau_m}{D_T}. \tag{156}$$

Note that ξ_m^2/τ_m can be interpreted as an order-parameter diffusion constant, denoted by D_m, so that p equals a ratio of diffusion constants $p = D_m/D_T$.

To fix the *boundary conditions*, we need to know four values: $m_\pm \equiv m(\pm\infty, t)$ and $u_\pm \equiv u(\pm\infty, t)$. We first require local equilibrium at $z = \pm\infty$, which gives two equations relating $m_\pm$ and $u_\pm$:

$$df_0/dm|_{m_\pm} = -\tfrac{1}{2}\delta u_\pm. \tag{157}$$

We could obtain the other two equations by fixing the temperature at $z = \pm\infty$, so that $u_\pm = -\Delta$. One would then study the growth of a solid germ that has nucleated at $z = 0$ and one would obtain $m_\pm$ by solving the algebraic equation (157).

For numerical convenience, one can also consider "steady-state" boundary conditions, where a semi-infinite amount of solid has already been created. We retain $u_+ = -\Delta$ but adopt conditions at $z = -\infty$ which specify the state of the solid. One can show that for constant-velocity fronts [278]

$$u_+ - m_+ = u_- - m_-. \tag{158}$$

Along with (157), (158) suffices to fix $u_\pm$ and $m_\pm$.

One can also consider "coexistence" boundary conditions [281], where one takes, in place of (158)

$$u_- = 0, \quad m_- = 1. \tag{159}$$

In this case, the solid is created at equilibrium. For a unique undercooling Δ_c, both the steady-state and coexistence boundary conditions are identical. For $\delta \to 0$, one has $\Delta_c = 1$. In the phase-field model, the δu term implies that the m-value of the minimum of the liquid depends slightly on the undercooling via (157). In particular, m will be positive in the metastable liquid phase if the liquid is undercooled. This means that Δ_c is slightly smaller than 1 and is a function of δ. Since for $\Delta = \Delta_c$, the amount of heat generated by freezing is just enough to heat the liquid back up to the coexistence temperature, we refer to this as *unit undercooling.*

Explicitly, combining eqs. (157) and (159), one finds for the Ginzburg–Landau model that $\Delta_c = 1 - (1 - \sqrt{1 - 2\delta})/4$ whereas in the parabolic model $\Delta_c = 1/(1 + \delta/2)$.

Physically one can now understand why one expects to see different kinds of freezing behaviour for small undercoolings ($\Delta < \Delta_c$) and for large undercoolings ($\Delta > \Delta_c$). In the former case, let one start with an entirely liquid sample. Then imagine that it is all converted to solid without the latent heat diffusing anywhere. The release of latent heat raises the temperature by Δ_c. This temperature rise, however, exceeds the original undercooling of the liquid. Were the heat truly to stay put and not diffuse, then the solid created would be superheated. The true equilibrium, in fact, requires that some of the heat be transported away to infinity and that the solid be at the coexistence temperature. Since the transport of heat to infinity is via diffusion, the front slows down via $v(t) \propto t^{-1/2}$.

By contrast, if $\Delta > \Delta_c$, the heat is not sufficient to raise the temperature of the solid back up to coexistence. The solid is then below its coexistence temperature, a thermodynamically stable situation. Since no heat needs to be transported out to infinity, solidification is limited only by the kinetics of transforming liquid to solid, and fronts travel at constant velocity.

The case $\Delta = \Delta_c$, where the latent heat is just enough to reheat the solid back to T_0 is a special point that divides the diffusion-limited from the kinetics-limited regimes. In this case, the phase-field model predicts *two types of behaviour* at Δ_c, depending on p: for $p > p_c$, there is a steady state solution, while for $p < p_c$ the velocity decays with an $-1/3$ power law $v(t) \propto t^{-1/3}$. Here, p_c is a critical value of p which depends on the coupling δ.

A final remark concerns the applicability of the phase field model to alloys. This was extensively discussed by Löwen et al. [281] and also by Wheeler et al. [284]. In this case, the temperature field has to be replaced by the concentration field of impurities. The equations formally are the same, but the parameters p, δ and Δ have another meaning and will be significantly different for inpurity-driven systems. There is also the attractive possibility of tuning δ by varying the impurity concentration.

6.3. *Phase-field model: review of results*

The original interest in the phase-field model for crystallization came mainly from an inadequacy of the purely diffusive model, with its sharp interface held at local equilibrium $u = 0$. This model implies that for $\Delta < 1$, fronts slow down via a $t^{-1/2}$ power law [285]. For $\Delta > 1$, the model has no solution. The latent heat will increase the temperature of the solid by 1 at most; this is inconsistent with the requirement that $u = 0$ at the interface. At $\Delta = 1$, the front will travel at a constant but indeterminate velocity [272]. Although there are three qualitatively different regimes in this model, the model breaks down when $\Delta \geq \Delta_c = 1$ For $\Delta \ll \Delta_c$, however, it is perfectly satisfactory.

The diffusive model may be improved by adding a phenomenological description of kinetics. Instead of assuming that the solid–liquid interface is at $T_i = T_0$, one sets the interface temperature to $T_i = T_0 - \beta^{-1}v$, where v is the interface velocity and β is known as a kinetic coefficient [286, 287]. In this model, fronts with $\Delta < 1$ slow down via a $t^{-1/2}$ power law, as before. For $\Delta > 1$, fronts travel at constant velocity $v \propto (\Delta - 1)$ The model thus gives sensible results for both $\Delta < \Delta_c$ and for $\Delta > \Delta_c$.

The phase-model provided another solution to the velocity-degeneracy problem of the pure diffusion model. Both Langer [275] and Collins and Levine [273] showed that the phase-field model has a unique, constant-velocity solution at unit undercooling which is selected by microscopic order-parameter kinetics. The lack of such microscopic length and time information leads to the velocity degeneracy in the diffusive model. The phase-field model reduces to the diffusive model with linear kinetics when $\delta \to 0$ and $p/p_c \to 0$, where the order parameter profile becomes essentially a step function and the heat or impurity field obeys the standard (uncoupled) diffusion equation. The most thorough discussion is by Caginalp [288].

Schofield and Oxtoby [278] then found that the $\Delta = \Delta_c$ steady-state solutions to the phase-field model discovered by Langer [275] and Collins and Levine [273] exist only for certain values of the material parameters p and δ. In particular, for $p < p_c(\delta)$, there are no steady-state solutions. They evaluated p_c perturbatively for small δ in the Ginzburg–Landau model and found $p_c = 2/(3\delta)$. Löwen et al. [279] then repeated the calculations of Schofield and Oxtoby for the parabolic model and found similar results. The advantage is that, in the parabolic model, the velocities and steady-state profiles can be calculated *analytically*. For example, $p_c(\delta)$ is exactly $2/(3\delta)$. Subsequently, Löwen and Bechhoefer [280] explored the effect of different values of Δ in the parabolic model. The steady state theory can be done analytically. If there is a steady state velocity v, it must satisfy the equation

$$1 - \Delta\delta = 4 \sum_{\mathrm{Re}\, x_j<0} \left[(x_j + 2pv) \left(x_j \prod_{i \neq j} (x_j - x_i) \right)^{-1} \right], \tag{160}$$

where $\{x_j, j = 1, 2, 3\}$ are the complex roots of the cubic equation

$$x^3 + 2v(p + 1)x^2 - 2(1 - 2pv^2)x - 2pv(2 + \delta) = 0. \tag{161}$$

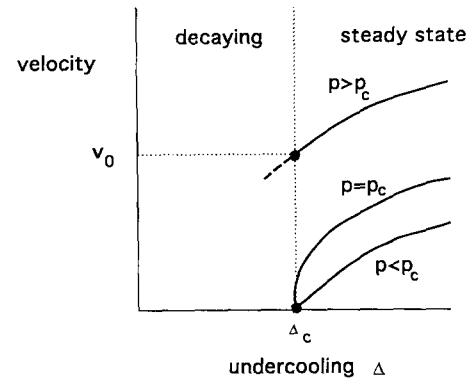

Fig. 6.1. Summary of the asymptotic behaviour of the phase-field model: velocity versus undercooling. For undercoolings $\Delta < \Delta_c$, fronts slow down with an asymptotic behaviour $v(t) \propto t^{-1/2}$, whereas for $\Delta > \Delta_c$, the fronts approach a steady-state velocity v. In the steady-state regime, there are three cases: (1) If $p < p_c$, near unit undercooling, the steady-state velocity is given by $v \propto (\Delta - \Delta_c)$. (2) If $p = p_c$, then $v \propto (\Delta - \Delta_c)^{1/2}$. (3) For $p > p_c$, the steady-state velocity is finite at Δ_c. At Δ_c and $p \leq p_c$, the velocity decay follows a $t^{-1/3}$ power law. Finally, for $p > p_c$, there are stable steady-state solutions even for $\Delta < \Delta_c$, which are shown as a heavy dashed line.

The main result of an analysis of (161) is a transition from a steady state to a diffusive regime at $\Delta = \Delta_c$ with the following scaling properties:

(i) *Above* the borderline, $\Delta > \Delta_c$, there is a nonzero steady state velocity v. Fronts approach their steady state value exponentially, i.e. $v(t) = v + A\exp(-t/\tau)$ where A and τ depend on Δ, p and δ. Near the borderline, $\Delta \gtrsim \Delta_c$, there are different scaling laws for v in $\Delta - \Delta_c$:

- For $p > p_c(\delta)$, v remains nonzero at Δ_c.
- For $p = p_c(\delta)$, v scales as $(\Delta - \Delta_c)^{1/2}$.
- For $p < p_c(\delta)$, v scales as $(\Delta - \Delta_c)$.
- At one special point $(\delta_0, p_0, \Delta_0) \equiv (\frac{4}{3}, \frac{1}{2}, \frac{3}{5})$ in (δ, p, Δ) parameter space, called *critical point*, v scales as $(\Delta - \Delta_c)^{1/3}$.

(ii) *Below* the borderline, $\Delta < \Delta_c$, there are two cases.

- For $p \leq p_c(\delta)$, there is a decaying velocity $v(t) \propto t^{-1/2}$.
- For $p > p_c(\delta)$, and for small $\Delta_c - \Delta$, there are dynamically stable steady-state solutions which lead to the creation of a *metastable* solid. At some undercooling $\overline{\Delta}_c < \Delta_c$ these solutions have a finite velocity v and then cease to exist. There is a crossover with a *velocity jump* from a steady state solution to a solution with decaying velocity $v(t) \propto t^{-1/2}$.

(iii) *On* the borderline, $\Delta \equiv \Delta_c$, there are three cases:

- For $p > p_c(\delta)$, there is a steady state solution with finite velocity.
- For $p = p_c(\delta)$, v is decaying $\propto t^{-1/3}$ as long as $\delta < \delta_0$ while for $\delta > \delta_0$ v is finite.
- For $p < p_c(\delta)$, v is decaying $\propto t^{-1/3}$. This *1/3-exponent* was proved by Marder [289] (for the derivation of this exponent in the diffusive model with linear kinetics, see also ref. [290]).

The asymptotic behaviour of the crystal growth velocity in the phase-field model is summarized in fig. 6.1, which shows the velocity versus undercooling, a plot that is typically encountered in experiments where one varies the undercooling [291, 292].

Complementary to these analytical results, numerical simulations of the Ginzburg–Landau form of the phase-field model equations were performed by Löwen et al. [281]. Typical profiles of $m(z,t)$ and $u(z,t)$ for different times t are shown in fig. 6.2. The interface starts to move but the produced latent heat diffuses more and more away, thus hindering crystal growth.

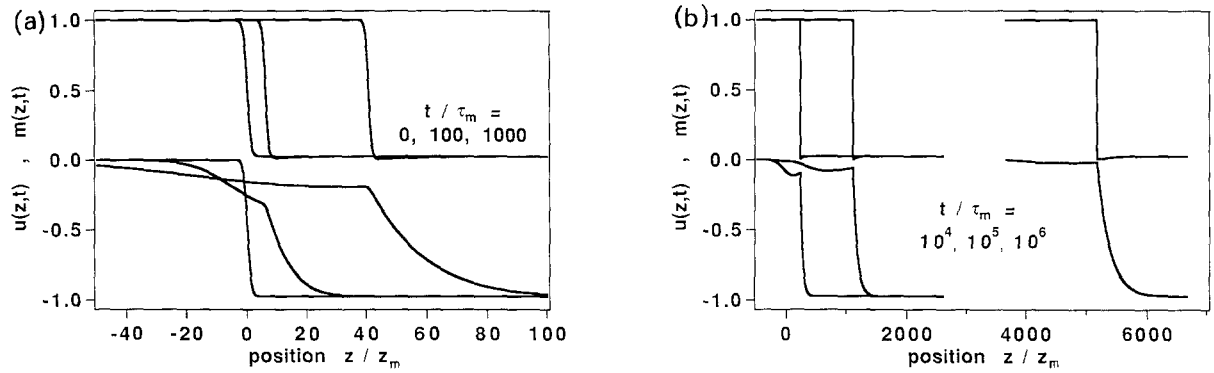

Fig. 6.2. Evolution of the order parameter $m(z,t)$ and heat field $u(z,t)$. The material parameters are $p/p_c = 0.1$ and $\delta = 0.1$. The undercooling is $\Delta = \Delta_c$. In both (a) and (b), the upper curves denote m and the lower ones u. The horizontal positions of the different curves show the overall displacement of the front at times $t/\tau_m = 0$, 100, and 1000 in (a) and $t/\tau_m = 10^4$, 10^5, and 10^6 in (b). The z-axis is scaled by z_m, the microscopic order-parameter length scale and the time by τ_m, the microscopic order-parameter time scale. From ref. [281].

A sensitive quantity to detect different power laws in the velocity decay is the time-dependent decay exponent $\nu(t)$, defined by

$$\nu(t) = \mathrm{d}\log_{10} v(t)/\mathrm{d}\log_{10} t = ta(t)/v(t) \tag{162}$$

where $a(t) \equiv \mathrm{d}v(t)/\mathrm{d}t$ denotes the interface acceleration. $\nu(t)$ is shown for different undercoolings Δ in fig. 6.3. Note the logarithmic axis in time. For $\Delta > \Delta_c$, $a(t)$ becomes zero, since there is a steady state solution. At $\Delta = \Delta_c$, there is a plateau at $\nu = 0.30$ with a very long-lived transient which prevents rapid appearance of the asymptotic state where $\nu = 1/3$. Finally, in the diffusive regime $\Delta < \Delta_c$, $\nu(t)$ saturates at $1/2$.

To summarize, there are three qualitatively new features inherent in the phase-field model: the $1/3$ power-law decay at $\Delta = \Delta_c$, the jump from a non-zero velocity steady-state solution to

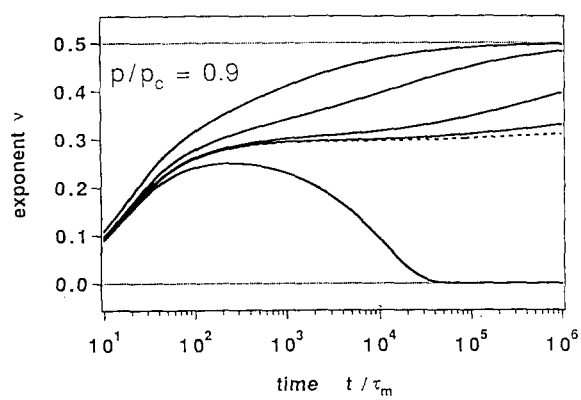

Fig. 6.3. The evolution of the velocity decay exponent ν for different undercoolings. From top to bottom, the undercoolings are $\Delta/\Delta_c = 0.9240$, 0.9753, 0.9959, 0.9994, 1.000, 1.027. The heavy dashed line is the $\Delta = \Delta_c$ curve. The material parameters are $p/p_c = 0.9$ and $\delta = 0.1$. From ref. [281].

a diffusive solution when $p > p_c$, and the critical point. All these features have not yet been detected in growth experiments. An estimation of material parameters, however, shows [281] that the boundary between the kinetics-dominated and the diffusive regime should be accessible for impurity-driven systems. Thus there are good reasons to believe that some of the new predictions of the phase-field model are verified experimentally in near future.

7. Kinetic glass transition and colloidal suspensions

As a common experience, liquids can be easily undercooled until to a certain temperature where they freeze into a glass where the particles are practically trapped into the cages formed by their nearest neighbours. This kinetic glass transition is not connected with a true thermodynamic phase transition but manifests itself as a sharp crossover with qualitative different dynamical relaxation of density perturbations. Since dynamics are different for atomic and colloidal systems, the relaxational scenario is – at least a priori – different, too. In this chapter we discuss similarities and differences of the kinetic glass transition in atomic and colloidal liquids.

7.1. Kinetic glass transition for atomic liquids

7.1.1. General

The relaxation time of a density perturbation in a supercooled liquid was studied as early as 1863 by Maxwell who defined a relaxation time τ_M as

$$\tau_M = \eta / G_\infty \tag{163}$$

where η is the shear viscosity and G_∞ the high frequency shear modulus of the liquid. The latter barely varies with temperature and is of the order of 10^{10} Pa. One can roughly define a glass transition by fixing τ_M to be a long experimental time, say $10^2 s$. This then corresponds to a viscosity of 10^{12} Pa s $= 10^{13}$ poise which is the usual definition of the glass transition point. Evidently, this definition is arbitrary. Experimentally, due to the finite time window of observation, it is often connected to an almost discontinuous behaviour of the measured specific heat since some degrees of freedom seem to be frozen. The scenario for this glass transition also depends on the cooling history and so there is no reproducible underlying sharp glass transition. In this section, we shall restrict ourselves to a dynamical phenomenon well above the "calorimetric" glass transition temperature which occurs at about $\eta \simeq 10^2$ poise where *fragile* glass formers show a significant deviation from the Arrhenius behaviour $\eta \sim \exp(-A/T)$, see the classification of Angell [293]. This behaviour is intrinsic, i.e. it does not depend on the cooling history, and may be called *kinetic glass transition*. However, one should bear in mind that it is not a sharp transition. One can also call it a change in the dynamical behaviour of a supercooled liquid well above the calorimetric glass transition. The important question concerns the microscopic origin of the deviation from the Arrhenius law. On the other hand, *strong* glass formers (like window glass) have already strong bondings in the supercooled liquid and their viscosity follows an Arrhenius law over several decades [293]. Consequently, there is no "kinetic glass transition" for strong glass formers.

These observations indicate that the kinetic glass transition has *dynamical* origin. There are also some changes in the statics of higher-order correlation functions, see e.g. ref. [294], but the pair structure is very much similar to that of an ordinary supercooled liquid. Thus, from studying the structure factor $S(k)$ alone, one cannot decide whether a given material is liquid- or glassy-like.

7.1.2. Experiments

In principle, dielectric relaxation methods, nuclear magnetic resonance, quasi-elastic light and inelastic neutron scattering experiments provide data for the time-dependent density autocorrelation function $F_d(k,t)$ respectively its spectrum $S_d(k,\omega)$ (see eq. (63)), which are the dynamical key quantities in studying the density relaxation near the kinetic glass transition. The technical problem is that simple atomic materials do crystallize on the experimental time-scale, they can hardly be undercooled sufficiently. Therefore, experiments have usually been performed at much more complex multi-component liquids. One relatively simple ionic fragile glass former is represented by a molten salt like $Ca_{0.4}K_{0.6}(NO_3)_{1.4}$ that was studied in detail by Mezei and collaborators [295, 296] and for which there are also simple expressions for the pair potential [297]. These measurements give excellent data over a broad time window. Two important features of the dynamical correlation functions are *scaling* and *stretching* near the kinetic glass transition. Scaling means that a set of correlation functions measured at different temperatures fall on a universal Master curve after a suitable scaling of the time. Stretching implies that the correlations function decays as a stretched exponential for large times $\sim \exp(-(t/t_0)^\nu)$, with an exponent $\nu < 1$ (Kohlrausch-law)

7.1.3. Mode coupling theory

The mode coupling approach is extensively reviewed by Götze [298] and Götze and Sjögren [299], also in connection with experiments. The starting point is the exact generalized Langevin equation for the normalized density autocorrelation function $\Phi(k,t) \equiv F_d(k,t)/S(k)$, see eq. (63), which can be cast in the form of the equation of motion for a damped harmonic oscillator

$$\ddot{\Phi}(k,t) + \gamma(k)\dot{\Phi}(k,t) + \Omega^2(k)\Phi(k,t) + \int_0^t \mathrm{d}t'\, M(k,t-t')\dot{\Phi}(k,t') = 0. \tag{164}$$

Here, $\gamma(k)$ is an instantaneous friction coefficient and $\Omega^2(k) = (k_B T k)^2/S(k)m^2$. The last term in (164) describes the retarded friction characterized by a memory kernel $M(k,t)$. In MCT, this kernel is approximated by a form quadratic in $\Phi(k,t)$ providing a closed set of equations with a nonlinear feedback mechanism.

By varying a control parameter, e.g. the density or the temperature, the nonlinear feedback leads to a bifurcation from a solution $\Phi(k,t)$ that decays to zero at long times to a solution that tends asymptotically to a constant $\Phi(k, t \to \infty) = \xi_k$, referred to as the Edwards–Anderson order parameter [300]. In other words, there is a transition from an ergodic to nonergodic behaviour at a certain sharp temperature T_0. This is called *ideal glass transition* which is directly connected with ergodicity breaking. Close to T_0, MCT predicts a two-step relaxation of $\Phi(k,t)$: a β-relaxation at "intermediate" times and a final α-relaxation, which obey *scaling* laws in $T - T_0$ with nonuniversal exponents.

However, MCT in its simplest form ignores thermal activated hopping processes that finally restore ergodicity. Strictly speaking an ideal glass transition does not exist. In a more extended version of MCT, Das [301] included this mechanism approximately and found a smeared transition. The resulting continuous behaviour unfortunately suppresses any clearcut diagnostics of the kinetic glass transition as in its ideal counterpart.

7.1.4. Molecular Dynamics (MD) simulations

The time-dependent correlation functions discussed in section 1.5.3 provide a dynamical diagnostics of the kinetic glass transition and are also accessible by Molecular Dynamics simulations.

However, for present day computers, one is still limited in the time window. The maximum time one can span is typically about 1000–10 000 times a typical microscopic time. Nevertheless in this time window MD simulations have provided "exact" data for simple supercooled atomic liquids, necessary for a detailed discussion of the decay scenario of density fluctuations. For a summary and extensive discussion of MD computer simulations at the kinetic glass transition, we refer to the review article of Barrat and Klein [302].

MD simulations have revealed that the kinetic glass transition is connected with a crossover between two different microscopic dynamical relaxations: hydrodynamic relaxation by collective diffusion as in usual liquids and relaxation by thermal activated jump processes. Then, as the temperature is lowered further, there is a separation of time scales between short time relaxation (phonons) and the so-called α-relaxation. The former can be thought of as a particle rattling in the cage formed by its nearest neighbours, the latter is related to thermal activated jumps and gives rise to a stretched exponential Kohlrausch decay. Between these two processes there may be a further relaxation, called β-relaxation, which can be attributed to the relaxation of the particle cages, but its definition and microscopic manifestation is much less clear, although it seems to be accepted now that it is a *localized* relaxation phenomenon. At this stage it may be useful to point out that simulations of Ernst et al. [303] and Dasgupta et al. [304] indicate that there is no diverging correlation length near the kinetic glass transition.

7.2. Kinetic glass transition for colloidal liquids

7.2.1. Experiments

Using dynamical light scattering, van Megen and coworkers [305–309] measured the time-dependent density autocorrelation function over a broad time window for a sterically stabilized colloidal suspension as a function of the packing fraction of the particles. Despite the enormous differences in timescales between atomic and mesoscopic glass formers, the supercooled colloidal liquid exhibits qualitative features very similar to that of an atomic liquid at the kinetic glass transition. The advantage for interpretation is that the experimental system is a rather simple: it represents a hard-sphere-like system with a small polydispersity.

Also the relaxation of spherical polystyrene micronetwork particles of mesoscopic size, swollen in a good solvent, was recently measured over a very broad time-window by Bartsch and coworkers [310–312], representing another type of colloidal suspension. The samples are a bit more polydisperse ($p_\sigma = 0.16$) than that used by van Megen and coworkers. Again the long-time relaxation was found to be very much similar to that of simple atomic liquids. Charge-stabilized colloidal suspensions also form glasses; experimental studies at the glass transition were done by Sirota et al. [313] and Meller and Stavans [314]. In the latter references, however, only static properties were investigated.

7.2.2. Mode coupling theory

The experimental results of van Megen and Pusey [306] were compared with predictions of mode coupling theory for a hard sphere system by Götze and Sjögren [315] and by Fuchs et al. [316]; good agreement was found between mode coupling theory and the experimental data. In the comparison, however, some fitting parameters were involved as e.g. the packing fraction of the (ideal) glass transition, i.e. the glass transition point is not an output but an input in the comparison. The fitted time-dependent density autocorrelation function is simply monotonically decaying and has no particular structure. However, one should not forget that the fits extends over several decades in time such that the agreement supports mode coupling theory.

The MCT was originally derived for Molecular Dynamics. It was shown explicitly by Szamel and Löwen [46] that the asymptotic predictions of MCT do not change for Brownian Dynamics. Hence, within MCT, the asymptotics of the density relaxation are universal with respect to the short-time dynamics. For example, the ideal glass transition occurs at the same temperature for MD and BD.

7.2.3. Brownian Dynamics (BD) simulations

Löwen et al. [317] performed an extensive simulation for a charge-stabilized polydisperse colloidal suspension near the kinetic glass transition for both BD and MD. So, a direct comparison of the density relaxation for both kind of dynamics could be made. To date this is the only simulation for the kinetic glass transition which takes solvent friction into account.

In ref. [317], a charge-polydisperse colloidal fluid, described by the potential

$$V_{ij}(r) = U_0 \frac{a}{r} \frac{Z_i Z_j}{\bar{Z}^2} \exp[-\kappa^*(r-a)/a)] \tag{165}$$

is chosen as a model system. U_0 sets the energy and a the length scale. $\kappa^* \equiv 7$ and $\rho \equiv a^{-3}$ are fixed. The system is then cooled from a temperature $T^* \equiv k_B T/U_0 = 0.45$ down to $T^* = 0.10$. The charge-distribution $P(Z)$ is taken to be a Schultz distribution with relative charge-polydispersity $p_Z = 0.5$. The characteristic time scales for BD and MD are $\tau_B = \xi a^2/U_0$ and $\tau_N = \sqrt{ma^2/U_0}$ in the BD/MD case.

As dynamical diagnostics for the kinetic glass transition the relaxation of the self part of the van Hove function, $G_s(r,t)$, can be used. As discussed in section 1.5.3 (see eq. (59)), $G_s(r,t)$ gives the probability distribution to find a particle after a time t at a distance r from the origin provided it was at the origin at time $t = 0$. In a normal liquid, $G_s(r,t)$ approaches rapidly (i.e. after few τ_N or τ_B) an exponential $\cong (4\pi D_L t)^{-3/2} \exp(-r^2/4D_L t)$ where D_L is the long time diffusion constant. As the system is gently cooled down further, there is a sudden drastic change in the relaxation. The function $r^2 G_s(r,t)$ shows now the buildup of a secondary peak roughly at a mean particle distance a whereas the position of the first peak remains frozen over "long" (i.e. $100\tau_B, \tau_N$) times. For Newtonian Dynamics, this function is shown for two different temperatures in fig. 7.1.

This gives a first indication that hopping processes do occur. Of course this qualitative change occurs gradually in a smooth manner but still in a relatively narrow temperature interval and it can be used to determine an estimate for the kinetic glass transition which is now microscopically connected with a change in the relaxation behaviour from hydrodynamic relaxation to relaxation by thermal activated jumps. Remarkably, the temperature interval in which this dynamical crossover occurs is the same for BD and MD. Also, the buildup of the secondary peak is present in BD, indicating that there is the *same* crossover to thermal activated jumps in the Brownian case. By this diagnostics one may estimate the temperature for the kinetic glass transition for both MD and BD to be within

$$0.115 < T^*_{\text{glass}} < 0.12. \tag{166}$$

The long time diffusion constant drops to very small values near T^*_{glass} and a power law with a small residual contribution ΔD due to jumps fits well the data of the supercooled liquid

$$D_L(T) = \Delta D + A(T - T^*_{\text{glass}})^\gamma \tag{167}$$

with $\gamma \approx 1.4$ for *both* BD and MD.

Another interesting quantity is the distinct part of the van Hove function, $G_d(r,t)$, defined in eq. (58), giving the probability distribution to find a particle at a distance r from the origin after a

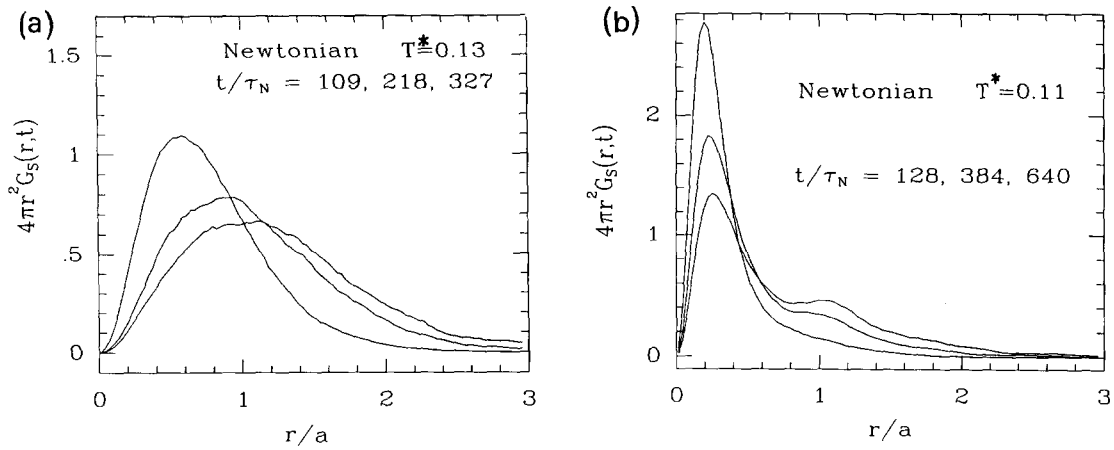

Fig. 7.1. Self part of the van Hove function, $G_s(r,t)$, multiplied by $4\pi r^2 a$ versus reduced distance r/a calculated with Newtonian dynamics; the curves from left to right (or top to bottom) are for increasing time arguments. (a) Results for $T^* = 0.13$ and $t^* = t/\tau_N = 109, 218, 327$. (b) Results for $T^* = 0.11$ and $t^* = 128, 384, 640$. From ref. [317].

time t provided *another* particle was at the origin at $t = 0$. At the kinetic glass transition, it turns out, again both for BD and MD, that a peak at $r = 0$ is built up giving again strong evidence for particle exchange hopping processes. In a dense supercooled liquid, however, these processes are more complicated than simple pair exchanges. In general, more than two particles (small clusters of particles) participate to a real position exchange process, see e.g. ref. [318].

Other interesting quantities are the spatial and time Fourier transformations of $G_s(r,t)$ and $G_d(r,t)$, denoted by $F_s(k,t)$, $F_d(k,t)$ respectively $S_s(k,\omega)$, $S_d(k,\omega)$, see eqs. (62) and (63). In fig. 7.2, $F_s(k,t)$ is plotted as a function of time t an a logarithmic scale for a fixed wave vector

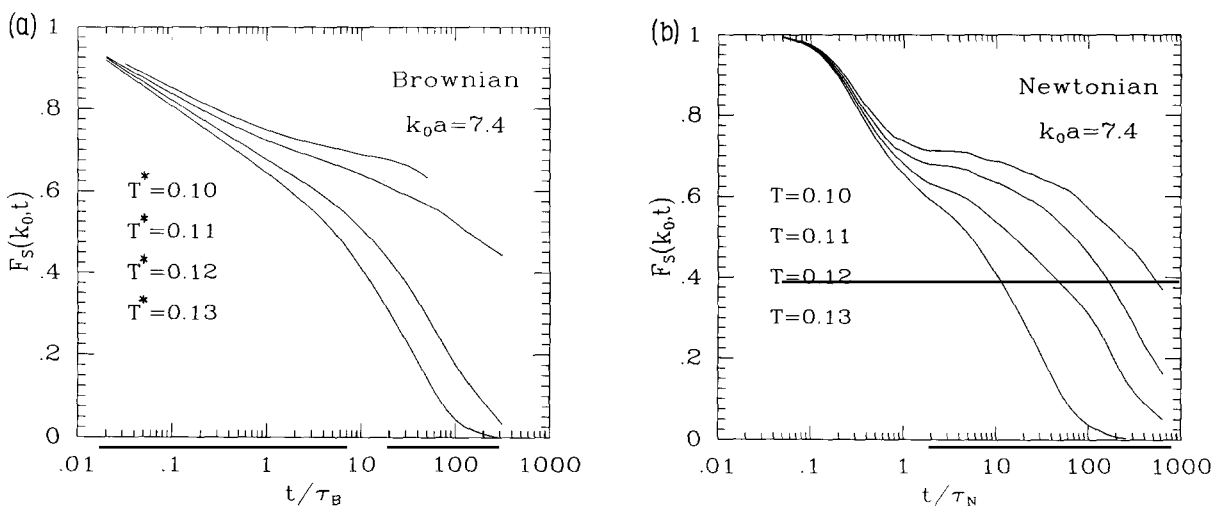

Fig. 7.2. Self part of the density autocorrelation function $F_S(k,t)$ versus reduced time $t^* = t/\tau_N, t/\tau_B$ (on a logarithmic scale) for $k = k_0 = 7.4/a$ and (from bottom to top) $T^* = 0.13$, 0.12, 0.11 and 0.10 (a) Brownian Dynamics; (b) Molecular Dynamics. From ref. [317].

k near the first peak of the static structure factor $S(k)$. From this figure it becomes evident that there are qualitative different relaxations for BD and MD. Of course, for short times t/τ_N, t/τ_B, the decay of the density autocorrelation function is different. As explained in section 1.5.3, it starts with $1 - O(t^2)$ in the MD and with $1 - O(t)$ in the BD case. For very long times, $F_s(k,t)$ and $F_d(k,t)$ can be fitted by a stretched exponential law $\sim \exp(-(t/t_0)^\nu)$, where t_0 is strongly temperature dependent and, as ν, also depends on k. The exponent ν is found to be practically the same for BD than for MD. So the α-relaxation scenario is quite similar. From fig. V7.2 it becomes clear that, for times small compared to α-relaxation but still larger than τ_B, τ_N, there are qualitative differences, i.e. the different short-time behaviour also induces a different crossover to the long-time behaviour. The decay is smoother in the BD-case and there is no clear indication for a buildup of a plateau near T^*_{glass}. (Of course, for smaller temperatures there must be a quasi-plateau.) If one looks at the time Fourier transforms of $F_d(k,t)$ or $F_s(k,t)$ $(ka = 7)$, one finds that there is a shoulder at the corresponding frequency for MD which is missing for BD. It is tempting to call this a β-relaxation and one main conclusion is that the dynamical onset of β-relaxation is qualitatively different for BD and MD. In mode coupling theory, β-relaxation is defined in a different way, namely by an additional scaling law near T^*_{glass} whose asymptotic behaviour can be studied analytically. Again, mode coupling theory predicts no difference for MD and BD in the asymptotic case. The difference obtained in the simulation, however, occurs for smaller times that are not yet in the asymptotic regime.

In ref. [317] the simulation was carried out for a polydisperse system in order to avoid spontaneous crystallization. Although the charge polydispersity is high ($p_Z = 0.5$), a mapping procedure to an effective size-polydisperse reference system [21] shows that the effective size polydispersity is $p_\sigma = 0.13$ which is a value typically encountered in experiments.

Summarizing, the kinetic glass transition manifests itself microscopically as a crossover from hydrodynamic relaxation to relaxation by thermal activated jumps. This crossover is not completely sharp but occurs on a very narrow temperature interval upon cooling. The transition temperature is the same for BD and MD. The dynamical onset of β-relaxation, however, is different. A shoulder in the dynamical structure factor at intermediate frequencies is present for MD but missing for BD. On the other hand, α-relaxation is similar, supporting the prediction of simple mode coupling theory.

7.3. Some further recent developments

7.3.1. Density functional theory of the glass transition

It is tempting to consider simply the phenomenological (e.g. Ginzburg–Landau or Cahn–Hilliard) equations for the relaxation of the density field near the kinetic glass transition instead of starting from microscopic dynamics. For the free energy density functional which enters into these dynamical equations one can use an approximation which describes freezing, see section 3.2. A necessary condition for a glass transition is the existence of secondary local minima in the functional with a glassy structure. For hard spheres, this was recently investigated by Dasgupta [319] and Dasgupta and Ramaswamy [320] using the Ramakrishnan–Yussouff approximation. As minima in the free energy functional they found frozen inhomogeneous structured density distributions. The associated free energy of these glassy states is in general higher than that of the solid state but smaller than that of a homogeneous density distribution characterizing a liquid.

Recently, Lust et al. [321] considered a phenomenological density dynamics based on nonlinear fluctuating hydrodynamics with Langevin random forces in order to address dynamical properties

of the liquid-to-glass transition. In the framework of Ramakrishnan–Yussouff density functional theory they found two-stage relaxation and stretched exponential decay of density correlations. Hence this approach can be considered as being complementary to mode coupling theory where one starts from microscopic dynamics. Still, however, the numerically accessible time-window is rather limited and thus the results have to be considered as preliminary.

7.3.2. Simulation of "complex" models

We have extensively described a Brownian Dynamics study for a polydisperse charged colloidal liquid. This is one step from usual MD designed for simple atomic liquids towards a more realistic description of the interactions and dynamics for real complex glass formers. Along these lines, Dzugutov [322] gives strong evidence of icosahedral ordering near the glass transition in a one-component system with a more complicated pair potential. There are also recent simulations with a realistic interactions for methanol by Sindzingre and Klein [323], and for ortho-terphenyl by Wahnström and Lewis [324].

Baschnagel et al. [325] performed Monte Carlo simulations of a lattice model for a polymer melt. In this model one elementary step consists of moving one polymer segment about a lattice constant and consequently a much larger time-window and smaller statistical error is available for the long-time dynamics than for usual MD or BD simulations where one needs much more tseps for such a movement. One should keep in mind that the Monte-Carlo short-time dynamics is fictitious. The conclusion of section 7.2, however, indicates that the explicit form chosen for the short-time dynamics is irrelevant if one is only interested in qualitative features of the long-time dynamics. This motivates the usage of simplified dynamical models in order to speed up the calculation of the long-time dynamics. This idea was also used by Kob and Anderson [326] who studied a non-deterministic kinetic lattice-gas model to simulate long-time relaxation. Their results essentially support predictions of mode coupling theory. Finally we mention simulational studies which directly focus on ergodicity of supercooled liquids by Thirumalai et al. [327, 328].

8. Conclusions

8.1. Summary

For melting and freezing phenomena in atomic and colloidal systems, various aspects of theory, computer simulation and experiments have been discussed. Both static and dynamical phenomena have been considered of bulk phases and interfaces between two phases. Particular emphasis was put on the following points:

- *Colloidal suspensions* represent excellent realizations of classical Statistical Mechanics systems with many advantages over atomic systems. A direct comparison of the experimental measured structure with predictions from theories and simulations of classical Statistical Mechanics is possible.
- Within the density functional approach, one can construct a theory of *freezing* which is based on the liquid state. Although it is somewhat ad hoc, it works well for strong repulsive potentials and is suitable to calculate bulk phase diagrams as well as the structure of interfaces and other inhomogeneous systems from first principles.
- *Melting* of a solid can be initiated at its surface. Surface melting occurs for quite a large number of different materials. Details of this cooperative phenomenon depend sensitively on the nature of the interparticle forces and on the surface orientation.

- Interfacial kinetics near three-phase coexistence can exhibit some interesting dynamical effects including a splitting instability by which a macroscopic portion of a *metastable phase* can be created.
- *Crystal growth* from its melt is hindered by diffusion of the emerging latent heat which leads to different scaling laws for the growth velocity.
- A supercooled liquid undergoes a *kinetic glass transition* which manifests itself microscopically as a dynamical crossover from hydrodynamic relaxation to a relaxation by thermal activated particle hopping. For long times the relaxation seems to be rather independent of the corresponding short-time dynamics implying that it is quite similar for colloidal and atomic liquids.

8.2. Outlook

In the following some interesting novel trends as well as some open problems in the area of melting and freezing are listed up. Both, simple liquids and more complex liquids (which were beyond the scope of this review) are briefly addressed.

8.2.1. Simple liquids

In a *gravitational field*, colloidal suspensions exhibit a sedimentation density profile. By inversion of this profile one can extract the complete isothermal equation of state [329, 330]. For charged colloids and high salt concentration the experimental density profiles are very similar to that expected for hard spheres although there are still some problems in interpreting the dilute wing of the density profile [331]. Until now there is no theory for the sedimentation dynamics which is also directly accessible in experiment. Also crystallization effects at the bottom of the sedimentation tube are presently investigated.

It is difficult to prepare strict *two-dimensional* systems in nature. Typical examples are rare gas films on graphite. Another promising system results by confining charged colloidal particles between two parallel charged plates. This yields a very good realization of a quasi-2d liquid on a mesoscopic length scale. The great advantage is that real-space methods are applicable, i.e. one can obtain typical particle configurations in real space by direct image processing, see e.g. ref. [332]. Structural and dynamical quantities are well-described by an effective two-dimensional Yukawa potential and two-dimensional Brownian Dynamics [333] and in principle a quantitative comparison with the experimental results is possible. The melting process is fundamentally different in two dimensions since it may be mediated by a hexatic phase with orientational long-range order. With these colloidal model systems, one can hope that the (non-)existence of a hexatic phase is clarified in near future. Also the phase diagram for hard disks is still controversial: the rigorous proof for the non-existence of long-range positional order in 2D-systems [54] does not apply to hard disks. Computer simulational studies for large system sizes are still not conclusive [334, 335] and the validity of density functional theories [64, 81, 336, 337, 108] is a priori unclear.

The two-dimensional analogon to surface melting of a 3d crystal is *line-melting* of a 2D crystal. The existence of this effect seems now to be established in experiments on e.g. low-coverage rare gas layers on graphite [338, 339].

Another question concerns a theory for the *dynamics of a concentrated colloidal suspension* treating properly solvent-mediated hydrodynamic interactions. At present, there is a lot of research focussing on a consistent theoretical explanation for such dynamical effects including the experimental facts.

The validity of the Yukawa pair potential as a model for concentrated charge-stabilized colloidal suspension was recently checked by *"ab initio" simulations* that combine Molecular Dynamics for the macroions and classical density functional theory for the counterions [7, 340, 341]. In

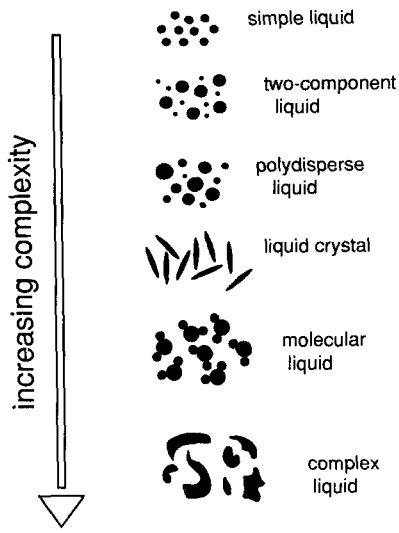

Fig. 8.1. From simple liquids to supramolecular aggregates: different kinds of fluid with increasing complexity (schematic). Since there is no exact measure for complexity, the arrow only gives a general trend.

this adiabatic approach effective counterion-induced many-body forces between the macroions are included. It was found that an effective Yukawa-model reproduces the pair-correlations [342]. In general, however, the Yukawa parameters differ from that of the classic DLVO theory. Much less understood is the influence of a discrete solvent on the effective pair interaction which may be relevant for micellar particles.

Details of the melting process at solid surfaces are still unclear. An interesting question is that of *edge-melting*: a two-dimensional solid surface necessarily has one-dimensional edges and steps. The question is whether the surface melting process is initiated first at this one-dimensional line or whether the solid surface melts as a whole.

8.2.2. Complex liquids

One main focus for future developments will be the extension of theories, simulations and experiments *from simple to more and more complex systems* which have a richer phase diagram with new bulk phases and a correspondingly more complex interfacial behaviour. In this review, we have considered rigid *spherical* colloidal particles. In the direction of increasing complexity, future work should put emphasis on *mixtures* of colloidal spheres, rod-like particles forming liquid crystals, polymers, etc. The increasing complexity is visualized in fig. 8.1. In particular, as regards theory, density functional theory will be used to study the structure and phase diagram of several kinds of liquids with increasing complexity. As the complexity increases, less informations from the liquid state are known, and the constructed functionals become less accurate.

One can prepare binary mixtures of sterically stabilized colloidal suspensions which represent a *two-component hard sphere mixture* characterized by the ratio α of their two diameters and their volume fractions η_A and η_B. The phase diagram of such mixtures depends on these three parameters and is thus much more complicated than that of a simple hard-sphere system. The investigation of the different phases in hard-sphere mixtures is an excellent example of how recent research makes progress involving experiments, computer simulation and density functional theory at the same

time! Detailed experimental data for the phase diagram were obtained for $\alpha = 0.58$ by Bartlett et al. [343], including an AB_2 phase and even an AB_{13} superlattice. The latter phase is familiar in metallic alloys (e.g. $NaZn_{13}$) and consists of a simple cubic lattice of A particles. In the middle of each A-cube, a B-particle surrounded by an icosahedral cluster of other B's is found. The full unit cell consists of eight such sub-cells with neighbouring icosehedra alternating in orientation by 90^o. Extensive computer simulations by Eldridge et al. [344, 345] confirm the existence of this AB_{13} superlattice as a stable bulk phase in the phase diagram even in a region where pure excluded volume considerations would predict a phase separation into a close packed A and B crystal. In parallel, a density functional theory was proposed which reproduced AB_{13} superlattice formation [346].

A strongly asymmetric hard-sphere mixture ($\alpha \to 0$ for fixed η_A and η_B) is a model for sterically-stabilized colloidal particles in a solvent, where the solvent is modelled as small spheres. Computer simulations are extremely difficult for such highly asymmetric models. A liquid integral equation study with the Rogers–Young closure predicts phase separation [347] which is a priori unexpected for a system which is governed by purely repulsive forces. The physical picture is that due to excluded volume effects the small spheres induce an effective attraction between the large spheres. Now experimental research is also looking for this phase separation.

The glass transition in a hard sphere mixture is also non-trivial as a function of α. For $\alpha \simeq 1$ one expects the same scenario as for a simple one-component system. On the other hand, for small α, only the big spheres should freeze into a glassy matrix whereas the smaller spheres remain liquid. Consequently there must be a transition at intermediate α between these two extreme cases. Although there are some mode coupling theory studies [348], it is still an open question whether this transition is continuous and connected to a tunneling probability of the small spheres between the matrix of the large spheres or not.

Finally we mention less recent density functional studies for two-component fluids including hard spheres [349–354], ionic [355–357] and Lennard-Jones mixtures [358].

The next level of complexity consists of multicomponent or polydisperse liquids which was already briefly discussed in section 1.3. Density functional theories for polydisperse hard spheres [359, 360] have been constructed in order to study the influence of polydispersity on the freezing transition.

In *liquid crystals* an additional orientational degree of freedom is present. One has mainly focussed on simple models like hard-rods or hard ellipsoids. We mention e.g. the density functional works of Holyst and Poniewierski [361–365], and others [366–370], as well as the computer simulations of Veerman and Frenkel [371] providing the complete phase diagram of sphero-cylinders. Again, the best characterized experimental systems are colloids ranging from concentrated aqueous suspensions of tobacco-mosaic viruses (TMV) [372] or bacterial fd viruses [373] to cylindrical micellar aggregates and ellipsoidal polystyrene latex particles. Recent experiments, mainly for TMV, have revealed a complex phase diagram with many different liquid-crystalline phases. Theoretically the interaction between charged colloidal rods like TMV has to be described by a Yukawa-segment model [374–376] which is more complicated than that of hard sphero-cylinders. Until now, there are no theoretical and simulational results for the phase diagram of a Yukawa-segment model.

In *molecular liquids*, the molecules can be assumed to be rigid or to exhibit certain internal degrees of freedom. There are extensive Molecular Dynamics simulations and experiments for many different materials. For a density functional study see e.g. ref. [377].

Finally, flexible *supramolecular aggregates*, like micelles or polymers, in general have an even higher degree of complexity if one describes them on a microscopic basis. Usually, one assumes that the length of a polymer chains is much bigger than its diameter which reduces again the complexity.

Polymer dynamics was recently successfully studied by computer simulation, see e.g. ref. [378], and also density functional theory was applied to polymer chains [379].

Summarizing, the application of classical statistical mechanics to complex systems will remain an interesting and important area of future research in order to contact more and more complex molecular and colloidal systems such as paint, milk and ink. One can expect that new structural and dynamical phenomena in complex systems are discovered which then may even lead to important industrial applications.

Acknowledgments

I would like to express my warmest thanks to Jean-Pierre Hansen (Lyon), Paul Madden (Oxford) and Herbert Wagner (München) for a very enjoyable collaboration and many useful discussions. For a productive cooperation and fruitful discussions, I am furthermore grateful to John Bechhoefer (Vancouver), Thomas Beier (München), Thierry Biben (Lyon), Lydéric Bocquet (Lyon), Reinhard Lipowsky (Jülich), Rüdiger Ohnesorge (München), David W. Oxtoby (Chicago), Thomas Palberg (Konstanz), Jean-Noël Roux (Paris), Sarah A. Schofield (Urbana), Rolf Simon (Konstanz), Grzegorz Szamel (Utrecht) and Laurette S. Tuckerman (Austin). I have to thank many colleagues for helpful correspondence and discussions; in particular, I would like to mention Jean-Louis Barrat (Lyon), H. P. Bonzel (Jülich), Jürgen Bosse (Berlin), Alan Denton (Guelph), Siegfried Dietrich (Wuppertal), Gerhard Gompper (München), Wolfgang Götze (München), Robert Holyst (Warsaw), Alberto Meroni (Milano), Patrick Oswald (Lyon), Peter Pusey (Edinburgh), Klaus Schätzel (Mainz), Herbert Spohn (München) and Per Stoltze (Copenhagen). This work is dedicated to Anne.

References

[1] J.A. Barker, R.O. Watts, J.K. Lee, T.P. Shafer, Y.T. Lee, J. Chem. Phys. 61 (1974) 3081.
[2] B.M. Axilrod, E. Teller, J. Chem. Phys. 11 (1943) 229.
[3] M. Tau, L. Reatto, R. Magli, P.A. Egelstaff, F. Barocchi, J. Phys. Cond. Matt. 1 (1989) 7131.
[4] J. Hafner, J. Phys. Condens. Matter 3 (1991) F23.
[5] R. Car, M. Parrinello, Phys. Rev. Lett. 55 (1985) 2471.
[6] B.V. Derjaguin, L.D. Landau, Acta Physicochim. USSR 14 (1941) 633;
E.J.W. Verwey, J.Th. Overbeek, Theory of the Stability of Lyophobic Colloids (Elsevier, Amsterdam, 1948).
[7] H. Löwen, P.A. Madden, J.P. Hansen, Phys. Rev. Lett. 68 (1992) 1081.
[8] W.G. Hoover, F.H. Ree, J. Chem. Phys. 49 (1968) 3609.
[9] W.L. Slattery, G.D. Doolen, H.E. de Witt, Phys. Rev. A 26 (1982) 2255.
[10] M.O. Robbins, K. Kremer, G.S. Grest, J. Chem. Phys. 88 (1988) 3286.
[11] E.J. Meijer, D. Frenkel, J. Chem. Phys. 94 (1991) 2269.
[12] E. Thiele, J. Chem. Phys. 39 (1963) 474.
[13] M.S. Wertheim, Phys. Rev. Lett. 10 (1963) 321.
[14] L. Verlet, J.J. Weis, Phys. Rev. 45 (1972) 939.
[15] D. Henderson, E.W. Grundke, J. Chem. Phys. 63 (1975) 601.
[16] L. Blum, G. Stell, J. Chem. Phys. 71 (1979) 42; 72 (1980) 2212.
[17] P. van Beurten, A. Vrij, J. Chem. Phys. 74 (1981) 2744.
[18] L. Blum, J.S.Høye, J. Stat. Phys. 19 (1978) 317.
[19] B. D'Aguanno, R. Klein, J. Chem. Soc. Faraday Trans. 87 (1991) 379.
[20] B. D'Aguanno, R. Klein, Phys. Rev. A 46 (1992) 7652.
[21] H. Löwen, J.N. Roux, J.P. Hansen, J. Phys. Cond. Matt. 3 (1991) 997.
[22] D.L. Ermak, J. Chem. Phys. 62 (1975) 4189, 4197.

[23] M.P. Allen, D.J. Tildesley, Computer Simulation of Liquids (Clarendon Press, Oxford, 1987).
[24] J.D. van der Waals, Z. phys. Chem. 13 (1894) 657.
[25] R. Evans, Adv. of Physics 28 (1979) 143.
[26] S. Dietrich, in: Phase transitions and Critical Phenomena, Vol. 12, eds C. Domb and J. Lebowitz (Academic Press, London, 1987) p. 1.
[27] R. Lipowsky, Habilitation Thesis, University of Munich, 1987.
[28] H. Dosch, Critical Phenomena at Surfaces and Interfaces, Springer Tracts in Modern Physics 126 (Springer, Berlin, 1992).
[29] J.D. Gunton, M. San Miguel, P.S. Sahni, in: Phase Transitions and Critical Phenomena, Vol. 8, eds C. Domb and J.L. Lebowitz (Academic Press, London, 1983) p. 267.
[30] A.P. Gast, Y. Monovoukas, Nature 351 (1991) 553.
[31] K. Schätzel, B.J. Ackerson, Phys. Rev. Lett. 68 (1992) 337.
[32] F.A. Lindemann, Phys. Z. 11 (1910) 609.
[33] A.R. Ubbelohde, The Molten State of Matter (Wiley, Chicester, 1978).
[34] E.L. Pollock, J.P. Hansen, Phys. Rev. A 8 (1973) 3110.
[35] M.J. Stephens, M.O. Robbins, J. Chem. Phys. 98 (1993) 2319.
[36] D.A. Young, B.J. Alder, J. Chem. Phys. 60 (1974) 1254.
[37] R. Ohnesorge, H. Löwen, H. Wagner, Europhys. Lett. 22 (1993) 245.
[38] M. Ross, Phys. Rev. 184 (1969) 233.
[39] J.P. Hansen, L. Verlet, Phys. Rev. 184 (1969) 151.
[40] Y. Rosenfeld, Phys. Rev. A 24 (1981) 2805.
[41] H. Löwen, T. Palberg, R. Simon, Phys. Rev. Lett. 70 (1993) 1557.
[42] M. Medina-Noyola, Phys. Rev. Lett. 60 (1988) 2705.
[43] R. Klein, W. Hess, in: Ionic Liquids, Molten States and Polyelectrolytes, eds K.H. Bennemann, F. Bouers and D. Quitmann, Lecture Notes in Physics 172 (1982) 199.
[44] G. Nägele, M. Medina-Noyola, R. Klein, J.L. Arauz-Lara, Physica A 149 (1988) 123.
[45] J.-P. Hansen, I.R. McDonald, Theory of Simple Liquids, 1st Ed. (Academic Press, London, 1976) p. 368.
[46] J.A. Leegwater, G. Szamel, Phys. Rev. A 46 (1992) 4999.
[47] H. Löwen, G. Szamel, J. Phys. Condensed Matter 5 (1993) 2295.
[48] B. Cichocki, Physica A 165 (1988) 191.
[49] J.C. McCoy, A.D.J. Haymet, Int. J. Thermophys. 10 (1989) 87.
[50] I. Bhattacharya, U.P. Singh, U. Mohanty, Physica A 175 (1991) 473.
[51] J.M. Kosterlitz, D.J. Thouless, J. Phys. C 6 (1973) 1181.
[52] D.R. Nelson, B.I. Halperin, Phys. Rev. B 21 (1980) 5312.
[53] K.J. Strandburg, Rev. Mod. Phys. 60 (1988) 161.
[54] J. Fröhlich, C. Pfister, Commun. Math. Phys. 81 (1981) 277.
[55] D. Kuhlmann-Wilsdorf, Phys. Rev. 140 (1965) A 1599.
[56] S.F. Edwards, M. Warner, Philos. Mag. 40 (1979) 257.
[57] H. Kleinert, Gauge Fields in Condensed Matter, Vol. II, Stresses and Defects (World Scientific, Singapore, 1989).
[58] T. Yanamoto, T. Izuyama, J. Phys. Soc. Japan 57 (1988) 3742.
[59] R.M.J. Cotterhill, W.D. Kristensen, E.J. Jensen, Phil. Mag. 31 (1974) 245.
[60] F. Lund, Phys. Rev. Lett. 69 (1992) 3084.
[61] J.P. Hansen, I.R. McDonald, Theory of Simple Liquids, 2nd Ed. (Academic Press, London, 1986).
[62] N.D. Mermin, Phys. Rev. 137 (1965) A1441.
[63] J.T. Chayes, L. Chayes, J. Stat. Phys. 36 (1984) 471.
[64] T.V. Ramakrishnan, M. Yussouff, Phys. Rev. B 19 (1979) 2775.
[65] A.D.J. Haymet, D.W. Oxtoby, J. Chem. Phys. 74 (1981) 2559.
[66] J.L. Barrat, J.P. Hansen, G. Pastore, Phys. Rev. Lett. 58 (1987) 2075.
[67] J.L. Barrat, Europhysics Lett. 3 (1987) 523.
[68] P. Tarazona, Phys. Rev. A 31 (1985) 2672.
[69] W.A. Curtin, N.W. Ashcroft, Phys. Rev. A 32 (1985) 2909.
[70] Y. Rosenfeld, D. Levesque, J. Weis, J. Chem. Phys. 92 (1990) 6818.
[71] W.A. Curtin, N.W. Ashcroft, Phys. Rev. Lett. 59 (1987) 2385.
[72] A.R. Denton, N.W. Ashcroft, Phys. Rev. A 39 (1989) 426.
[73] W.A. Curtin, J. Chem. Phys. 93 (1990) 1919.
[74] A.R. Denton, N.W. Ashcroft, Phys. Rev. A 39 (1989) 4701.
[75] R. Leidl, H. Wagner, J. Chem. Phys. 98 (1993) 4142.

[76] W.A. Curtin, K. Runge, Phys. Rev. A 35 (1987) 4755.
[77] J. Percus, J. Stat. Phys. 52 (1988) 1157.
[78] R. Ohnesorge, H. Löwen, H. Wagner, Phys. Rev. A 43 (1991) 2870.
[79] M. Baus, J. Phys. Cond. Matter 2 (1990) 2111.
[80] R. Evans, in: Fundamentals of Inhomogeneous Fluids, ed. D. Henderson (Marcel Dekker, New York, 1992).
[81] P. Tarazona, Mol. Phys. 52 (1984) 81.
[82] M. Baus, J.L. Colot, Mol. Phys. 55 (1985) 653.
[83] M. Baus, J. Stat. Phys. 48 (1987) 1129.
[84] J.F. Lutsko, M. Baus, Phys. Rev. Lett. 64 (1990) 761.
[85] J.F. Lutsko, M. Baus, Phys. Rev. A 41 (1990) 6647.
[86] J.F. Lutsko, Phys. Rev. A 43 (1991) 4124.
[87] T.F. Meister, D.M. Kroll, Phys. Rev. A 31 (1985) 4155.
[88] F. Igloi, J. Hafner, J. Phys. C 19 (1986) 5799.
[89] R.D. Groot, J.P.van der Eerden, Phys. Rev. A 36 (1987) 4356.
[90] C. Ebner, W.F. Saam, D.G. Stroud, Phys. Rev. A 14 (1976) 2264.
[91] C. Ebner, H.R. Krishnamurthy, R. Pandit, Phys. Rev. A 43 (1991) 4355.
[92] Y. Rosenfeld, Phys. Rev. Lett. 63 (1989) 980.
[93] G.L. Jones, S.-C. Kim, J. Stat. Phys. 56 (1989) 709.
[94] M.Q. Zhang, J.K. Percus, J. Chem. Phys. 92 (1990) 6779.
[95] X.C. Zeng, D.W. Oxtoby, Phys. Rev. A 41 (1991) 1219.
[96] A.R. Denton, N.W. Ashcroft, Phys. Rev. A 44 (1991) 1219.
[97] A. Kyrilidis, R.A. Brown, Phys. Rev. A 44 (1991) 8141; 45 (1992) 5654; Phys. Rev. E 47 (1993) 427.
[98] J.A. Cuesta, C.F. Tejero, M. Baus, Phys. Rev. A 45 (1992) 7395.
[99] C.F. Tejero, J.A. Cuesta, Phys. Rev. E 47 (1993) 490.
[100] M. Popovic, M.V. Jaric, Phys. Rev. B 38 (1988) 808.
[101] J.L. Colot, M. Baus, H. Xu, Mol. Phys. 57 (1986) 809.
[102] B.B. Laird, J.D. McCoy, A.D.J. Haymet, J. Chem. Phys. 87 (1987) 5449.
[103] A.D.J. Haymet, D.W. Oxtoby, J. Chem. Phys. 84 (1986) 1769.
[104] A.D.J. Haymet, Phys. Rev. Lett. 52 (1984) 1013.
[105] B. Bagchi, C. Cerjan, U. Mohanty, S.A. Rice, Phys. Rev. B 29 (1984) 2857.
[106] M. Rovere, M.P. Tosi, J. Phys. C 18 (1985) 3445.
[107] H. Iyetomi, S. Ichimaru, Phys. Rev. B 38 (1988) 6761.
[108] X.C. Zeng, D.W. Oxtoby, J. Chem. Phys. 93 (1990) 2692.
[109] Z. Badirkhan, M. Rovere, M.P. Tosi, J. Phys. Condensed Matter 3 (1991) 1627.
[110] C. Likos, N.W. Ashcroft, Phys. Rev. Lett. 69 (1992) 316.
[111] J.L. Barrat, J.P. Hansen, G. Pastore, E.M. Waisman, J. Chem. Phys. 86 (1987) 6360.
[112] A. de Kuijper, W.L. Vos, J.L. Barrat, J.P. Hansen, J. A. Schouten, J. Chem. Phys. 93 (1990) 5187.
[113] X.G. Wu, M. Baus, Mol. Phys. 62 (1987) 375.
[114] B.B. Laird, D.M. Kroll, Phys. Rev. A 42 (1990) 4810.
[115] J.F. Lutsko, M. Baus, J. Phys. Cond. Matt. 3 (1991) 6547.
[116] R. Kesavamoorthy, B.V.R. Tata, A.K. Arora, A.K. Sood, Phys. Lett. A 138 (1989) 208.
[117] S. Sengupta, A.K. Sood, Phys. Rev. A 44 (1991) 1233.
[118] A. Kloczkowski, A. Samborski, J. Chem. Phys. 88 (1988) 5834.
[119] L. Verlet, D. Levesque, Physica 36 (1967) 245.
[120] C. Marshall, B.B. Laird, A.D.J. Haymet, Chem. Phys. Lett. 122 (1985) 320.
[121] W.A. Curtin, N.W. Ashcroft, Phys. Rev. Lett. 56 (1986) 2775.
[122] W.A. Curtin, Phys. Rev. Lett. 59 (1987) 1228.
[123] W.A. Curtin, Phys. Rev. B 39 (1989) 6775.
[124] D.W. Marr, A.P. Gast, Phys. Rev. E 47 (1993) 1212.
[125] D.W. Oxtoby, A.D.J. Haymet, J. Chem. Phys. 76 (1982) 6262.
[126] S.M. Moore, H.J. Raveché, J. Chem. Phys. 85 (1986) 6039.
[127] W.H. Shih, Z.Q. Wang, X.C. Zeng, D. Stroud, Phys. Rev. A 35 (1987) 2611.
[128] W.E. McMullen, D.W. Oxtoby, J. Chem. Phys. 88 (1988) 1967.
[129] H. Löwen, T. Beier, H. Wagner, Europhys. Lett. 9 (1989) 791.
[130] H. Löwen, T. Beier, H. Wagner, Z. Phys. B 79 (1990) 109.
[131] A.J. Bray, M.A. Moore, Phys. Rev. Lett. 49 (1982) 1545.
[132] E. Velasco, P. Tarazona, Phys. Rev. A 36 (1987) 979.

[133] H. Xu, M. Baus, Phys. Rev. A 38 (1988) 4348.
[134] G. Jones, U. Mohanty, Mol. Phys. 54 (1985) 1241.
[135] R. McRae, J.D. McCoy, A.D.J. Haymet, J. Chem. Phys. 93 (1990) 4281.
[136] T.V. Ramakrishnan, Phys. Rev. B 37 (1988) 1936.
[137] M.C. Mahato, H.R. Krishnamurty, T.V. Ramakrishnan, Phys. Rev. B 44 (1991) 9944.
[138] M. Ferconi, M.P. Tosi, J. Phys. Cond. Matt. 3 (1991) 9943; Europhys. Lett. 14 (1991) 797.
[139] S. Sachdev, D.R. Nelson, Phys. Rev. B 32 (1985) 4592.
[140] Y. Singh, J.P. Stoessel, P.G. Wolynes, Phys. Rev. Lett. 54 (1985) 1059.
[141] M. Baus, J.L. Colot, J. Phys. C 19 (1986) L135.
[142] H. Löwen, J. Phys. Cond. Matt. 2 (1990) 8477.
[143] E. Kierlik, M.L. Rosinberg, Phys. Rev. A 42 (1990) 3382.
[144] E. Kierlik, M.L. Rosinberg, Phys. Rev. A 44 (1991) 5025.
[145] J.L. Barrat, H. Xu, J. Phys. Cond. Matt. 2 (1991) 9445.
[146] F. Igloi, G. Kahl, J. Hafner, J. Phys. C 20 (1987) 1863.
[147] J.D. McCoy, S.W. Rick, A.D.J. Haymet, J. Chem. Phys. 90 (1990) 4622.
[148] J.D. McCoy, S.W. Rick, A.D.J. Haymet, J. Chem. Phys. 92 (1990) 3034.
[149] J.D. McCoy, S.W. Rick, A.D.J. Haymet, J. Chem. Phys. 92 (1990) 3040.
[150] A.R. Denton, P. Nielaba, K.J. Runge, N.W. Ashcroft, Phys. Rev. Lett. 64 (1990) 1529.
[151] A.R. Denton, P. Nielaba, K.J. Runge, N.W. Ashcroft, J. Phys. Cond. Matt. 3 (1991) 593.
[152] G. Senatore, G. Pastore, Phys. Rev. Lett. 64 (1990) 303.
[153] S. Moroni, G. Senatore, Phys. Rev. B 44 (1991) 9864.
[154] F. Dalfovo, J. Dupont-Roc, N. Pavloff, S. Stringari, J. Treiner, Europhysics Lett. 16 (1991) 205.
[155] S. Sengupta, C. Dasgupta, H.R. Krishnamurthy, G.I. Menon, T.V. Ramakrishnan, Phys. Rev. Lett. 67 (1991) 3444.
[156] T. Munakata, J. Non-Cryst. Solids 117/118 (1990) 875.
[157] W. Dieterich, H.L. Frisch, A. Majhofer, Z. Physik B 78 (1990) 317.
[158] M. Pokorny, G. Grimvall, J. Phys. F 14 (1984) 931.
[159] C.H. Martin, S.J. Singer, Phys. Rev. B 44 (1989) 477.
[160] R. Kikuchi, J.W. Cahn, Phys. Rev. B 21 (1980) 1893.
[161] G. Ciccotti, M. Guillopé, V. Pontikis, Phys. Rev. B 27 (1983) 5576.
[162] J.R. Broughton, G.H. Gilmer, Phys. Rev. Lett. 56 (1986) 2692.
[163] S.R. Phillpot, J.F. Lutsko, D. Wolf, S. Yip, Phys. Rev. B 40 (1989) 2831.
[164] J. Daeges, H. Gleiter, J.H. Perpezko, Phys. Lett. A 119 (1986) 79.
[165] J. Broughton, Phys. Rev. Lett 67 (1991) 2990.
[166] M. Faraday, Proc. R. Soc. London 10 (1860) 440.
[167] M. Faraday, reported in: The Athenaeum 1181 (1933) 640.
[168] J.G. Dash, Contemp. Phys. 30 (1989) 89.
[169] G. Tammann, Z. Physik. Chemie 68 (1910) 205.
[170] I.N. Stranski, Die Naturwissenschaften 28 (1942) 425.
[171] J.W.M. Frenken, J.F. van der Veen, Phys. Rev. Lett. 54 (1985) 134.
[172] J.W.M. Frenken, P.M.J. Maree, J.F. van der Veen, Phys. Rev. B 34 (1986) 7506.
[173] B. Pluis, A.W. Denier van der Gon, J.W.M. Frenken, J.F. van der Veen, Phys. Rev. Lett. 59 (1987) 2678.
[174] B. Pluis, T.N. Taylor, D. Frenkel, J.F. van der Veen, Phys. Rev. B 40 (1989) 1353.
[175] J.W.M. Frenken, B.J. Hinch, J.P. Toennies, C. Wöll, Phys. Rev. B. 41 (1990) 938.
[176] B. Pluis, J.M. Gay, J.W.M. Frenken, S. Gierlotka, J.F. van der Veen, J.E. MacDonald, A.A. Williams, N. Piggins, J. Als-Nielsen, Surface Sci. 222 (1989) L845.
[177] P.H. Fuoss, L.J. Norton, S. Brennan, Phys. Rev. Lett. 60 (1988) 2046.
[178] U. Breuer, O. Knauff, H.P. Bonzel, J. Vac. Sci. Technol. A 8 (1990) 2489.
[179] U. Breuer, O. Knauff, H.P. Bonzel, Phys. Rev. B 41 (1990) 10848.
[180] H.M. van Pinxteren, J.W.M. Frenken, Surface Sci. 275 (1992) 383.
[181] K.C. Prince, U. Breuer, H.P. Bonzel, Phys. Rev. Lett. 60 (1988) 1146.
[182] U. Breuer, H.P. Bonzel, K.C. Prince, R. Lipowsky, Surface Sci. 223 (1989) 258.
[183] H.N. Yang, T.-M. Lu, G.-C. Wang, Phys. Rev. Lett. 63 (1989) 1621.
[184] W. Dürr, D. Pescia, J.W. Kremer, W. Gudat, Solid State Commun. 73 (1990) 119.
[185] D.M. Zhu, J.G. Dash, Phys. Rev. Lett. 57 (1986) 2959.
[186] D.M. Zhu, J.G. Dash, Phys. Rev. Lett. 60 (1988) 432.
[187] L. Brushi, G. Torzo, H.W. Chan, Europhys. Lett. 6 (1988) 541.
[188] K.D. Stock, E. Menzel, Surface Sci. 61 (1976) 272.

[189] K.D. Stock, E. Menzel, J. Crystal Growth 43 (1978) 135.
[190] K.D. Stock, B. Grosser, J. Crystal Growth 50 (1980) 485.
[191] J. Krim, J.P. Coulomb, J. Bouzidi, Phys. Rev. Lett. 58 (1987) 583.
[192] P. Chiarello, J.P. Coulomb, J. Krim, C.L. Wang, Phys. Rev. B 38 (1989) 8967.
[193] M. Bienfait, Europhys. Lett. 4 (1987) 79.
[194] M.S. Pettersen, M.J. Lysek, D.L. Goodstein, Phys. Rev. B 40 (1989) 4938.
[195] P. von Blanckenhagen, W. Schommers, V. Voegele, J. Vac. Sci. Technol. A 5 (1987) 649.
[196] W. Theis, Diploma thesis, FU Berlin, 1989.
[197] A.W. Denier van der Gon, R.J. Smith, J.M. Gay, D.J. O'Connor, J.F. van der Veen, Surface Sci. 227 (1990) 143.
[198] H. Dosch, T. Höfer, J. Peisl, R.L. Johnson, Europhys. Lett. 15 (1991) 527.
[199] E.G. McRae, R.A. Malic, Phys. Rev. Lett. 58 (1987) 1437.
[200] S.G.J. Mochrie, D.M. Zehner, B.M. Ocko, D. Gibbs, Phys. Rev. Lett. 64 (1990) 2925.
[201] B.M. Ocko, D. Gibbs, K.G. Huang, D.M. Zehner, S.G.J. Mochrie, Phys. Rev. B 44 (1991) 6429.
[202] A. Hoss, U. Romahn, P. von Blanckenhagen, O. Meyer, Europhys. Lett. 20 (1992) 125.
[203] Y. Cao, E.H. Conrad, Phys. Rev. Lett. 64 (1990) 447.
[204] S. Chandavarkar, R.M. Geertman, W.H. de Jeu, Phys. Rev. Lett. 69 (1992) 2384.
[205] A. Lied, H. Dosch, J. Peisl, to be published, 1993.
[206] R.T. Lyzhva, A.Y. Mitus, A.Z. Patashinskii, Sov. Phys. JETP 54 (1981) 1168.
[207] R. Lipowsky, W. Speth, Phys, Rev. B 28 (1983) 3983.
[208] R. Lipowsky, U. Breuer, K.C. Prince, H.P. Bonzel, Phys. Rev. Lett. 62 (1989) 913.
[209] A. Levi, E. Tosatti, Surface Sci. 189/190 (1987) 641.
[210] G. Gompper, D. Kroll, Phys. Rev. B 40 (1989) 7221.
[211] T.A. Cherepanova, A.V. Stekolnikov, J. Crystal Growth 99 (1990) 88.
[212] T.A. Cherepanova, A.V. Stekolnikov, P. Bennema, to be published.
[213] L.S. Tuckerman, J. Bechhoefer, Phys. Rev. A 46 (1992) 3178.
[214] J.Q. Broughton, G.H. Gilmer, J. Chem. Phys. 79 (1983) 5095, 5105, 5119.
[215] L. Pietronero, E. Tosatti, Solid State Comm. 32 (1979) 255.
[216] C.S. Jayanthi, E. Tosatti, A. Fasolino, Surface Sci. 152/153 (1985) 155.
[217] C.S. Jayanthi, E. Tosatti, L. Pietronero, Phys. Rev. B 31 (1985) 3456.
[218] A. Trayanov, E. Tosatti, Phys. Rev. Lett. 59 (1987) 2207.
[219] A. Trayanov, E. Tosatti, Phys. Rev. B 38 (1988) 6961.
[220] J.Q. Broughton, L.V. Woodcock, J. Phys. C 11 (1978) 2743.
[221] V. Pontikis, V. Rosato, Surface Sci. 162 (1985) 150.
[222] V. Rosato, G. Ciccotti, V. Pontikis, Phys. Rev. B 33 (1986) 1860.
[223] V. Pontikis, P. Sindzingre, Physica Scripta T 19 (1987) 375.
[224] J.P. van der Eerden, H.J.F. Knops, A. Roos, J. Chem. Phys. 96 (1991) 714;
J.P. van der Eerden, T.H.M. van den Berg, J. Huinink, H.J.F. Knops, J. Crystal Growth 128 (1993) 57.
[225] W. Schommers, Phys. Rev. B 37 (1985) 6845.
[226] W. Schommers, P. von Blanckenhagen, Surface Sci. 162 (1985) 144.
[227] S. Valkealahti, R.M. Nieminen, Physica Scripta 36 (1987) 646.
[228] X. Chen, PhD Thesis, Trieste, 1990.
[229] P. Carnevalli, F. Ercolessi, E. Tosatti, Phys. Rev. B 36 (1987) 6701.
[230] P. Stoltze, J.K.Nørskov, U. Landman, Phys. Rev. Lett. 61 (1988) 440.
[231] P. Stoltze, J.K. Nørskov, U. Landman, Surface Sci. 220 L693 (1989) L693.
[232] E.T. Chen, R.N. Barnett, U. Landman, Phys. Rev. B 40 (1989) 925.
[233] E.T. Chen, R.N. Barnett, U. Landman, Phys. Rev. B 41 (1990) 439.
[234] P. Stoltze, J. Chem. Phys. 92 (1990) 6306.
[235] A.W. Denier van der Gon, D. Frenkel, J.W.M. Frenken, R. Smith, P. Stoltze, Surface Sci. 256 (1991) 385.
[236] P. Stoltze, J.K.Nørskov, 1993, to be published.
[237] R.N. Barnett, U. Landman, Phys. Rev. B 44 (1991) 3226.
[238] P.D. Ditlevsen, P. Stoltze, J.K.Nørskov, Phys. Rev. B 44 (1991) 13002.
[239] A. Boutin, A.H. Fuchs, J. Chem. Phys. 98 (1993) 3290.
[240] L.V. Mikheev, A.A. Chernov, Sov. Phys. JETP 65 (1987) 971.
[241] H. Löwen, T. Beier, Phys. Rev. B 41 (1990) 4435.
[242] H. Löwen, Phys. Rev. Lett. 64 (1990) 2104.
[243] R. Lipowsky, Z. Phys. B 55 (1984) 345.
[244] H. Löwen, T. Beier, Z. Phys. B 79 (1990) 441.

[245] J.M. Victor, J.P. Hansen, J. Phys. (Paris) Lett. 45 (1984) L307.
[246] H.N.W. Lekkerkerker, W.C.-K. Poon, P.N. Pusey, A. Stroobants, P.B. Warren, Europhys. Lett. 20 (1992) 559.
[247] G. Wulff, Z. Krist. 34 (1901) 449.
[248] J.J.Métois, J.C. Heyraud, Ultramiscroscopy 31 (1989) 73.
[249] J.C. Heyraud, J.J.Métois, J.M. Bermond, J. Cryst. Growth 98 (1989) 355.
[250] J.J.Métois, J.C. Heyraud, J. Phys. (Paris) 50 (1989) 3175.
[251] A. Pavlovska, K. Faulian, E. Bauer, Surface Sci. 221 (1989) 233.
[252] P. Stoltze, 1993, to be published.
[253] G. Bilalbegovic, F. Ercolessi, E. Tosatti, Europhys. Lett. 17 (1992) 333.
[254] H.M. van Pinxteren, J.W.M. Frenken, Europhys. Lett. 21 (1993) 43.
[255] P. Nozières, J. Phys. (Paris) 50 (1989) 2541.
[256] H. Löwen, Surface Sci. 234 (1990) 315.
[257] J. Stewart, Phys. Rev. Lett. 71 (1993) 887.
[258] P.R. Harrowell, D.W. Oxtoby, J. Chem. Phys. 86 (1987) 2932.
[259] E. Montroll, in: Statistical Mechanics, eds S. Rice, K. Freed and J. Light (University of Chicago, Chicago, 1972).
[260] S. Chan, J. Chem. Phys. 67 (1978) 5755.
[261] H. Löwen, D. Oxtoby, J. Chem. Phys. 93 (1990) 674.
[262] D.E. Sullivan, Phys. Rev. B 20 (1979) 3991.
[263] D.E. Sullivan, J. Chem. Phys. 74 (1981) 2604.
[264] E.H. Hauge, M. Schick, Phys. Rev. B 27 (1983) 4288.
[265] H. Löwen, R. Lipowsky, Phys. Rev. B 43 (1991) 3507.
[266] R. Lipowsky, D.A. Huse, Phys. Rev. Lett. 57 (1986) 353.
[267] J. Bechhoefer, H. Löwen, L.S. Tuckerman, Phys. Rev. Lett. 67 (1991) 1266.
[268] D.A. Porter, K.E. Easterling, Phase Transformations in Metals and Alloys (Van Nostrand Reinhold, Berkshire, 1981) ch. 6.
[269] L.A. Bendersky, R.J. Schaefer, Physica A 140 (1986) 298.
[270] L. Bocquet, H. Löwen, to be published, 1993.
[271] R.J. Schaefer, M.E. Glicksman, J. Cryst. Growth 5 (1969) 44.
[272] J.S. Langer, in Chance and Matter, Proceedings of the Les Houches Summer School, Session XLVI, eds J. Souletie, J. Vannimenus, R. Stora (Elsevier, Amsterdam, 1987).
[273] J.B. Collins, H. Levine, Phys. Rev. B 31 (1985) 6119.
[274] J.B. Collins, A. Chakrabarti, J.D. Gunton, Phys. Rev. B 39 (1989) 1506.
[275] J.S. Langer, in: Directions in Condensed Matter Physics, eds G. Grinstein, G. Mazenko (World Scientific, Singapore, 1986) p. 165.
[276] A.R. Umantsev, A.L. Roitburd, Sov. Phys. Solid State 30 (1988) 651.
[277] A. Umantsev, Sov. Phys. Crystallography 30 (1985) 87.
[278] S.A. Schofield, D.W. Oxtoby, J. Chem. Phys. 94 (1991) 2176.
[279] H. Löwen, S.A. Schofield, D. Oxtoby, J. Chem. Phys. 94 (1991) 5685.
[280] H. Löwen, J. Bechhoefer, Europhys. Lett. 16 (1991) 195.
[281] H. Löwen, J. Bechhoefer, L.S. Tuckerman, Phys. Rev. A 45 (1992) 2399.
[282] R. Kupfermann, O. Shochet, E. Ben-Jacob, Z. Schuss, Phys. Rev. B 46 (1992) 16045.
[283] C. Charach, B. Zaltzman, Phys. Rev. E 47 (1993) 1230.
[284] A.A. Wheeler, W.J. Boettinger, G.B. McFadden, Phys. Rev. A 45 (1992) 7424; Phys. Rev. E 47 (1993) 1893.
[285] C. Zener, J. Appl. Phys. 20 (1949) 950.
[286] E.A. Brener, D.E. Temkin, Europhys. Lett. 10 (1989) 171.
[287] C. Misbah, H. Müller-Krumbhaar, D.E. Temkin, J. Phys. (Paris) I 1 (1991) 585.
[288] G. Caginalp, Phys. Rev. A 39 (1989) 5887.
[289] M. Marder, Phys. Rev. A 45 (1992) R2158.
[290] A. Umantsev, J. Chem. Phys. 96 (1992) 605.
[291] J. Bechhoefer, A.J. Simon, A. Libchaber, P. Oswald, Phys. Rev. A 40 (1989) 2042.
[292] P. Oswald, J. Malthête, P. Pelcé, J. Phys. (Paris) 50 (1989) 2121.
[293] C.A. Angell, J. Phys. Chem. Solids 49 (1988) 863.
[294] N. Pistoor, PhD thesis, University of Mainz, 1991.
[295] F. Mezei, W. Knaak, B. Farago, Phys. Rev. Lett. 58 (1987) 571.
[296] W. Knaak, F. Mezei, B. Farago, Europhys. Lett. 7 (1988) 529.
[297] G.F. Signorini, J.L. Barrat, M.L. Klein, J. Chem. Phys. 92 (1990) 1294.

[298] W. Götze, in: Liquids, Freezing and the Glass Transition, eds J.P. Hansen, D. Levesque, J. Zinn-Justin (North-Holland, Amsterdam, 1991).
[299] W. Götze, L. Sjögren, Rep. Prog. Phys. 55 (1992) 241.
[300] S.F. Edwards, P.W. Anderson, J. Phys. F 5 (1975) 965.
[301] S.P. Das, Phys. Rev. A 42 (1990) 6116.
[302] J.L. Barrat, M.L. Klein, Annu. Rev. Phys. Chem. 42 (1991) 23.
[303] R.M. Ernst, S.R. Nagel, G.S. Grest, Phys. Rev. B 43 (1991) 8070.
[304] C. Dasgupta, A.V. Indrani, S. Ramaswamy, M.K. Phani, Europhys. Lett. 15 (1991) 307.
[305] P.N. Pusey, W. van Megen, Phys. Rev. Lett. 59 (1987) 2083.
[306] P.N. Pusey, W. van Megen, Phys. Rev. A 43 (1991) 5429.
[307] W. van Megen, S.M. Underwood, P.N. Pusey, Phys. Rev. Lett. 67 (1991) 1586.
[308] W. van Megen, S.M. Underwood, Phys. Rev. Lett. 70 (1993) 2766.
[309] W. van Megen, S.M. Underwood, Phys. Rev. E 47 (1993) 248.
[310] E. Bartsch, M. Antoinetti, W. Schupp, H. Sillescu, J. Chem. Phys. 97 (1992) 97.
[311] E. Bartsch, V. Frenz, S. Möller, H. Sillescu, Physica A 201 (1993) 363.
[312] H. Sillescu, E. Bartsch, in: Disorder Effects on Relaxational Processes, eds R. Richert, A. Blumen (Springer, Berlin, 1993).
[313] E.B. Sirota, H.D. Ou-Yang, S.K. Sinha, P.M. Chaikin, J.D. Axe, Y. Fuji, Phys. Rev. Lett. 62 (1989) 1524.
[314] A. Meller, J. Stavans, Phys. Rev. Lett. 68 (1992) 3646.
[315] W. Götze, L. Sjögren, Phys. Rev. A 43 (1991) 5442.
[316] M. Fuchs, I. Hofacker, A. Latz, Phys. Rev. A 45 (1992) 898.
[317] H. Löwen, J.P. Hansen, J.N. Roux, Phys. Rev. A 44 (1991) 1169.
[318] H. Migayawa, Y. Hiwatari, B. Bernu, J.P. Hansen, J. Chem. Phys. 88 (1988) 3879.
[319] C. Dasgupta, Europhysics Lett. 20 (1992) 131.
[320] C. Dasgupta, S. Ramaswamy, Physica A 186 (1992) 314.
[321] L.M. Lust, O.T. Valls, C. Dasgupta, Phys. Rev. E 48 (1993) 1787.
[322] M. Dzugutov, Phys. Rev. A 46 (1992) R2984.
[323] P. Sindzingre, M.L. Klein, J. Chem. Phys. 96 (1992) 4681.
[324] G. Wahnström, L.J. Lewis, to be published, 1993.
[325] J. Baschnagel, K. Binder, H.-P. Wittmann, J. Phys. Condensed Matter 5 (1993) 1597.
[326] W. Kob, H.C. Anderson, Phys. Rev. E 47 (1993) 3281.
[327] D. Thirumalai, R.D. Mountain, T.R. Kirkpatrick, Phys. Rev. A 39 (1989) 3563.
[328] D. Thirumalai, R.D. Mountain, Phys. Rev. E 47 (1993) 479.
[329] J.L. Barrat, T. Biben, J.P. Hansen, J. Phys. Condensed Matter 4 (1992) L11.
[330] T. Biben, J.P. Hansen, J.L. Barrat, J. Chem. Phys. 98, (1993) 7330.
[331] T. Bellini, R. Piazza, V. Degiorgio, to be published, 1993.
[332] D.G. Grier, C.A. Murray, in: Structure and Dynamics of Strongly Interacting Colloids and Supramolecular Aggregates in Solution, eds S.H. Chen, J.S. Huang, P. Tartaglia, Nato ASI (Kluwer, Deventer, 1992).
[333] H. Löwen, J. Phys. Condensed Matter 4 (1992) 10105.
[334] J.A. Zollweg, G.V. Chester, Phys. Rev. B 46 (1992) 11186.
[335] J. Lee, K.J. Strandburg, Phys. Rev. B 46 (1992) 11190.
[336] J.L. Colot, M. Baus, Phys. Lett. A 119 (1986) 135.
[337] B.B. Laird, J.D. McCoy, A.D.J. Haymet, J. Chem. Phys. 88 (1988) 3900.
[338] D.M. Zhu, D. Pengra, J.G. Dash, Phys. Rev. B 37 (1988) 5586.
[339] H. Shechter, R. Brener, M. Folman, J. Suzanne, Phys. Rev. B 41 (1990) 2748.
[340] H. Löwen, J.P. Hansen, P.A. Madden, J. Chem. Phys. 98 (1993) 3275.
[341] M. Fushiki, J. Chem. Phys. 97 (1992) 6700.
[342] H. Löwen, G. Kramposthuber, Europhys. Lett. 23 (1993) 673.
[343] P. Bartlett, R.H. Ottewill, P.N. Pusey, Phys. Rev. Lett. 68 (1992) 3801.
[344] M.D. Eldridge, P.A. Madden, D. Frenkel, Mol. Phys. 79 (1993) 105.
[345] M.D. Eldridge, P.A. Madden, D. Frenkel, to be published, 1993.
[346] H. Xu, M. Baus, J. Phys. Condensed Matter 4 (1992) L663.
[347] T. Biben, J.P. Hansen, Phys. Rev. Lett. 66 (1991) 2215.
[348] J.S. Thakur, J. Bosse, Phys. Rev. A 43 (1990) 4378; 43 (1990) 4388.
[349] J.L. Barrat, M. Baus, J.P. Hansen, Phys. Rev. Lett. 56 (1986) 1063.
[350] J.L. Barrat, M. Baus, J.P. Hansen, J. Phys. C 20 (1987) 1413.
[351] S.J. Smithline, A.D.J. Haymet, J. Chem. Phys. 88 (1988) 2004.

[352] X.C. Zeng, D.W. Oxtoby, J. Chem. Phys. 93 (1990) 4357.
[353] A.R. Denton, N.W. Ashcroft, Phys. Rev. A 42 (1990) 7312.
[354] A.R. Denton, N.W. Ashcroft, Phys. Rev. A 43 (1991) 3161.
[355] M. Rovere, M.P. Tosi, N.H. March, Phys. Chem. Liq. 12 (1982) 177.
[356] J.L. Barrat, J.P. Hansen, R. Moshkovitch, Astron. Astrophys. 199 (1988) 15.
[357] S. Ichimaru, H. Iyetoni, S. Ogata, Astrophys. J. 334 (1988) 17.
[358] S.W. Rick, A.D.J. Haymet, J. Chem. Phys. 90 (1989) 1188.
[359] J.L. Barrat, J.P. Hansen, J. Phys. (Paris) 47 (1986) 1547.
[360] R. McRae, A.D.J. Haymet, J. Chem. Phys. 88 (1988) 1114.
[361] R. Holyst, A. Poniewierski, Phys. Rev. A 38 (1988) 1527.
[362] A. Poniewierski, R. Holyst, Phys. Rev. Lett. 61 (1988) 2461.
[363] A. Poniewierski, R. Holyst, Phys. Rev. A 38 (1988) 3721.
[364] R. Holyst, A. Poniewierski, Phys. Rev. A 39 (1989) 2742.
[365] A. Poniewierski, R. Holyst, Phys. Rev. A 41 (1990) 6871.
[366] A.M. Somoza, P. Tarazona, Phys. Rev. Lett. 61 (1988) 2566.
[367] U.P. Singh, U. Mohanty, Y. Singh, Phys. Rev. A 38 (1988) 4377.
[368] M.C. Mahato, M.R. Lakshni, R. Pandit, H.R. Krishnamurty, Phys. Rev. A 38 (1988) 1049.
[369] P.I. Teixera, M.M. Telo da Gama, J. Phys. Cond. Matt. 3 (1991) 111.
[370] H. Xu, H.N.W. Lekkerkerker, M. Baus, Europhys. Lett. 17 (1992) 163.
[371] J.A.C. Veerman, D. Frenkel, Phys. Rev. A 41 (1990) 3237.
[372] S. Fraden, A.J. Hurd, R.B. Meyer, M. Cahoon, D.L.D. Caspar, J. Phys. Colloque C3 (1985) C3-85.
[373] S.F. Schulz, E.E. Maier, R. Weber, J. Chem. Phys. 90 (1989) 7.
[374] J. Schneider, W. Hess, R. Klein, J. Phys. A: Math. Gen. 18 (1985) 1221.
[375] J. Schneider, D. Karrer, J.K.G. Dhont, R. Klein, J. Chem. Phys. 87 (1987) 3008.
[376] H. Löwen, to be published, 1994.
[377] P. Frodl, S. Dietrich, Phys. Rev. A 45 (1992) 7330.
[378] K. Kremer, B. Dünweg, M.S. Stevens, Physica A 194 (1993) 321.
[379] W.E. McMullen, K.F. Freed, J. Chem. Phys. 92 (1990) 1413.